Genome organization by SATB1 binding to base-unpairing regions (BURs) provides a scaffold for SATB1-regulated gene expression

Short title: SATB1 binds BUR genomic elements to organize chromatin

Yoshinori Kohwi[1*], Xianrong Wong[2^], Mari Grange[1], Thomas Sexton[3], Hunter W. Richards[1], Yohko Kitagawa[4†], Shimon Sakaguchi[4], Ya-Chen Liang[5], Cheng-Ming Chuong[5], Vladimir A. Botchkarev[6], Ichiro Taniuchi[7], Karen L. Reddy[2] and Terumi Kohwi-Shigematsu[1*]

[1] Department of Orofacial Sciences, University of California San Francisco, San Francisco, CA, 94143, USA

[2] Department of Biological Chemistry, School of Medicine, Johns Hopkins University, Baltimore, MD, 21205, USA

[3] Institute of Genetics and Molecular and Cellular biology (IGBMC), INSERM U1258, Illkirch, France.

[4] Laboratory of Experimental Immunology, Immunology Frontier Research Center, Osaka University, Osaka, 565-0871, Japan

[5] Department of Pathology, University of Southern California, Los Angeles, CA, 90033, USA

[6] Department of Dermatology, Boston University School of Medicine, Boston, Massachusetts, 02118, USA

[7] Laboratory for Transcriptional Regulation, RIKEN Center for Integrative Medical Sciences, Yokohama, 230-0045, Japan

† present address: Center of iPS Research and Applications, Kyoto University, Kyoto, 606-8507, Japan

^ Agency for Science, Technology, and Research (A*STAR) Skin Research Labs (A*SRL), Singapore 138632

* co-corresponding authors: TKohwi-Shigematsu@lbl.gov, YKohwi@lbl.gov

Abstract

Mammalian genomes are organized by multi-level folding, yet how this organization contributes to cell type-specific transcription remain unclear. A nuclear protein SATB1 forms a SATB1-rich subnuclear structure that resists high-salt extraction. SATB1 binds in the minor groove of double-stranded base-unpairing regions (BURs), genomic elements with high unwinding propensities. We uncovered that SATB1 establishes a two-tiered chromatin organization, one through indirect binding and another by direct binding of BURs. Published ChIP-seq datasets show SATB1 binding to highly accessible chromatin at enhancers and CTCF sites, but not to BURs. By employing urea ChIP-seq, which retains only directly bound protein:DNA complexes, we found that BURs, but not CTCF sites, are direct SATB1 binding targets genome-wide. BURs bound to the SATB1 nuclear substructure interact with accessible chromatin crossing multiple topologically associated domains (TADs). SATB1 is required for these megabase-scale interactions linked to cell type-specific gene expression. BURs are highly enriched within lamina associated domains (LADs), but some (~10%) are found in gene-rich accessible chromatin outside LADs as well. Only a subset of BURs is bound to SATB1 depending on cell type. Notably, despite the mutually exclusive SATB1-binding profiles uncovered by the two ChIP-seq methods, we found most peaks in both profiles are valid and require SATB1. Based on these and previous data, we propose that the SATB1 protein network forms a chromatin scaffold, providing an interface that connects accessible chromatin to a subnuclear architectural structure, thereby facilitating the three-dimensional organization linked to cell type-specific gene expression.

Introduction

Three-dimensional (3D) chromatin architecture, formed by chromatin folding at multiple hierarchical levels, is thought to play a fundamental role in genome activity such as gene expression (*1-7*). Whether and how genome folding contributes to gene regulation, however, remains largely unknown. High resolution chromatin interaction maps, generated by chromosome conformation capture methods such as Hi-C (all-to-all contacts), have revealed chromatin to be partitioned mainly into two types of megabase (Mb)-sized compartments, A and B (*8*). The euchromatic A compartment is gene-rich, transcriptionally active and enriched in histone marks associated with active chromatin, conferring high chromatin accessibility. On the other hand, the B compartment is gene-poor, transcriptionally repressive, and enriched in repressive histone marks. The largely transcriptionally repressive lamina-associated domains (LADs) are among the B compartment chromatin displaying the typical features of heterochromatin (*9, 10*). LADs have been identified by the lamin B1-mediated adenine methyltransferase identification (DamID) method (*11*) as genomic regions that are spatially proximal to the nuclear lamina, an intermediate filament meshwork adjacent to the inner nuclear membrane. LADs represent discrete chromatin domains of 40kb to 30 Mb in size (*9*). Approximately 1000-1500 LADs have been identified in mouse and human cells and, in a given cell type, typically cover ~30% of the genome (*2*). By sequestering chromatin to the repressive nuclear compartment, the nuclear lamina is thought to play an important role in genome organization.

At sub-megabase scales, using Hi-C, chromatin domains called “topological-associated domains” (TADs) were previously detected that are relatively insulated from adjacent TADs by preferentially making intra-domain contacts via looping (*12-14*). CTCF and cohesin are the two major architectural proteins required for folding chromatin into loops. The loop extrusion model postulates that cohesin functions in loop extrusion until it encounters the CCCTC-binding factor (CTCF) bound to its target sites in a convergent orientation (*15, 16*). CTCF- and cohesin-binding sites are enriched at the boundaries of TADs (*12, 17*) and LADs (*9*). Acute depletion of CTCF (*18*), cohesin (*19, 20*) or induced removal of cohesin loading factor NIPBL (*21*) results in a major loss of TADs. Unexpectedly, the majority of protein-coding genes remained largely unchanged in their expression levels in the absence of TADs. These results challenge the view that TADs provide a unit of gene expression control by insulating enhancer-promoter interactions from neighboring TADs. In the last few years, using super-resolution live-cell imaging, genome interactions were studied at the single cell levels. These studies revealed that chromatin looping formed by CTCF and cohesin are highly dynamic and variable among individual single cells, suggesting that TADs are an emergent property of the cell population average of heterogeneous chromatin folding (*22-26*). Therefore, TADs, enriched in contacts, may not represent a stable structural unit of chromatin flanked by two boundary loci stably bound by CTCF and cohesin [reviewed in (*25, 27, 28*)]. Super-resolution microscopy detected not only single cohesin-mediated loops but also radially stacked loops forming “rosette” like structures in individual single cells. These loops

were also transient and a single cell spends a minority of its time in the configuration, and depletion of cohesin led to increased variability in gene expression at single cell levels (*29*). As such, although research on CTCF and cohesin has greatly advanced our understanding on chromatin loop formation, there is still much to learn about how and what functional 3D chromatin structure underlies gene activity, especially cell-type specific gene expression. It is increasingly clear that it is necessary to explore additional nuclear factors that potentially drive chromatin folding. In this paper, we studied function of a tissue-specific architectural protein SATB1 in genome organization.

SATB1 was originally identified by virtue of its specific binding to genomic sequences called Base Unpairing Regions (BURs). Previous *in vitro* studies have shown that SATB1 directly binds BURs without requiring additional molecules, such as RNA or proteins (*30-32*). BURs have a strong unwinding property under negative superhelical stress, and BURs are empirically identified using unpaired DNA-specific chemical probes (*30, 33*) because they lack primary sequence consensus. However, BURs have a unique sequence context: a typical BUR (~200-300bp) contains a cluster of short sequence segments (25-50 bp/segment) containing exclusively As, Ts, and Cs on one strand (ATC context) (*30, 32*). BURs are at least 65% AT-rich, but importantly, not all AT-rich sequences are BURs. Importantly, SATB1 binds to BURs in the minor groove of double-stranded DNA, recognizing the altered phosphate backbone structure; it does not bind to single-stranded DNA (*32*). Disruption of the ATC context by mutagenesis, without affecting the AT content, results in loss of unwinding property of a BUR and SATB1 binding. While BURs are obviously present in the genome across cell types, SATB1 protein is cell-type restricted, most abundantly expressed in thymocytes and among multiple adult progenitor cells (*34-36*), as well as terminal differentiated postnatal neurons in the cortex and amygdala (*37, 38*). Located in nuclear interior, SATB1 has an interconnected cage-like distribution in thymocytes (*39*) and a fine spider web-like distribution in neurons (*37*) forming a unique SATB1 subnuclear structures that are resistant to high-salt extraction. Some BURs have been identified and characterized as *in vivo* SATB1 binding sites and, when bound to SATB1, are also resistant to salt extraction (*39, 40*). SATB1 has been shown to be essential for loop formation connecting a subset of these BURs and recruiting chromatin remodeling complexes, epigenetic factors and transcription factors to specific gene loci (*41*) Of particular interest, SATB1 regulates expression of hundreds of protein-coding genes in a cell-type specific manner to enable cells to acquire new phenotypes, such as during T cell activation (*42*), development of many adult progenitor cells (*34-37, 43-49*), and cancer metastasis (*41, 50-52*). For example, by directing lineage-specific transcriptional programs, SATB1 plays an essential role in development of $CD4^+$ T cells, $CD8^+$ T cells, NKT cells, and $Foxp3^+$ regulatory T cells (Treg) in the thymus(*46, 47*) as well as in promoting the pathogenic effector program of tissue Th17 cells in autoimmune disease in mice(*48*). These activities have been shown to mediate co-induction of interleukin genes in T helper cells (*42*) and regulate ~1000 genes in cancer to promote metastasis(*50*). Thus, SATB1 has long been thought to play a role in regulating genome architecture and in gene expression.

Although BURs have been identified to be specific and direct binding target sequences of SATB1, mysteriously the genome-wide SATB1 binding profiles obtained by the widely used, standard chromatin immunoprecipitation-deep sequencing (ChIP-seq) does not detect SATB1 interaction with BURs. Instead, SATB1 has been mapped mainly to enhancers and to a region that would become an active super-enhancer upon differentiation (*45-47*). In line with this, recent studies on chromatin looping with Hi-C also shows that SATB1 mediates interactions involving a subset of enhancers and promoters for cell identity gene expression and that SATB1 binding sites coincide with many CTCF-bound loci (*53-55*). These results align with SATB1's role in assembling transcription complexes at regulatory regions. However, they are also puzzling, considering that BURs have been identified as the direct binding targets of SATB1 by *in vitro* binding assays. We therefore hypothesized that SATB1-BUR interactions are somehow undetectable by the standard ChIP-seq approach and CUT&Tag methods, and if identified, would provide additional mechanisms for chromatin looping events *in vivo* that link to gene expression.

ChIP-seq has been a gold standard for profiling chromatin-protein interactions. However, standard ChIP-seq approaches have several drawbacks. First, chromatin structure can introduce biases into ChIP-seq analysis. Fragmentation of crosslinked chromatin in whole cells/nuclei can result in biased capture of transcriptionally active, highly accessible "open" chromatin and generation of false-positive "phantom" peaks (*56-60*). Second, it fails to distinguish between direct and indirect (piggybacking) chromatin binding of a protein of interest. Here, we optimized urea-ChIP-seq, a modified ChIP-seq that first isolate stringently purified whole intact genomic DNA that retains only its directly bound proteins from crosslinked cells prior to fragmentation and immunoprecipitation. This captures the entire genome, regardless of its original chromatin accessibility status. This approach has allowed us to identify genomic sites directly bound by SATB1 and revealed BURs to be the primary *direct* SATB1 target sites, previously hidden by standard ChIP-seq. The SATB1-bound BURs are mutually exclusive with enhancer-enriched SATB1-bound sites mapped by standard ChIP-seq. Instead, a majority of BURs are mapped within LADs, and depending on cell type, SATB1 binds *in vivo* to selective subsets of these BURs. Using the urea 4C-seq (one-to-all contacts), select SATB1-bound BURs were found to interact extensively over the >5.7Mb gene-rich region within DNase 1 hypersensitive (DNase 1 HS) regions, but not with adjacent gene-poor regions. SATB1 is essential for both megabase-level chromatin interactions and proper expression of multiple genes in this gene-rich region. Collectively, our results suggest that SATB1-mediated genome organization exhibits two distinct features, a "skeletal framework" where SATB1 binds BURs directly, and a network of gene-rich open chromatin that is tethered to BURs indirectly through SATB1-mediated chromatin looping, which is correlated to gene expression.

Results

Development of urea ChIP-seq method to detect genome-wide SATB1-binding profiles

166 Unlike many nuclear proteins (e.g. transcription and chromatin modifying factors), SATB1 resides in
167 nuclear substructures exhibiting resistance to extraction with high salt or lithium 3,5-diidosalicylate (LIS)
168 (*40, 44*). Consistent with this, after extraction of nuclei with buffer containing 2M NaCl that removed
169 most of the proteins from DNA, individually cloned SATB1-bound BURs remained anchored to the
170 residual SATB1 protein network (SATB1-rich subnuclear architecture) found in the interior of nuclei (*39*).
171 By contrast, in high-salt extracted *Satb1*$^{-/-}$ (SATB1-KO) thymocyte nuclei, these BURs lost their
172 anchored sites and were exclusively found in the distended DNA halos that spread around the residual
173 nuclei, which is illustrated (*Figure 1A*) (*39*). Thus, we hypothesized that SATB1-BUR interactions are
174 likely embedded in an insoluble subnuclear structure that could not be detected to date by the widely
175 used standard ChIP-seq methods. It is possible that ChIP-seq experiments have inherent biases arising
176 from chromatin structure such as heterochromatin and transcriptionally active regions (*61*).

177 To detect BURs as the primary targets of SATB1 genome wide, we devised a urea ChIP-seq
178 method to purify genomic DNA with only its directly bound proteins. Through this apporach, we found
179 that a vast majority of *in vivo* SATB1-binding sites are BURs in the genome. In this method, cells are
180 first crosslinked with formaldehyde. Then, cells are lysed in a 4% SDS-containing buffer and subjected to
181 ultracentrifugation with 8M urea. In this manner, crosslinked chromatin is stringently purified by removing
182 all free-floating proteins and proteins bound to DNA indirectly. Therefore, urea ChIP-seq is performed with
183 the genomic DNA retaining only directly bound proteins. It is important to note that without prior
184 formaldehyde crosslinking, urea centrifugation removes 99.9% of chromatin-associated protein from
185 chromatin and sediments unsheared pure genomic DNA at the bottom of the tube (*62*). As a denaturant
186 for DNA, RNA, and proteins, high concentrations of urea (e.g. 6-8M) disrupt the secondary structures
187 of nucleic acids and the three-dimensional structure of proteins (*63-65*). Crucially, purified genomic DNA
188 obtained from 8M urea ultracentrifugation remains double-stranded and can therefore be readily
189 digested with restriction enzymes (this study and (*66*). Additionally, the proteins that remain bound to
190 urea-purified DNA from crosslinked cells can still be detected with the antibodies compatible with
191 standard ChIP protocols. By acting as both a hydrogen bond donor and acceptor, high concentrations
192 of urea destabilize double-stranded DNA by weakening the hydrogen bonds between base pairs,
193 thereby decreasing the melting temperature of DNA (*67, 68*). However, even 6-8 M urea alone, without
194 heat treatment, is insufficient to convert double-stranded DNA into single-stranded DNA (*69*).
195 Denaturing polyacrylamide electrophoresis for separating DNA oligonucleotides by size typically uses
196 6-8 M urea. For this, DNA samples need to be heat denatured first to make them single-stranded (*70*).
197 Our 8 M urea centrifugation protocol lacks heat treatment and includes prior formaldehyde fixation, thus
198 allowing genomic DNA to remain double-stranded and bound by interacting proteins

199 Critically, the urea ChIP-seq method (*66*) allows detection of genomic regions solely based on
200 their direct protein binding regardless of their original chromatin status, such as 'accessible' or
201 'inaccessible' chromatin. To obtain reproducible direct binding profiles of SATB1 at the genome-wide
202 scale, it was necessary to make additional optimizations. The modified urea ChIP-seq protocol allows

203 quantitative solubilization of the unsheared crosslinked genomic DNA fiber after urea ultracentrifugation,
204 while still maintaining intact chromatin-protein interactions during fragmentation. The critical steps that
205 are different between urea and standard ChIP-seq are highlighted (*Figure 1B*). A putative scenario as
206 to how DNA-binding sites of chromatin-associated factors are captured by the two different ChIP-seq
207 methods is illustrated (*Figure 1C*). Urea ChIP-seq allows detection of chromatin-bound proteins
208 regardless of the chromatin's accessibility because the whole genome is purified. In contrast, standard
209 ChIP-seq discards most of the insoluble fraction and retains primarily the soluble fraction for the
210 subsequent chromatin immunoprecipitation step (*61*). This results in samples that are enriched in
211 accessible "open" chromatin. Because a fraction of SATB1 proteins can be easily extracted from cells
212 with a high salt-containing buffer whereas other fraction resists extraction, both soluble and insoluble
213 fractions are expected to contain SATB1(*40*). This could reflect SATB1 proteins being heterogeneous
214 with regards to their mobility. By fluorescence recovery after photobleaching (FRAP) assay in
215 thymocytes, we found one fraction of SATB1 essentially immobile and the other with high mobility (our
216 unpublished results). Due to the lack of specific markers to distinguish these SATB1 proteins, we cannot
217 confirm the exact relationship between fast-mobile SATB1 and immobile SATB1 to the soluble and
218 insoluble fractions, respectively. Comparing the two ChIP-seq protocols, standard ChIP-seq, therefore,
219 captures both directly and indirectly bound proteins for chromatin fragments in the soluble fraction, and
220 their binding profiles cannot be distinguished. In contrast, urea ChIP-seq strongly enriches for directly
221 bound proteins, including those in chromatin regions that are difficult to solubilize. Thus, urea ChIP-seq
222 is uniquely suited for detecting direct DNA binding profiles of SATB1 that resides in the high-salt
223 extraction resistant subnuclear structure.

224 **Urea ChIP-seq detects BURs as direct binding targets of SATB1 *in vivo.***

225 To determine whether SATB1 binds to BURs *in vivo*, it is essential to validate *in vivo* SATB1-bound
226 sites as BURs. We previously generated a genome-wide BUR reference map by deep sequencing DNA
227 fragments generated from purified genomic DNA bound by recombinant SATB1 protein *in vitro (66)*.
228 Since SATB1 binds specifically to BURs *in vitro*, we used SATB1 as a biological probe to identify all
229 potential BURs in the genome. Using this approach, we reproducibly identified approximately 240,000
230 BURs ($q<0.01$), establishing a BUR reference map for both mouse and human genomes. Comparing
231 ChIP-seq peaks for SATB1 with the BUR reference map allows us to assess whether SATB1 binding
232 sites *in vivo* correspond to BURs.

233 We performed urea ChIP-seq for SATB1 in thymocytes and compared the results with standard
234 ChIP-seq for this protein and the BUR reference map. Strikingly, urea ChIP-seq produced SATB1
235 binding profiles that are entirely different from those produced by the standard ChIP-seq method (*Figure*
236 *2A*). The genome-wide analysis in mouse thymocytes using deepTools revealed that only 0.92% (an
237 average of two replicates per ChIP-seq method) of peaks in urea SATB1 ChIP-seq coincided with those
238 in standard SATB1 ChIP-seq (*supplementary Table 1 and Table 2*). In a large genomic region covering

239 a 4.48Mb region in chromosome 17 (*Figure 2A, top*), a gene-rich region was found in the valley between
240 BUR-enriched domains (*Figure 2A, track 3*), and standard ChIP-seq detects clusters of SATB1 binding
241 sites in this gene-rich region (*Figure 2A, tracks 1 and 2*). In contrast, urea ChIP-seq detected SATB-
242 binding to the domains surrounding the gene rich region, corresponding to regions heavily enriched in
243 BUR sites (*Figure 2A, tracks 3-5*). In a zoomed-in view, covering a 430 kb region, SATB1 sites identified
244 from urea ChIP-seq precisely coincided with BUR peaks and are excluded in the standard SATB1 ChIP-
245 seq peaks (*Figure 2B, tracks 1-3*). SATB1 bound sites uncovered from urea ChIP-seq avoided CTCF
246 sites (*Figure 2B, tracks 4 and 5 versus track 6)*, H3K27ac-marked sites and DNase 1 HS (*Figure 2B*
247 *tracks 7 and 8)*, whereas SATB1 sites from standard ChIP-seq primarily co-mapped to these sites
248 (*Figure 2B, tracks 1,2,6-9*). To unequivocally demonstrate that urea ChIP-seq peaks for SATB1 coincide
249 with BURs, we examined these peaks shown in Figure 2B at a higher resolution (Figure 2—*figure*
250 *supplement 1*). All four SATB1 peaks in Figure 2B precisely co-map with BURs. For one of these peaks,
251 a typical BUR sequence is shown that contains a cluster of DNA sequence stretches in which either Gs
252 or Cs are lacking from one strand. This DNA sequence context is referred to as the ATC sequence
253 context. We confirmed the relationship of SATB1-binding sites by urea ChIP-seq and BURs at the
254 genome-wide level using deepTools. Among SATB1 urea ChIP-seq peaks, an average of 77% of two
255 replicates coincided with BURs identified in our reference maps (*Figure 2C*). The statistical significance
256 of enrichment of BURs compared to a random overlap in either urea ChIP-seq or standard ChIP-seq
257 peaks is $p<0.001$ or $p=1$, respectively, using 1000 bootstrapped genomic intervals sampled using the
258 *bootRanges* approach (*71*) (*Figure 2C*). Consistent with this, genome-wide distribution profile analyses
259 show that while SATB1 binding profiles by standard ChIP-seq specifically exclude BURs, showing a
260 sharp indentation at the peak of BUR distribution, SATB1-binding profiles by urea ChIP-seq coincide
261 with BUR distribution (*Figure 2D*). Heatmap analyses were also conducted to examine SATB1-binding
262 sites among all BURs and BURs occurrence in all SATB1-bound sites in thymocytes *(Figure 2E).*
263 Consistent with results shown in *Figures 2C and 2D*, the heatmap study shows that the majority of
264 SATB1-binding sites coincide with BURs. Also, SATB1 binds a small subpopulation of BURs in
265 thymocytes (see below for cell-type dependent SATB1 occupancy of BURs). These results indicate
266 that SATB1 predominantly and directly targets BURs genome-wide *in vivo* and that the SATB1-binding
267 profiles obtained by standard and urea ChIP-seq methods are mutually exclusive. We conclude that our
268 urea ChIP-seq, which solely captures DNA with its directly bound proteins, unmasks SATB1 direct
269 binding profiles missed by standard ChIP-seq.

270 **CTCF-binding profiles remain unchanged between urea and standard ChIP-seq**

271 To investigate the potential cause for the discrepancy in the SATB1-binding profiles between the two
272 ChIP-seq approaches, we applied the urea ChIP-seq method to other factors and asked whether
273 binding profiles differed between urea and standard ChIP-seq. We investigated the DNA-binding profile
274 for CTCF by urea ChIP-seq and found its profile to be very similar to that obtained by standard ChIP-

275 seq from ENCODE, which largely overlapped with DNase 1 HS (*72*) (*Figure 3A, tracks 2, 4, 5 and 6*).
276 Similarly, we also found that urea ChIP-seq generated essentially identical DNA-binding profiles for
277 polycomb repressive complex 2 (PRC2) core subunits, SUZ12, JARID2 and EZH2 as generated by
278 others using standard ChIP-seq (*73*) (*Figure 3—figure supplement 1*). In line with recent studies (*53-*
279 *55*), 37% of SATB1 peaks from standard ChIP-seq (ENCODE) (average of two replicates,
280 *supplementary Table 1*) intersected with CTCF peaks genome-wide. In contrast, only 0.8% of SATB1
281 peaks from urea ChIP-seq coincided with CTCF peaks (average of two replicas, *supplementary Table*
282 *1*), confirming the UCSC browser track views (*Figure 2A and 3A*). These results verify that urea ChIP-
283 seq can accurately identify the DNA-binding sites of chromatin associated proteins. Thus, urea ChIP-
284 seq, compared to standard ChIP-seq, produces contrasting DNA-binding profiles for SATB1, but this is
285 not necessarily the case for other nuclear proteins. Thus, we conclude that for SATB1, urea and
286 standard ChIP-seq produces contrasting SATB1 binding profiles. Importantly, only urea ChIP-seq can
287 faithfully detects direct and specific SATB1 interactions with BURs, suggesting a different mode of
288 chromatin interactions. As mentioned in the introduction, it is important to note that these urea ChIP-
289 seq results support a large body of prior binding assay and cytological data for SATB1, indicating that
290 SATB1 forms salt-extraction resistant subnuclear protein network, and that the genomic sites directly
291 bound to SATB1 reside in the "inaccessible" chromatin.
292
293 **CTCF and SATB1 have distinct and independent binding profiles**
294 Our results above indicate that CTCF and SATB1 *direct* binding sites do not overlap. However, because
295 both CTCF and SATB1 are known to affect chromatin organization, there might be a functional link
296 between the two proteins. Recently, CTCF-binding sites mapped by CUT&Tag were found to be SATB1
297 independent in specific gene loci (*55*). We validated this result by generating the CTCF-binding profiles
298 by urea ChIP-seq in *Satb1*$^{-/-}$ (SATB1-KO) and *Satb1*$^{+/+}$ (SATB1-WT) thymocytes. These CTCF-binding
299 profiles showed no major changes depending on SATB1 (*Figure 3A, compare tracks 2 and 3*), as shown
300 in a randomly chosen region in chromosome 17 in wild-type (WT) and SATB1-KO thymocytes. This was
301 confirmed by genome-wide analyses which showed that CTCF urea ChIP-seq peak distributions from
302 SATB1-WT and SATB1-KO thymocytes coincided (*Figure 3B*). This indicates that CTCF binding to
303 genomic DNA is SATB1-independent genome wide.
304 To corroborate the independence of CTCF/cohesin and SATB1, we next examined whether
305 SATB1 interacts with CTCF and/or cohesin or both, components known to be important for loop
306 formation. Distinct from protein-protein co-immunoprecipitation (co-IP) using whole cell or nuclear
307 extracts, we examined the direct co-binding status on chromatin *in vivo* of SATB1 and CTCF or cohesin
308 by urea ChIP-Western. Urea-purified crosslinked-chromatin fragments immunoprecipitated with anti-
309 SATB1 antibody (SATB1-bound urea-ChIP fragments) contained SATB1 as expected, detected by
310 Western-blot of the de-crosslinked urea-ChIP sample. However, neither CTCF nor RAD21 (a cohesin
311 complex component) was detected in the SATB1 urea-ChIP samples. Reciprocal experiments using

312 either CTCF or RAD21-bound urea ChIP samples confirmed lack of SATB1 co-binding to these
313 chromatin fragments (*Figure 3C*, *Figure 3—figure supplement 2A*). We confirmed that a similar amount
314 of urea-purified crosslinking chromatin was used for each ChIP-Western sample with an anti-H3
315 antibody (which is, as expected, retained on urea-purified crosslinked chromatin). Therefore, these
316 results from urea ChIP-Western indicate that at least for the direct DNA co-binding status of SATB1
317 with either CTCF or RAD21, SATB1 does not co-bind chromatin with either of these proteins (*Figure*
318 *3C*). These results are consistent with mutually exclusive direct binding sites of CTCF and SATB1
319 (*Figure 3A* and *3B*).

320 If cohesin and CTCF bind directly to chromatin for loop formation according to the loop extrusion
321 model, then we expect that the urea ChIP-Western results will show that cohesin-bound DNA fragments
322 are co-bound by CTCF at the base of loops. As expected, we do find co-binding, however, fragments
323 co-bound by RAD21 and CTCF represent only a small fraction of either total RAD21-bound or CTCF-
324 bound chromatin fragments (*Figure 3C*). These results show that CTCF and RAD21 direct co-binding
325 to chromatin occurs much less frequently than their individual binding to chromatin. This result agrees
326 with a recent report which used super-resolution imaging of individual cells to show that the stable
327 CTCF-mediated loops are rare, and >95% of the time, the loops are either only partially extruded, or no
328 loops are formed (*25*).

329 Given that CTCF deletion causes most TADs to disappear, we next examined whether SATB1
330 depletion has any effects on TAD formation. We compared bulk Hi-C results between thymocytes
331 isolated from wild-type (*Satb1*$^{+/+}$: *Cd4-cre*) and SATB1-deficient (*Satb1*$^{F/F}$:*Cd4-cre*) mice in duplicates
332 (*Figure 3—figure supplement 2B*). Our Hi-C results revealed largely indistinguishable TAD profiles
333 between the two thymocytes (*Figure 3D*) examined at 10kb resolution**.** Neither TAD number nor TAD
334 sizes were changed by SATB1 depletion from thymocytes (*Figure 3—figure supplement 2C).* Intra-TAD
335 interactivity (the sum of Hi-C chromatin contacts inside the TAD) also remained mostly unchanged
336 (*Figure 3—figure supplement* 2D). These bulk Hi-C results upon SATB1 deletion are in good agreement
337 with recently published studies (*53, 54*). Similar to the results from the CTCF depletion study (*18*),
338 SATB1 depletion also did not alter segregation of active (A) and inactive chromatin
339 compartmentalization (B) (*Figure 3E*). Furthermore, our scaling plot displaying how the Hi-C contacts
340 decrease as a function of genomic distance shows that SATB1 depletion does not affect chromosome
341 compaction (*Figure 3—figure supplement* 2F). These Hi-C results taken together with SATB1-
342 independent CTCF-binding to DNA and non-overlapping direct genomic DNA-binding of SATB1 and
343 CTCF/cohesin, strongly suggest that SATB1 and CTCF are two independent proteins that have distinct
344 roles in chromatin organization, consistent with SATB1 having no roles in TAD organization.

345 **Non-specific peaks appear in *Satb1*$^{-/-}$ thymocytes by standard SATB1 ChIP-seq**
346
347 An important question is whether SATB1-binding profiles obtained by standard ChIP-seq are strictly
348 SATB1 dependent. If so, these binding sites likely reflect real but indirect SATB1 association with

349 chromatin. To address this question, we performed standard ChIP-seq on *Satb1*$^{-/-}$ (KO) thymocytes
350 using two different anti-SATB1 antibodies (1583 and ab109112, both of which are validated for
351 immunoprecipitation). The results are highlighted in two randomly chosen ~3Mb regions in chromosome
352 17 and in X chromosome, each containing a gene-rich region surrounded by gene-poor regions. Both
353 antibodies generated similar peaks in KO thymocytes (KO peaks) by standard ChIP-seq. These KO
354 peaks (false-positive) were predominantly detected in gene-rich, open chromatin regions in KO
355 thymocytes, and many of them coincided with peaks originally detected in WT thymocytes (WT peaks)
356 (*Figure 4—figure supplement 1 A and 1B, top and bottom, tracks 9 and 10*). This is in agreement with
357 an earlier report that ChIP-seq generate false-positive peaks in highly accessible, transcriptionally
358 active chromatin region (*56-60*). Intersection analyses with deepTools show that 4.1% of SATB1
359 standard ChIP-seq peaks obtained from our experiments are false-positive peaks (based on average
360 of two standard KO ChIP-seq samples) (*supplementary* Table 3 and 4). Besides those KO peaks that
361 overlapped with WT peaks, there were several thousands of KO-specific peaks generated by standard
362 ChIP-seq in our study. In contrast, SATB1 urea ChIP-seq had no false-positive peaks (0.0%). Also, only
363 ~100 KO-specific peaks (not overlapping with WT peaks) were detected (average of two samples)
364 compared to ~40,000 total WT peaks from SATB1 urea ChIP-seq (*supplementary Table 3 and 4*).
365 Therefore, validation using knockout cells is critical to distinguish real peaks that depend on SATB1
366 from SATB1-independent phantom peaks derived from the standard ChIP-seq method. The
367 percentages of phantom peaks in standard ChIP-seq likely depend on the specificity of antibodies used
368 and the condition of sample preparation.

369 After validation with SATB1-KO cells, we conclude that most SATB1 sites detected from
370 standard ChIP-seq are bound by SATB1, but most likely through indirect binding, as these peaks are
371 not detected by urea ChIP-seq, which removes any indirect binding proteins by urea ultracentrifugation.
372 SATB1 proteins are found in high salt-resistant fraction as well as salt-extracted fraction (*40*). Thus, it
373 is possible that soluble SATB1 may associate with "open" chromatin. In order to further understand
374 these differences and potential proximity of SATB1 binding sites detected by the two ChIP-seq methods,
375 we focused on three individual gene loci, i. e. *Rag1* and *Rag2* genes (*45*), *Foxp3* (*47*), and *Runx3* (*46*),
376 for which specific SATB1-binding sites by standard ChIP-seq have been reported (*Figure 4*). In addition,
377 these genes are known to be regulated by SATB1 in thymocytes and are thus excellent candidate
378 regions to investigate how SATB1 is regulating chromatin and gene expression. By either direct urea-
379 ChIP or standard ChIP, we found SATB1-bound sites within all three loci (*Rag1/2*, *Foxp3*, and *Runx3*)
380 to be SATB1-dependent. These sites were detected only in WT (*Figure 4, track 3*) but not in SATB1
381 KO-thymocytes (*Figure 4, tracks 7 and 9 for Rag/Rag2* and *Runx3*, *and tracks 9 and 11 for Foxp3*). In
382 these regions, input sample (without antibodies) had no peaks (*Figure 4*, *tracks 8 and 10 for Rag1/Rag2*
383 *and Runx 3, and tracks 10 and 12 for Foxp3*). For the *Rag1* and *Rag2* loci, SATB1 has been shown by
384 standard ChIP-seq to bind the anti-silencer element (ASE) and this binding is thought to counteract the
385 activity of an intergenic silencer, thus promoting expression of *Rag 1* and *Rag 2* (*45*). During

386 development of Foxp3^{+}-regulatory T cells (Treg) in the thymus, SATB1 expression in Treg precursor cells
387 is essential for the future establishment of a Treg cell–specific super-enhancers at the *Foxp3* locus in
388 Treg cells (*47*). Thus, thymocyte precursor-specific SATB1 deficiency, using *Satb1*$^{fl/fl}$ CD4-cre mice but
389 not *Satb1*$^{fl/fl}$ *Foxp3*-cre mice, impairs Treg super-enhancer activation and expression of *Foxp3*(*47*).
390 Impaired Treg cell development results in autoimmune disease (*46, 47, 74, 75*). Finally, SATB1 is also
391 essential for generation of CD4^{+} and CD8^{+} T cells and NKT cells (*46*). In response to T cell receptor
392 signaling by MHC class I and II, SATB1 regulates enhancer function in gene loci encoding lineage-
393 specifying factors (e.g. *Runx3*) and directs lineage-specific transcriptional programs in the thymus (*46*).
394 Strikingly, in these three regions, SATB1-bound BURs, as detected by urea ChIP-seq, are found
395 infrequently, and appear as isolated single peaks within 30-50kb regions. Such SATB1-bound BUR
396 sites are located close to but not overlapping with the cluster of enhancers marked by H3K27ac and
397 H3Kme1 modifications. These SATB1-bound BUR sites reside within 3kb of the nearest putative
398 SATB1-bound enhancers (detected by standard ChIP-seq) for the *Rag1/Rag2* and *Runx3* loci as well
399 as from the super-enhancer that becomes established at the *Foxp3* loci in matured Treg cells. Results
400 from these three loci show that, while the SATB1-bound peaks generated by urea ChIP and standard
401 ChIP-seq did not overlap, they were nonetheless proximal to each other, and both were SATB1
402 dependent. The two distinct ChIP-seq protocols are likely detecting two different modes of DNA binding
403 for SATB1 i.e., direct binding to BURs and indirect binding to open chromatin regions.
404

405 **Long-distance chromatin interactions involving a BUR depend on SATB1**

406 We next explored whether there is any three-dimensional relationship between SATB1-bound
407 BURs detected by urea-ChIP-seq and SATB1-bound sites in the open chromatin region detected by
408 standard ChIP-seq. We hypothesized that chromatin architecture formed by direct binding of SATB1 to
409 BURs may recruit open chromatin regions by indirect association with their chromatin-bound protein
410 complexes by SATB1. If so, such interactions would necessarily be dependent on SATB1, and they
411 might be correlated to gene expression. To address these questions, we studied a gene-rich region in
412 chromosome 2 that contains the *Rag1* and *Rag2* genes whose expression is SATB1 dependent (*45*).
413 We first examined genome-wide interactions from a SATB1-bound BUR that appeared as a single,
414 strong peak (*Figure 4, top track2, and 5, top)* as the viewpoint or bait (BUR-1). The BUR-1 primer
415 sequence is located near the border between the 3.9 Mb gene-desert region and the 5.8Mb gene rich
416 region on chromosome 2 where the major BUR bound to SATB1 is located. BUR-1 resides in the latter
417 accessible chromatin region and 1.4 kb away from the ASE (*Figure 4, top, track2*), which is essential
418 for proper *Rag1* and *Rag2* expression in double-positive thymocytes and for differentiation of single-
419 positive thymocytes (*76*).

420 To study interactions from the SATB1-bound BUR, we performed 4C-seq using urea purified
421 chromatin (urea 4C-seq, one-to-all) to better access and capture BUR-mediated interactions, which are

422 expected to emanate from the SATB1 subnuclear architectural structure. In our urea 4C-seq, we used
423 *Hind*III for initial digestion. The 6-base cutter, *Hind*III, was used instead of a 4-base cutter like *Dpn*II
424 (frequently used for 4C-seq), because multiple *Dpn*II sites are often found within individual SATB1-
425 bound BURs, thus producing small fragments, likely disrupting SATB1-binding to BURs. The "BUR-1"
426 bait region at a SATB1-bound BUR is designed at the end of the *Hind*III fragment, which is adjacent to
427 the *Hind*III fragment containing ASE. We examined interaction events from the fragment containing
428 BUR-1 and its interaction sites were mapped on the genome for visualization.

429 While urea purification removes indirectly associated protein and thus may reduce some
430 chromatin interactions, we speculated that the overall 3D chromatin structure of fixed chromatin will still
431 retain its proximity events, especially in the environment of chromatin which is strongly anchored to the
432 subnuclear structure (as we predicted for SATB1 scaffold anchoring at BURs) to enable detection in
433 urea 4C-seq. In the ChIP-seq protocol (in general), we expect that in the absence of a ligation step as
434 is routinely done in 4C protocols (as described below), subsequent steps for ChIP-seq (sonication,
435 stringent washes of immunoprecipitated fragments, etc) results in dissociation of interacting fragments.
436 We carried out urea 4C-seq experiments to test if we could indeed detect such strong SATB1-mediated
437 3D interactions. Briefly, for urea 4C-seq (outlined in *Figure 5—figure supplement 1*), crosslinked
438 chromatin purified by urea ultracentrifugation is first digested with a restriction enzyme (*Hind*III).
439 Digestion is followed by ligation of chromatin fragments whose physically proximity status in 3D space
440 was fixed at the time of formaldehyde crosslinking. After these steps, DNA was purified. Beyond this
441 point urea-4C-seq differs from the commonly used 4C-seq called circular chromosome conformation
442 capture (referred to here as circular 4C-seq)(*77-82*). In circular 4C-seq, ligated DNA fragments are
443 circularized after second restriction enzyme digestion before PCR amplification. In contrast, in urea 4C-
444 seq a single strand DNA capture strategy was used to isolate a specific pool of single strand DNA, each
445 containing a ligation-captured DNA fragment surrounded by the bait fragment and the DNA linker (see
446 details in *Figure 5—figure supplement 1* legend and Materials and Methods). The captured DNA
447 sequences in the single strand DNA were PCR amplified using a primer from the bait sequence and
448 another primer from the DNA linker, thus avoiding amplification of any non-specific DNA fragments.
449 This was confirmed by the lack of PCR products using either primer alone (data not shown). This critical
450 step results in highly specific signals with very low background signals. The high signal-to-noise ratio in
451 urea 4C-seq contrasts with uniform and strong genome-wide background signals typically seen with
452 circular 4C-seq, which are thought to reflect random chromatin interaction events. Some non-interacting
453 sequences could also be trapped at the circulization step, and even if such incidence is rare, would
454 result in background signals upon PCR amplification. Because the background signals for urea 4C-seq
455 are extremely low in contrast to circular 4C-seq, the visual appearances of the interacting profiles from
456 the two methods are greatly different. Nevertheless, urea 4C-seq detects large-scale interactions
457 involving BURs that are strictly dependent on SATB1 as described below.

458 In wild-type thymocytes, we detected BUR-1 making extensive long-distance interactions
459 covering most of the ~5.8Mb adjacent gene-rich region (*Figure 5A*). Interestingly, BUR-1 interactions
460 are found to be scarce over the gene-desert region upstream of BUR-1, despite the presence of many
461 SATB1-bound BURs in this region (*Figure 5A, top track for urea SATB1 ChIP-seq, Figure 5—figure*
462 *supplement 2*). Though 4C-seq can detect both up- and downstream interactions from a chosen single
463 bait site, we observed heavily direction-biased interactions of BUR-1 with the gene-rich region, perhaps
464 indicative of its involvement in gene regulation. BUR-1 interactions were found particularly concentrated
465 over the ~3 megabase (Mb) gene-rich region, containing SATB1-dependent *Rag1* and *Rag2* genes.
466 These dense and strong interaction signals must not be due to their spatial proximity from the bait
467 because similar dense interactions were not detected with the SATB1-KO cells. In fact, most of the
468 BUR-1 interactions were absent in SATB1-KO cells (*Figure 5A, track KO-BUR1*), indicating that SATB1
469 is required for the numerous long-distance interactions over the gene-rich region. We also validated
470 these interactions using a second bait (BUR-2) as an experimental control as BUR-1 interacts with the
471 *Hind*III fragment containing BUR-2, located in the second intron of *B230118H07Rik* gene (see *Figure*
472 *5B* for specific location). This fragment contains two strong BUR peaks. Although weakly, SATB1 binds
473 to one of these BURs. Hence, urea 4C-seq using BUR-2 serves as a reciprocal experiment of BUR-1
474 to validate reproducibility of the BUR-1 interaction profile. By comparing with the Hi-C heatmap in this
475 5.8Mb region we found that BUR-1 interactions traverse multiple TADs and are not constrained by any
476 specific TADs (*Figure 5—figure supplement 2*), further supporting the CTCF independent nature of
477 these SATB1-mediated interactions. Within this gene rich region, numerous interactions from BUR-1
478 were detected within DNase 1 HS containing enhancers marked by H3K27ac and H3Kme1
479 modifications. Therefore, dense chromatin looping events involving these SATB1-bound BURs indicate
480 a highly interactive chromatin architecture for the gene-rich region, bringing together many gene
481 regulatory sequences into proximity. We further examined a wider region covering >44Mb that includes
482 distal neighboring gene-rich regions *(Figure 5 and Figure 5—figure supplement 3A and 3B).* Although
483 interaction frequencies were lower than that within the first ~5.8Mb gene-rich region, we detected BUR-
484 1 interactions with further distal gene-rich region coinciding with enhancer-rich DNase 1 HS regions,
485 where clusters of SATB1 binding sites were detected by standard ChIP-seq, skipping over gene-poor
486 regions and a gene-rich region containing transcriptionally silent olfactory receptor genes.
487 A zoomed-in view (chr2:101,308,846-101,599,827; 291Kb) of BUR-1 interactions confirmed a
488 marked difference in BUR-1 interactions (~200Kb) over the *Rag1* and *Rag 2* loci between wild-type and
489 *Satb1*$^{-/-}$thymocytes, confirming BUR-1 interactions require SATB1 (*Figure 5B*). In addition to many BUR-
490 1 interacting chromatin fragments close to or containing enhancers (marked by H3K27ac and H3Kme1),
491 some of these fragments contain additional BUR sites, including BUR-2 adjacent to enhancer(s) *(Figure*
492 *5B,* gray shaded with red stars*).* BUR-2 interacted heavily over the *Rag1* and *Rag2* loci in wild-type
493 thymocytes and well reproduced the interactions observed with BUR-1, consistent with the larger region
494 (*Figure 5A*), suggesting that both BUR-1 and BUR-2 are part of the common interaction network that

495 requires SATB1. Concerning the correlation of chromatin interactions and gene expression, among 43
496 genes identified with official gene symbols mapped in the 5.8Mb gene rich region, 8 genes display
497 various levels of SATB1-dependent expression ($p<0.05$) (*54*). These genes were either up or
498 downregulated upon SATB1 deletion in thymocytes based on RNA-seq data (*Figure 5-figure*
499 *supplement 4*), and *Rag1* and *Rag2* were most strongly downregulated by SATB1 depletion in this
500 region. Collectively, these data suggest a strong correlation between SATB1-dependent gene
501 expression and extensive looping events over long distance linking SATB1-bound BURs and regulatory
502 regions in the open chromatin regions. Therefore, SATB1 function on chromatin is not limited to merely
503 connecting a specific target gene locus with nearby enhancers and promoters within TADs. Instead,
504 SATB1 appears to form a large interaction network covering the entire gene-rich regions.
505
506 **SATB1 binds BURs in a cell-type dependent manner**
507 We next examined whether SATB1 binds different subsets of BURs depending on cell type, by studying
508 SATB1-binding profiles in three different types of mouse tissues– thymus, frontal cortex and skin – that
509 contain SATB1-expressing cells. SATB1 expression is primarily restricted to adult progenitor cells, such
510 as thymocytes and in basal layer of epidermis. SATB1 is also expressed in differentiated neurons in
511 specific brain subregions (e.g. frontal cortex and amygdala). We compared UCSC browser images of
512 two selected regions, a ~2.4 Mb region in chromosome 6 containing the *Cd4* locus expressed in
513 thymocytes (*Figure 6A*) and a 406kb region in chromosome 5 containing *Gabra2* and *Gabrg1* loci
514 expressed in the mammalian brain (*Figure 6B*). BURs were most frequently bound by SATB1 in brain
515 compared to thymocytes, and the least frequently bound in skin. Whereas SATB1-bound BURs show
516 cell-type dependency, CTCF binding sites that largely coincide with DNase1 HS were largely similar
517 between these three types of cells (*Figure 6A*).
518 We analyzed whether BURs are targeted by SATB1 depending on cell type. Consistent with the
519 cell-type specific function of SATB1, we observed cell-type dependent differences in BUR occupancy
520 by SATB1. For all three types of cells, high percentages of urea ChIP-seq peaks (close to 80%,
521 *supplementary Table 1*) correspond to BURs, as revealed by peak intersection studies using deepTools
522 (*83*) and comparing to the BUR reference map (*Figure 6C*, *supplementary Table 1*). Despite similar total
523 aligned sequence reads in urea ChIP-seq, the number of SATB1-bound BUR peaks greatly differed
524 between cell types (*supplementary Table 2*). Among 238,380 mapped BURs ($q<0.01$), the percentage
525 of SATB1-bound BURs in skin, thymocytes, and brain were 3.7%, 13.5% and 35.0% (based on average
526 of two replicas/cell type), respectively (*Figure 6D and supplementary Table 1*). These results indicate
527 that frequency of BURs targeted by SATB1 *in vivo* can vary more than 10-fold depending on cell type.
528 Interestingly, while the number of BURs bound by SATB1 greatly differs between cell types, the majority
529 (83.9%) of BURs targeted by SATB1 in skin were bound to SATB1 in thymocytes, and nearly all (91.6%)
530 SATB1-bound BURs in thymocytes were bound to SATB1 in brain. Therefore, each cell type has an
531 overlapping set of SATB1-bound BURs in common, with increasing/decreasing numbers of sites

532 depending on cell type, rather than distinct subsets. Despite the highest BUR occupancy by SATB1
533 was observed in the brain, this is not due to the brain expressing the highest levels of SATB1 protein.
534 In fact, the thymus expresses by far the highest levels of SATB1, which comprises ~0.3% of the total
535 protein (*84*).
536
537 **BURs are enriched in LADs**
538
539 LADs are large mostly heterochromatic domains in close contact with the nuclear lamina and are known
540 to be enriched in AT-rich sequences (*85*). Although AT-rich sequences are not necessarily BURs, BURs
541 have a minimum of 65% AT content (many of them have a higher AT content) with the ATC sequence
542 context with an exceptionally strong unwinding propensity (*41*). We therefore asked whether and to
543 what extent any of the ~240,000 BURs identified in the genome could be found within LADs. We first
544 visually compared the distribution of all potential BURs with LADs mapped by DamID (*86-88*) and noted
545 some correlation of BURs and LADs. As an example, the 9 Mb region in chromosome 5 containing the
546 neuronal gene cluster locus that encodes subunits of $GABA_A$ receptor complex (*Gabrg1,* and *Gabra1,*
547 *Gaba6, Gabrb2)* has a BUR-enriched region overlapping with LADs obtained from thymocytes (*Figure*
548 *7A*). We checked if this LAD-BUR overlap is not restricted to this specific region by examining a larger
549 view of a randomly chosen region covering 47.4 Mb in chromosome 3 (*Figure 7—figure supplement 1*).
550 In this region CTCF-binding sites, DNase1 HS, and standard SATB1 ChIP-seq peaks all converge in
551 the gene-rich inter-LAD regions, whereas distribution of LADs and BURs largely overlap, and these
552 regions are enriched in SATB1 urea ChIP-seq peaks.
553 We then examined the relationship between BUR and LAD distribution at the genome-wide
554 scale. We compared the genomic proximity to lamin B1 (as measured by Dam), SATB1-bound genomic
555 sites (from standard ChIP-seq), SATB1-bound BURs (from urea ChIP-seq) over LADs and flanking
556 regions (+/- 10% outside of the LADs). We found that the genome-wide distribution of LADs coincides
557 with the majority of SATB1-bound BURs, but it is mutually exclusive with SATB1-bound genomic sites
558 that are mapped by standard ChIP-seq, which avoid LADs (*Figure 7B*). In agreement with the result
559 shown in *Figure2A*, CTCF-bound sites mapped by urea-ChIP-seq coincide with those mapped by
560 standard ChIP-seq and are found at LAD borders and inter-LAD regions (*Figure 7C*), as previously
561 described (*9*). Collectively, these analyses confirmed that the majority of potential BURs from the BUR
562 reference map as well as directly SATB1-bound BURs overlap with LADs (Figure 7B and C), whereas
563 CTCF-binding sites avoid LAD-BUR regions and are confined to inter-LADs and LAD boundaries
564 (*Figure 7C*). We conclude that, at the genome-wide scale, the majority of BURs overlap with LADs,
565 suggesting that BURs represent as an important sequence component of LADs, some of which are
566 specifically targeted by SATB1. This agrees with earlier findings that LADs are enriched in AT
567 sequences as many BURs are AT-rich (>65% AT) and further identifies LADs as specifically enriched
568 in BURs.

569 Within larger LAD domains identified, there are smaller regions (<10kb) that display localized
570 looping away from the lamina (*89-91*). These DiPS (Depleted in Peripheral Signal) display all the
571 hallmarks of poised or active promoters or enhancers and are flanked by CTCF and cohesin. Thus,
572 these small regions embedded in larger LADs, are akin to small inter-LADs that are constrained at the
573 lamina due to their short lengths. We next asked if SATB1 binds BURs in these active regions within
574 LAD (DiPS). We examined the distribution of average signals of SATB1-bound BURs relative to
575 enhancers in DiPS marked by H3K4me1 and H3K27ac modifications over a +/- 3kb window centered
576 at H3K4me1 peaks. The peaks of enhancer histone marks (H3K27ac and H3K4me1) corresponded to
577 minimum occupancies of SATB1 in DiPS and also excluded BURs, indicating that enhancers are largely
578 excluded from BURs and SATB1-directly bound BURs in DiPS (*Figure 7D*).
579 We also examined SATB1-bound BURs outside LADs (inter-LADs) as well. Although less-
580 densely distributed compared to LADs, SATB1-bound BURs are detected in inter-LAD regions enriched
581 in actively transcribed genes. As an example, we show SATB1-bound BUR distribution in representative
582 inter-LADs containing *Rag1/Rag2* (this region was used for 4C analyses above) as well as other two
583 other SATB1-regulated loci*: Foxp3,* and *Runx3* relative to nearby LADs (*Figure 7—figure supplement*
584 *2*). Genome-wide analyses showed that in inter-LAD regions, SATB1-bound BURs are generally
585 excluding the peaks of enhancers marked by H3K4me1 and H3K27ac (Figure 7E). Although the
586 positions are not precisely coincident, ~10% of SATB1-bound BURs in inter-LADs are located close
587 (within +/- 5kb) to the peaks of H3K4me1 or H3K27ac. We viewed relative occupancies of BURs and
588 SATB1-bound sites in LADs and inter-LADs by heatmap *(Figure 7—figure supplement 3)*. Consistent
589 with the results described above, SATB1 occupancy is restricted to BUR sites, a fraction of BURs is
590 targeted by SATB1 in both inter-LADs and LADs (the former being a much fewer number of BURs).
591 Also, for both LADs and inter-LADs, most of the SATB1-bound regions coincide with BURs. We also
592 examined the distribution of urea4C-detected BUR-1 or BUR-2 interactions relative to LADs. These
593 SATB1-mediated interactions were found to be well constrained within inter-LADs enriched in histone
594 marks for enhancers *(Figure 7—figure supplement 4).* This remains the case even for sites with much
595 longer interactions, as these sites are located in accessible regions between LADs, confirmed by
596 viewing individual sites at high resolution. These results demonstrate that the inter-LAD BURs (BUR-1
597 and BUR-2), bound to SATB1 are contacting accessible chromatin at numerous locations over long
598 distances.
599

600 # Discussion

601 Here we used a systematic approach to compare and interrogate the chromatin binding profiles of a
602 genome organizing protein SATB1 detected by two alternative ChIP-seq approaches. Critically, by
603 establishing a urea purification-based ChIP-seq method that enriches for direct DNA-binding events,
604 we found that SATB1 directly binds BURs genome-wide. This is in stark contrast to previously identified

605 SATB1 binding to enhancers and promoters in open chromatin by standard ChIP-seq. Nevertheless,
606 the two contrasting DNA-binding profiles for SATB1 are both valid, requiring SATB1 for the ChIP-seq
607 peaks. These differing SATB1-binding profiles suggest that SATB1 is engaged in chromatin
608 organization through both direct binding to BURs, anchoring them to the subnuclear SATB1 protein
609 meshwork, as well as by indirect binding to the accessible (active) chromatin region, enriched in genes
610 and regulatory regions. We show that SATB1 is required for megabase-level interactions, connecting
611 select BURs to "open" chromatin, and that such interactions are linked with cell-type specific gene
612 expression regulated by SATB1 in thymocytes.

613 Using urea ChIP-seq, which stringently purifies chromatin, we identified a new type of chromatin
614 organization formed by direct binding of SATB1 with BURs, genomic elements distributed across the
615 mouse genome. While this SATB1-mediated chromatin organization contrasts with previous data from
616 standard ChIP-seq or CUT&Tag assays, which indicate SATB1 mainly interacts with enhancers and
617 promoters located within the "open chromatin" regions, our data agree with even earlier *in vitro* findings
618 that SATB1 binds to AT-rich BURs. Thus, standard ChIP-seq (or Cut&Tag) and urea ChIP-seq enrich
619 different and almost mutually exclusive SATB1 profiles, suggesting that these approaches are
620 interrogating the genome in different ways. It is important to note that while urea ChIP-seq and standard
621 ChIP-seq for SATB1 showed very different profiles, the binding profiles of CTCF and other proteins did
622 not differ between the two methods. This is consistent with SATB1 interacting with chromatin in a unique
623 way by forming a subnuclear proteinaceous network anchoring a subset of BURs (*39*).

624 **Differences between standard and urea ChIP-seq**

625 In order to understand why chromatin binding proteins might show different binding modalities in urea
626 ChIP-seq versus more standard approaches, it is important to understand the differences in the
627 protocols. Standard ChIP-seq protocols use crosslinked whole cells or nuclei without purification of
628 crosslinked chromatin, and immunoprecipitation is typically performed with the 'cleared' suspension
629 after extracts of sonicated crosslinked chromatin are centrifuged, thus removing most of the insoluble
630 material. Even if this fraction is not cleared in this way, the insoluble material does not perform well in
631 immunoprecipitation assays (*61*). Previous studies have identified SATB1 as a salt-extraction resistant
632 (nuclear matrix) protein (*39, 40*). Thus, using canonical ChIP-seq approaches, SATB1-directly bound
633 BURs in the inaccessible nuclear substructure would necessarily be lost in the insoluble fraction.
634 Conversely any SATB1-associated genomic regions in open chromatin regions (direct or indirect),
635 would become the predominantly captured fraction that is amplified during PCR-based library
636 preparations. Thus, SATB1 directly bound to BURs in the high-salt extraction resistant nuclear
637 substructure is likely missed by standard ChIP-seq (*53, 54*) and by CUT&Tag (*55*), which is also known
638 to preferentially detect protein interactions in open chromatin regions. In contrast, in urea ChIP-seq,
639 whole, intact crosslinked chromatin is purified through urea ultracentrifugation, first removing all
640 indirectly bound proteins from chromatin. Subsequently, the entire urea-purified crosslinked chromatin
641 is quantitatively solubilized. The two main advantages of urea ChIP-seq are that (1) only direct-binding

642 profiles will be obtained for a protein of interest, and (2) chromatin tightly associated with nuclear
643 substructures, which are typically discarded in the insoluble fractions in standard ChIP-seq, are retained
644 as whole intact crosslinked genomic DNA in urea ChIP-seq. Therefore, all direct DNA binding profiles
645 can be obtained, regardless of the original chromatin state (i.e. no bias toward open chromatin). Thus,
646 urea ChIP-seq is uniquely suited to detect direct binding sites of SATB1 as well as other BUR-binding
647 proteins genome wide. For non-BUR-binding proteins (e.g. CTCF and PRC2 core subunits), urea ChIP-
648 seq generates identical DNA binding profiles as standard ChIP-seq. Although we detected some
649 "phantom" or false-positive peaks using SATB1-KO cells by standard ChIP-seq (Table 3 and 4), under
650 our experimental conditions, we confirmed that the majority of SATB1-binding peaks are SATB1-
651 dependent. Importantly, these SATB1 peaks from standard ChIP-seq were essentially undetected by
652 urea ChIP-seq, suggesting that SATB1 indirectly binds to these sites presumably by associating with
653 nuclear proteins bound to their target sites in "open" chromatin. SATB1 is equipped with domains
654 responsible for specific binding to BURs (*92-95*) as well as for associating with or recruiting chromatin
655 binding proteins to specific genomic sites (e.g. CHRAC and ACF1 nucleosome mobilizing complex
656 subunits, Brg1, p300, Hdac1, Gata3, Stat6, c-Maf, Pit1, and β-catenin) (*39, 42, 44, 50, 96-100*).
657 Therefore, we anticipate that SATB1 binds indirectly and dynamically to regulatory regions in open
658 chromatin by associating with many chromatin-modifying and transcription factors to form protein
659 complexes to support tissue-specific gene expression. Despite the contrasting SATB1-binding profiles
660 obtained from standard ChIP-seq and urea ChIP-seq, generation of the peaks from both methods
661 require SATB1. Therefore, SATB1-mediated chromatin organization appears to have two components:
662 one involves direct binding to BURs, while the other involves indirect binding to other chromatin-
663 interacting proteins at genomic sites in accessible chromatin.

664 **Two-tiered chromatin organization mediated by SATB1**

665 Considering that the two contrasting SATB1-binding profiles require SATB1, an important
666 question emerges as to whether there is a functional or structural link between the two SATB1-bound
667 chromatin regions. We conceive that SATB1 might have a role in bringing together chromatin structure
668 formed by BURs tightly bound to nuclear substructure and a highly accessible "open" chromatin
669 enriched in transcription related proteins. Our urea 4C-seq results suggest that these two regions are
670 connected via SATB1-mediated interactions involving BURs. The ligation step in urea 4C-seq enabled
671 us to capture chromatin sites that were in close spatial proximity to the bait site (e.g. a BUR) at the time
672 of crosslinking. Apparently, 3D structures fixed by formaldehyde retained sufficient chromatin proximity
673 after urea purification to enable capture of BUR-interacting fragments. The urea 4C-seq revealed that
674 a SATB1-bound BUR site (BUR-1 as a bait), located at the border of a gene desert and a gene-rich
675 region containing SATB1-regulated genes (*Rag 1* and *Rag2*), interacts extensively over a 5.8Mb gene-
676 rich region with many gene loci, such as enhancers, promoters, BURs, and intergenic regions. Such

677 ultra-long-distance interactions from BUR-1 predominantly cover the entire 5.8Mb gene-rich region,
678 mostly avoiding the gene desert region. Such interactions were confirmed with another bait (BUR-2).
679 The SATB1-mediated chromatin interactions from BUR-1 and BUR-2 (validation control) as
680 baits, covering the 5.8Mb *Rag1/Rag2*-containing gene-rich region, are tightly linked to SATB1-
681 dependent expression of eight genes including *Rag1* and *Rag2* (P<0.05) out of 43 genes in this region
682 in thymocytes. BUR-1 further interacts with far distal gene-rich regions *in cis* in chromosome 2 (>44Mb),
683 skipping interstitial gene desert regions in a SATB1-dependent manner, albeit through weaker
684 interactions (*Figure 5—figure supplement 3*). These chromatin interactions are at a much greater scale
685 than those previously observed, such as T helper 2 cell activation induced dense chromatin looping in
686 the 200kb cytokine gene cluster, including several BURs and regulatory regions, tightly linked to
687 activation of the cytokine genes (*42*) and interactions at the subTAD levels (or <~500Kb) between
688 specific enhancers or enhancers to promoters in thymocytes (*53-55*). Combining results from SATB1-
689 binding profiles derived from urea ChIP-seq and standard ChIP-seq as well as urea 4C-seq, a model is
690 illustrated how the two chromatin regions might interact depending on SATB1 (*Figure 8*). In this model,
691 the stable SATB1 binding to BURs in the SATB1-rich nuclear substructure forms a foundational
692 chromatin scaffold and SATB1 tethers highly accessible "open" chromatin regions to this scaffold by
693 binding to regulatory protein complexes—the SATB1 proteinaceous matrix would serve as a scaffold
694 and interface. We anticipate that the latter interactions to be dynamic and form the highly interacting
695 chromatin architecture over gene-rich accessible chromatin regions, bringing regulatory sequences in
696 close vicinities. Both components of SATB1-mediated chromatin organization likely underlie regulation
697 of gene expression. This two-tier model of SATB1 chromatin organization is highly reminiscent of
698 previously published results on SATB1's role in transcription factor Pit1-regulated gene expression in
699 pituitary glands (*44*). SATB1 associates with Pit1 and β-catenin, and SATB1 is required for tethering
700 Pit1-bound enhancers to the subnuclear architectural structure that is resistant to salt extraction (note:
701 it is referred to as matrin-3 rich network, as matrin-3 is enriched in such substructure as well). A naturally
702 occurring mutation of human PIT1 (R271W) that causes combined pituitary hormone deficiency fails to
703 associate with SATB1 and β-catenin. Further studies with mutated R271WPit1 revealed that the
704 tethering of Pit1-bound enhancers to the insoluble nuclear substructure is essential for effective
705 activation of the Pit1-regulated transcriptional program.
706 Additional research will deepen our understanding of how SATB1 regulates cell-type specific
707 gene expression. The Wnt signaling pathway plays pivotal roles in carcinogenesis and development
708 (*101, 102*) and it will be important to investigate the role and nature of SATB1's involvement in this
709 pathway. Beta-catenin is the key component of the canonical Wnt signaling pathway; upon nuclear
710 translocation, it associates with the TCF/LEF family of transcription factors to activate target genes.
711 Because SATB1 also associates with beta-catenin, it is expected that SATB1 may influence target gene
712 expression, similar to its effects on Pit1's target genes. In addition, non-coding RNAs may have an
713 important role in SATB1 chromatin organization and gene expression. Especially, specific long non-

714 coding RNAs (lncRNAs) that remain associated with crosslinked chromatin after urea purification may
715 deserve attention (unpublished results). Most non-coding RNA is associated with RNA-binding proteins
716 (RBP) to form the ribonucleoprotein network which provides RNA structural scaffolds for the 3D
717 chromatin organization and function (*103-106*). The SATB1 subnuclear architecture has a prominent
718 cage-like distribution in thymocytes while neurons have a spider-web like distribution. It would be of
719 interest to address whether RNA, including lncRNAs, plays a role in the SATB1-rich subnuclear
720 proteinaceous scaffold formation depending on cell type and directing SATB1 to target specific sets of
721 BURs in a cell function-specific manner.

722 **Lack of overlapping function for SATB1 and CTCF**

723 Results obtained using urea-purified crosslinked chromatin show no relationship between CTCF and
724 SATB1. Several pieces of evidence support this conclusion. First, genome-wide CTCF-binding profiles
725 and Hi-C profiles remained largely unaltered by SATB1 deletion in thymocyte (*Figure 3*), a finding
726 supported by other studies (*53, 54*). Second, by urea ChIP-seq, SATB1:BUR binding sites precisely
727 exclude CTCF-binding sites, which contrasts with recent findings that SATB1 and CTCF-binding profiles
728 overlap by standard ChIP-seq(*54, 55*) or by CUT&Tag (*55*).Third, chromatin interactions (>5.7Mb) from
729 a SATB1-bound BUR are not constrained to individual TADs but span multiple TADs. Fourth, by urea
730 ChIP-Western, SATB1 does not interact with CTCF or cohesin on chromatin. Fifth, CTCF does not bind
731 to BURs. Therefore, chromatin organization mediated by SATB1 through direct binding to BURs is
732 distinct from that mediated by CTCF and cohesion.

733 **Potential biological significance of BURs mostly enriched in LADs**

734 We identify BURs as genomic elements enriched in LADs which are large chromatin domains located
735 proximal to the nuclear lamina. LADs and LAD borders have critical roles in gene regulation (e.g. the
736 *Tcrb* locus) (*2, 86*). Except for being generally AT-rich, genomic features of LADs have thus far been
737 poorly characterized. BURs are not simply any AT-rich sequence, but rather, are characterized by a
738 specific ATC sequence context. BURs are important genomic elements that are specifically targeted
739 by SATB1 which has a role in cell-type specific gene expression (*41*). Thus, discovering BUR
740 enrichment in LADs uncovers mechanistic insights into the biological function of LADs in gene
741 regulation. Although LADs form heterochromatin proximal to the nuclear envelope, LAD organization is
742 dynamic. While LADs are certainly constrained to the nuclear lamina, regions within LADs extend well
743 into the nuclear interior and display dynamic interactions with the lamin proteins. In addition, LADs are
744 dynamic during differentiation or other cell-state changes. For instance, during differentiation of mouse
745 cells, hundreds of genes display dynamic intranuclear spatial repositioning relative to the nuclear lamina
746 (*107*). Some LAD regions dynamically contact the nuclear lamina, and gene movement in and out of
747 the nuclear periphery in a circadian rhythm has been reported (*108*). Recently, relocation of the
748 *hunchback* gene in *Drosophila* neuroblasts to nuclear lamina has been shown to require polycomb
749 proteins binding to a specific intronic element of the gene locus. This process is important for heritable

750 gene silencing to regulate neuroblast competence (*109*). The organization of genomic DNA at the
751 lamina has been linked to both inactive chromatin state and the nuclear lamins, along with other nuclear
752 membrane proteins (*2, 110-115*). While chromatin state is likely important for both positioning at and
753 de-localization from the lamina, little information is available concerning *in vivo* mechanisms specifying
754 which regions within LADs could be targeted for de-localization and subsequent cell-type specific gene
755 activation. The SATB subnuclear architecture is found mostly in the nuclear interior of thymocytes where
756 many individually cloned BURs have been detected by DNA-FISH. Among such interiorly localized
757 BURs, a BUR 5' of *Myc* was confirmed to co-localize with SATB1 by immunoDNA-FISH in thymocytes
758 (*39, 40*). A closer look at immunostaining profiles of SATB1 distribution in thymocyte nuclei, however,
759 shows that a small reproducible fraction of SATB1 resides in the peripheral zone of nuclei and in some
760 cells the tip of the SATB1 network extends to and touches this region of the nucleus (*39*).

761 Future studies are needed to investigate the spatial context of a subset of BURs and LADs in
762 relation to SATB1 subnuclear architecture, depending on the cell type. For instance, many SATB1-
763 bound BURs are identified in the *Gabrg1* and *Gabra2* loci in neurons, but not in thymocytes (Fig. 6B),
764 even though thymocytes express SATB1 at high levels. Therefore, studies on nuclear positioning of
765 select BURs in neurons, thymocytes, and in non-SATB1-expressing cells would provide valuable
766 insights. In addition to LADs, transcriptionally active gene-rich regions outside LADs also contain BURs,
767 albeit at a considerably lower density compared to LADs (e.g. Rag1/Rag2, Foxp3, Runx3 loci). Some
768 of these BURs located near enhancers are bound by SATB1. It is of interest that the number of BURs
769 targeted by SATB1 greatly varies depending on cell type, where neurons have by far the greatest
770 number of BURs captured by SATB1. This may reflect the level of plasticity for gene transcription or
771 number of genes that must be dynamically regulated in each cell type in which SATB1 is expressed.
772 There is growing evidence supporting the critical roles of chromatin topology and nuclear architecture
773 in neuronal response to external stimuli to establish precise expression program associated with
774 cognition (*116*). In fact, SATB1 has roles in early postnatal cortical neuron development and neuronal
775 connectivity (*37, 117*). The exceptionally large number of BURs directly interacting with SATB1 in
776 cortical neurons may reflect specialized function of neurons that might require highly dynamic
777 transcriptional regulation to enable rapid response to a wide variety of environmental stimuli. How
778 SATB1 selects specific subsets of BURs and if and how SATB1's selection of BURs contributes to cell-
779 type specific gene expression are important topics for future research.

780 **A broader significance of BUR-binding proteins beyond SATB1**

781 Importantly, SATB1 is not the only BUR-binding protein, indicating the broader biological significance
782 of BURs as genomic elements. Although SATB1 confers by far the highest affinity to BURs, several
783 other nuclear factors (e.g. nucleolin, HMGI/Y, PARP1, Ku70/86 heterodimer) have also been verified to
784 directly and specifically bind BURs *in vitro* (*84, 118, 119*). Recently, we identified Tip5/Baz2a as an
785 additional strong BUR-direct binding protein from mouse embryonic stem cells (mESCs) that is essential
786 for pluripotency (submitted for publication). Similar to SATB1, this nuclear protein also binds specifically

787 to BURs in mESCs, and identification of BURs as its direct targets in mESCs requires urea ChIP-seq
788 as well. Despite the identical BUR binding specificity of SATB1 and this stem cell factor, these two
789 proteins confer entirely different functions in distinct cell types. Therefore, BURs may serve as core
790 genomic marks that can be selectively targeted by distinct BUR-binding proteins to form unique 3D
791 chromatin regulatory network depending on the BUR-binding protein for specific cell functions. BURs
792 in the mammalian genome may have similarities in function with the "tethering elements" in *Drosophila*
793 (*120, 121*).These elements can be bound by regulators such as pioneering factors and polycomb
794 proteins and were shown promote interactions of regulatory regions up to ~250kb within TADs to
795 regulate transcription of genes. Most recently, meta-loops constituting a meta-domain spanning
796 numerous TADs in CNS of *Drosophila* were reported (*122, 123*). Although meta-loops are similar in size
797 with SATB1-mediated chromatin interactions, the CNS meta-loops have different features. They are
798 formed by transcription factors (e.g. CTCF and GAF), the half of them is anchored at the TAD borders,
799 and the metadomain boundaries are CTCF-bound. It appears that clusters of very long chromatin
800 looping events linked to gene expression may form by multiple mechanisms across species. Future
801 research on BUR-mediated genome organization regulated by distinct BUR-binding proteins will likely
802 provide more in-depth understanding about cell-type specific mechanisms driving 3D chromatin
803 architecture that contributes to major changes in gene expression and cell phenotypes.
804

805 # Materials and Methods

806

807 ## Experimental design
808

809 ### Primary cells

810 All animal studies were performed under Institutional Animal Care & Use Program at University of
811 California San Francisco for collecting brain and thymus and the Boston University for collecting skin.
812 Thymi were isolated from 2 weeks-old *Satb1*$^{+/+}$ and *Satb1*$^{-/-}$ mice, as well as from *Satb1*$^{+/+}$:*Cd4*-cre and
813 *Satb1* $^{F/F}$:*Cd4*-cre mice. Brain was isolated from 6-10 weeks-old *Satb1*$^{+/+}$ mice. Thymocytes were
814 prepared from thymi and cortex was excised from brain for this study. Skin was isolated from postnatal
815 day 0.5 of C57Bl/6 mice.
816

817 ### Antibodies

818 Antibodies used and for their purposes are the followings. CTCF for ChIP-seq: Active MOTIF (61311.
819 lot# 34614003), CTCF for Western: Abcam (ab129973) and Millipore (07-729; lot#-3429114), RAD21 for
820 ChIP-seq and Western: ABclonal (A18850, lot# 3521809001), SATB1 for ChIP-seq and Western: rabbit
821 polyclonal 1583 prepared by Kohwi-Shigematsu's laboratory and Abcam (ab109122, lot#GR137720-
822 13) and Histone H3 for Western: Abcam (ab1791, lotGR3236305-2).

823

824 **Urea-purified chromatin immunoprecipitation and urea ChIP-seq**

825 Thymocytes and single cell suspension prepared for cortex and skin were cross-linked with 1%
826 formaldehyde for 10 min at room temperature, followed by addition of glycine at 0.125 M for 5 min to
827 quench cross-linking reaction. These cells were washed with 1X PBS, suspended in 1% BSA-PBS and
828 cells were precipitated in a tube. These cells were re-suspended in lysis buffer (4% SDS, 50 mM Tris-
829 HCl [pH 8.0], 10 mM EDTA, 100 mM NaCl) with Protease inhibitor (Roche) and RNase inhibitor. The
830 resulting cell lysate was incubated for 30 min at room temperature and loaded on top of 8 M urea followed
831 by ultracentrifugation in a Beckman TL-100 Ultracentrifuge for 4-5 hrs at 45K rpm (181,000g, g=relative
832 centrifugation force or RCF; TLS55 rotor). Recovered chromatin pellet was sonicated to generate
833 fragment size ranging 300–1,000bp using Branson sonifier (20% power, 10 sec on and 30 sec off for 4-
834 6 cycles) in 300μl of sonication buffer [0.5% Na-laurylsarcosine, 0.1% deoxycholate (DOC), 1mM EDTA,
835 0.5mM EGTA, 10mM TrisHCl, 100mM NaCl] with Protease inhibitor and RNase inhibitor. Note: urea-
836 purified crosslinked chromatin is highly vulnerable to sonication, therefore, it needs to adjust the
837 sonication condition depending on cell type and/or the size of the precipitate DNA. The sonicated
838 chromatin with 1% Triton X-100 were dialyzed against dialysis buffer (10 mM Tris-HCl [pH 8.0], 100 mM
839 NaCl, 1 mM EDTA, 5% glycerol), and dialyzed for 16 hrs at 4°C (this dialysis is optional). The chromatin
840 sample was centrifuged at 15,000g for 5 min at 4°C to remove a trace amount of residual insoluble
841 components. The test-reverse cross-linking of chromatin aliquot (5-10μl of the final volume) was done at
842 65°C for 2-3 hrs in buffer containing 1% SDS, 100 mM NaCl, 1 mM EDTA, 10mMTris. Samples were
843 further treated by 100 μg/ml RNase A at 37°C for 1 hr, 200 μg/ml proteinase K at 60°C for more than 3
844 hrs, followed by DNA purification using QIAquick PCR purification kit (Qiagen), and shearing efficiency
845 was examined by Bioanalyzer 2100 (Agilent Technologies Inc.). For chromatin-immunoprecipitation, 1 μg
846 of an antibody of choice were added to 10 ~ 20 μg of sonicated solubilized chromatin in 350 μl in dilution
847 buffer (1% Triton X-100, 0.01% SDS, 1 mM EDTA, 15 mM Tris-HCl, 100 mM NaCl) and incubated
848 overnight with rotation at 4°C. At least three chromatin samples were prepared for ChIP-seq from
849 independent experiments to confirm the results. The chromatin fragments bound to antibodies (after
850 incubation overnight) were captured using 20 μl of protein-A, protein-G or protein AG Dynabeads
851 (Invitrogen; pre-washed with 0.1% BSA [Fraction V, Sigma), by 4 hrs incubation time at 4°C. Dynabeads
852 bound to chromatin fragments were washed twice with Binding buffer (10 mM Tris, pH8.0, 1 mM EDTA,
853 1 mM EGTA, 0.5% Triton X-100, 0.1% DOC, 100 mM NaCl), twice with LiCl buffer (100 mM Tris [pH 8.0],
854 1 mM EDTA, 250 mM LiCl, 0.5% NP-40, and 0.5% DOC). The tubes were changed and washed twice
855 with 0.1M NaCl-TE buffer. The immunoprecipitated samples were eluted from Dynabeads by elution
856 buffer (10 mM Tris-HCl [pH 8.0], 1 mM EDTA, 100 mM NaCl and 1% SDS) at 65ºC for 20 min. After
857 elution, ChIP DNAs was reverse-crosslinked at 65ºC for 6 hrs, followed by RNase-A treatment at 37°C
858 for 1 hr and proteinase K treatments for 3 hrs at 60°C. The recovered DNA was further purified with a
859 QIAquick PCR purification kit (Qiagen), with elution in 15μl of Qiagen Elution Buffer (alternatively, phenol-

860 chloroform extraction and ethanol precipitation). Briefly for library construction, ChIP DNA fragments were
861 end-repaired and ligated to indexed sequencing adapters (NEB or Rubicon kit) and amplified with 8-11
862 rounds of PCR, depending on the DNA amount. Using SPRI beads (Beckman coulter), small fragments
863 (<200bp) were removed from the amplified library. The size-selected library was sequenced to 50bp
864 single-end read lengths on an HiSeq4000 (Vincent J. Coates Genomic Sequencing Laboratory, UC
865 Berkeley).

866 **Standard ChIP-seq**

867 For standard ChIP-seq, the protocol described by Kitagawa et al was employed (*47*).

868

869 **Urea Chromatin immunoprecipitation (urea ChIP)-Western analysis**

870 Urea-purified chromatin prepared as described above (~10μg of chromatin-DNA) was
871 Immunoprecipitated with indicated antibody to produce urea ChIP samples, and the chromatin fragments
872 bound by the antibody was trapped by Protein-A beads. The antibody-bound chromatin fragment-trapped
873 beads were washed with binding buffer/washing buffer/NaCl-TE (total 6 times), and the chromatin
874 fragments were released and isolated from beads (65°C for 20 min) in 100 μl of 1% SDS, 10 mM Tris,
875 pH7.6, 1mM EDTA, 100mM NaCl solution. The isolated chromatin fragments were subjected to reverse-
876 crosslinking by incubation at 65°C for additional 6 hrs. The released proteins were dissolved in the
877 Laemmli buffer, boiled and subjected to Western blot assay. To compare multiple samples, we confirmed
878 that we used a similar amount of original urea-purified crosslinked chromatin before ChIP by subjecting
879 each chromatin sample to Western blot using anti-H3 antibody. The similar amount of urea-purified
880 crosslinked chromatin was then used for ChIP-Western studies.

881

882 **Urea 4C-seq**

883 Urea-purified crosslinked chromatin (described above for its preparation) was processed for urea-4C-
884 seq basically as described(*66*) with some modifications. For the current experiment, the purified
885 crosslinked chromatin (appears as a transparent pellet at the bottom of a centrifugation tube) after urea
886 centrifugation was briefly sonicated in 100μl of the *Hind*III digestion buffer with Branson sonifier (20%
887 power, 10 sec, once). Next, *Hind*III was added to digest chromatin (10-20 units/μg DNA) overnight at
888 37°C. *Hind*III was heat inactivated at 80°C for 20 min, ligation was performed in 1.0 ml with 1X ligation
889 buffer with ligase (600 units) at 16°C for overnight, followed by reverse-crosslinking at 65°C for
890 overnight. The DNA was then purified by phenol-chloroform extraction or by spin column (NucleoSpin,
891 Macherey-Nagel). The purified DNAs (1-4μg) was further digested with *Hae*III (100-125 units) overnight.
892 The *Hind*III-*Hae*III digested DNA fragments were treated with Klenow. The resulting blunt-end *Hind*III-
893 *Hae*III DNA fragments were ligated with our custom double-stranded (ds) Linker DNA with one strand-
894 Biotin modified,

895 Linker-top strand sequence with Biotin modified (marked by *):

896 5'-aattcggtacctctagaga**t***a**t***ccgatcgctcgag(XhoI)aagctt(*Hind*III)-3';

897 Linker-bottom strand sequence: 5'-aagcttctcgagcgatcggatatctctagaggtaccgaatt-3'
898 as described (*66*). The Linker-ligated dsDNA fragments were purified by spin column to remove free
899 Linker. The Linker-ligated dsDNA fragments were further digested with *Xho*I at the linker site (next site
900 from *Hind*III). Single stranded DNAs were isolated from the *Xho*I digested DNA fragments by coupling to
901 StreptAvidin Dynabeads (Invitrogen, Dynabeads M-280 streptavidin) followed by incubation in 40μl of
902 0.15M NaOH for 10 min at 25°C, followed by neutralization. Only single-stranded DNA, containing biotin
903 coupled with streptavidin, were retained on the Dynabeads, releasing the non-biotin modified single-
904 stranded DNA (single strand DNA capture) (*66*). The released non-biotin modified single strand DNAs
905 were amplified by PCR (AmpliTaq Gold system, Applied Biosystems); 10 cycles at 94C for 30", 55°C for
906 60" and 72°C for 60", followed by 15-20 cycles at 94°C for 30", 65°C for 60", 72°C for 60", using the
907 custom Illumina sequence-bait oligomers and Illumina sequence-linker oligomer for library preparations
908 as described below. The PCR amplified DNAs were purified by high and low size selection by beads
909 (SPRIselect, Beckman Coulter). The purified DNAs were analyzed by Bioanalyzer to confirm their
910 average size of ~300-500 bp with mostly uniform distribution, followed by the Illumina sequencing using
911 custom bait-specific sequence oligomers and Linker specific barcode oligomer. We used two bait
912 sequences: 5' gaagggggtaggaaagaaagctt 3' (BUR-1 bait: adjacent to a SATB1-bound BUR, located1.4
913 kb from ASE) and 5' cgactcattcctactgaagctt 3' (BUR-2-bait: enhancer located in the second intron of
914 B230118H07Rik close to a SATB1-bound BUR), both including a *Hind*III site.
915 The library was constructed by amplification using either Illumina sequence-BUR-1-bait or Illumina
916 sequence-BUR-2-bait primer with Illumina sequence-linker oligomer. (Capital letters represent Illumina
917 sequence, lower case letters represent bait sequences or the linker sequence)
918 Illumina sequence-BUR-1-bait oligomer:
919 5'-AATGATACGGCGACCACCGAGATCTACACTCTTTCCCTACACGAC-gaagggggtaggaaagaaagctt
920 Illumina sequence-BUR-2-bait oligomer:
921 5'-AATGATACGGCGACCACCGAGATCTACACTCTTTCCCTACACGAC-cgactcattcctactgaagctt
922 Illumina sequence-linker oligomer: 5'-CAAGCAGAAGACGGCATACGAGAT (barcode; e.g. CGTGAT)
923 GTGACTGGAGTTC-gcgatcggatatctctagaggtaccgaattc
924 To validate successful experiments, we confirmed that no PCR amplified product was generated by
925 using either the bait oligomer or linker oligomer alone.
926 For the library construction, Taq-Gold polymerase (NEB) was used for PCR by the following condition:
927 94°C for 5-10min (one cycle), 94C for 30 seconds, 55C for 30 seconds, 72C for 60 seconds (for 5-10
928 cycles), 94°C for 30 second, 65°C for 30 seconds, 72°C for 60 seconds (for 20 cycles), followed by 72°C
929 for 10 min. PCR products were purified by phenol-chloroform extraction twice, CHCl3 extraction once,
930 followed by EtOH precipitation (Optional; PCR purification by spin column, Qiagen).
931 The 4C libraries were sequenced by Illumina-HiSeq4000, using BUR-1-bait sequence and BUR-2-bait
932 sequence as custom sequence oligomers as follows:
933 BUR-1-bait sequence oligomer: 5'-CTTTCCCTACACGAC-gaagggggtaggaaagaaagctt

934 BUR-2-bait sequence oligomer: 5'-ACTCTTTCCCTACACGAC-cgactcattcctactgaagctt
935 Each library sequence was identified with Linker specific barcode oligomer;
936 5'-gaattcggtacctctagagatatccgatcgc-GAACTCCAGTCAC. (Capital letters represent Illumina sequence
937 and lower-case letters represent linker sequence). For sequencing, the above custom barcode
938 sequence oligomer was required instead of the common Illumina barcode sequencing oligomer.

939 **Hi-C**

940 Hi-C was performed as described (*17*). Primary thymocyte samples from *Satb1*$^{+/+}$:*Cd4*-cre and *Satb1*
941 $^{F/F}$:*Cd4*-cre mice were formaldehyde crosslinked at 2% at room temperature for 10 min. Two biological
942 replica per sample were prepared for Hi-C. Hi-C libraries was prepared using the Arima HiC^{+} kit (Arima
943 Genomics) exactly following the associated protocol. Paired-end sequencing was performed by Illumina
944 NovaSeq 6000.

945 ## Statistical analysis

946 **Significance of overlap of SATB1 with BURS**

947 We used the *bootRanges* function that is part of the *nullranges* bioconductor package (*71, 124*)
948 It was used to compute the significance of overlap of two sets of genomic regions (e.g., BUR versus
949 the called peaks for each of the ChIP-seq data sets). This method is based on subsampling genomic
950 regions of a given size from within genomic segments of the same stateHere the mouse genome mm9
951 was segmented into regions capturing 3 states based on density of known genes using the
952 segmentDensity function using the CBS method 4 (*125*) and assuming a segment length of 2Mb.
953 Regions represented blacklisted regions (queried using the terms "excluderanges" and "mm9") in the
954 AnnotationHub package were excluded from the analysis. For each comparison [reference regions
955 (known BUR peak calls) versus query regions (SATB1 Urea or Standard Chip-seq peak calls)], the
956 observed number of overlapping regions is first computed, 1000 sets of random query region peak calls
957 were sampled given the estimated genome segmentation using blocks of length 300kb, the overlaps
958 for each of these 1000 random query regions with the reference regions were then computed and finally,
959 the estimated p-value is based on the fraction of 1000 random overlaps greater than or equal to the
960 observed number of overlaps. These results were validated by evaluating the statistical enrichment of
961 SATB1 binding at BURs using the regioneR package (v1.30.0) in R (*126*), generating a P value of
962 0.000999, Z-score of 543.37, and a one-sided test confirmed greater than expected overlap. SATB1-
963 bound genomic regions (satb1_gr) and BURs (bur_gr) were represented as GRanges objects. To
964 determine whether SATB1 binding events occur more frequently at BURs than expected by chance, we
965 performed a permutation test using permTest with 1,000 iterations. SATB1 regions were randomly
966 shuffled across the mm9 mouse genome using randomizeRegions, while excluding masked regions
967 such as repeats and assembly gaps via the built-in soft masking available in the
968 BSgenome.Mmusculus.UCSC.mm9 reference. Enrichment was evaluated using numOverlaps to count

969 the number of overlapping SATB1–BUR events in each permutation. A one-sided test was used to
970 assess whether observed overlaps were significantly greater than the randomized distribution.
971 For genome-wide heatmaps we quantified SATB1 chromatin occupancy relative to mapped base
972 unpairing regions (BURs). BURs were provided in narrowPeak format, and the SATB1 ChIP-seq peaks
973 were obtained from a processed peak file containing signal intensity. Using the
974 normalizeToMatrixfunction from the EnrichedHeatmap package (v1.30.0)(*127*), we computed SATB1
975 signal intensity in 50 bp bins across a ±3 kb window centered on each BUR. BURs were either plotted
976 as a total genome-wide dataset or stratified into lamina-associated domains (LADs) and inter-LADs
977 (iLADs) based on overlap with DamID-defined LAD intervals using the LADetector script(*86, 88*).
978 Normalized signal matrices were used to generate heatmaps of SATB1 enrichment using
979 ComplexHeatmap, with LADs and inter-LADs plotted separately. Line plots above the heatmaps show
980 the average SATB1 signal across all BURs in each category. Color scaling was applied using
981 colorRamp2 from the circlize package (v0.4.15)(*128*). All visualizations were constructed using
982 ComplexHeatmap (v2.18.0), with rasterization enabled for performance.

983 To assess the alignment of BURs to SATB1-bound loci, we performed the inverse analysis by
984 quantifying BUR signal intensity around SATB1 binding peaks. SATB1 peaks were split into LAD- and
985 iLAD-associated groups using genomic overlap with LAD intervals. BURs were used as a quantitative
986 signal (score column from the narrowPeak file), and enrichment around each SATB1 site was computed
987 in 50 bp bins across a ±3 kb window using normalizeToMatrix function from the EnrichedHeatmap R
988 package (v1.30.0). The resulting matrices were visualized as heatmaps and line plots of average BUR
989 signal genome-wide or in each domain context (LAD vs iLAD). All visualizations were constructed using
990 ComplexHeatmap (v2.18.0).

991 **Hi-C data processing**

992 Hi-C datasets were analyzed using the HiC-bench platform (*129*). The application of this method is
993 described in detail(*130*). Briefly, data were aligned against the mouse reference genome (mm10) by
994 bowtie2 (version 2.3.1)(*131*) with mostly default parameters (specific settings: --very-sensitive-local --
995 local). For Hi-C, aligned reads were filtered by the GenomicTools(*132*) tools-hic filter command
996 integrated in HiC-bench. Interaction matrices for each chromosome separately were created by the
997 HiC-bench platform at a 10kb resolution. The Hi-C filtered contact matrices were normalized using
998 "iterative correction and eigenvector decomposition" (ICE) algorithm (*133*) build into HiC-bench. To
999 account for variances of read counts of more distant loci, distance normalization for each matrix was
1000 performed as recently described(*134*). TADs were called using the algorithm developed within HiC-
1001 bench(*129*) at 10kb bin resolution with the insulating window of 100kb. For visualization of Hi-C data, we
1002 generated HiC files using the Juicer(*135*).

1003 **Quality Control**

1004 The total numbers of reads per biological replicate for each genotype ranged from 200 to 230 million
1005 reads. The percentage of reads aligned was >98% in all samples. The percentage of accepted reads
1006 (ds-accepted-intra" and "ds-accepted-inter") was in the range of 50% to 55.5%. The absolute number
1007 of accepted intra-chromosomal read-pairs were ~90-100 million reads for each sample. We analyzed
1008 data from individual samples as well as combined data from two replicates (~200 million reads) for each
1009 genotype.

1010 Scaling plot was performed by aggregating the counts per 10kb distance bins. Values were cpm-
1011 normalized by dividing by the total number of valid intra-chromosomal pairs.

1012 **Compartments**

1013 Compartment analysis was performed using the Homer pipeline (v4.6)(*136*). Homer performs a principal
1014 component analysis of the normalized interaction matrices and uses the PCA1 component (cis-
1015 Eigenvector 1) to predict regions of transcriptionally active (A compartments) and transcriptionally
1016 inactive chromatin (B compartments). Homer works under the assumption that gene-rich regions with
1017 active chromatin marks have similar PC1 values, while gene deserts show the opposite
1018 (http://homer.ucsd.edu/homer/interactions/HiCpca.html). HiC filtered matrices were given as input to
1019 Homer together with a list of house-keeping genes for compartment prediction. The house-keeping
1020 genes coordinates are used by Homer as prior information of active regions. We generated density
1021 plots to compare the cis-eigenvector 1 values of the knock-out and wild-type samples with 10kb genomic
1022 bins. Pearson correlation coefficients were calculated ('Cor' function in R) between the counts for
1023 every pair of 10kb bins on chromosome 2. Heatmaps representing the Pearson correlation of interactions
1024 of chromosome 2 for WT and KO thymocytes are displayed by juice box (500kb resolution).

1025 **urea ChIP-seq analysis**

1026 Sequenced reads were quality-checked using FastQC prior to downstream analysis. Unaligned reads
1027 were mapped to the mouse reference genome (NCBI37/mm9) using bowtie2 (version 2.3.1)(*131*)
1028 allowing for three mismatches in the seed region and only unique matches. Candidate binding sites were
1029 called using MACS2 (v2.2.7)(*137*) using a q-value threshold of 0.01. Coverage tracks are presented in
1030 RPM (read pileups per million reads) and utilities from UCSC were used for creating browser tracks (*138*).
1031 To determine intersection of peaks across ChIP-seq samples, deepTools(*83*) was used.

1032 **urea 4C-seq analysis**

1033 Reads were mapped with Bowtie, then assigned to *HindIII* sites with the same utility tools used in (*77*).
1034 These same tools also normalized the counts to per million intrachromosomal reads and removed reads
1035 to restriction fragments comprising more than 2% of the total reads (namely the contiguous adjacent
1036 restriction fragment corresponding to undigested chromatin during the urea 4C, and a rare (<5) numbers
1037 of fragments with extreme PCR duplications). The generated bedGraph files and these were converted
1038 to bigWig format using the bedGraphToBigWig program for direct visualization of the peaks on the
1039 UCSC browser.

1040

1041 **Analysis of SATB1 bound sites and other genomic features**

1042 LADs were identified as genomic intervals using the previously described LADetector algorithm
1043 (https://github.com/thereddylab/pyLAD) or sequencing data
1044 (https://github.com/thereddylab/LADetector) (*114, 139*).SATB1 urea-ChIP data from thymocytes were
1045 tested for statistically significant overlap of LADs using the GenometriCorr package(*140*). The
1046 GenometriCorr package applies multiple spatial tests of independence including a relative distance test
1047 (i.e., if two elements such as LADs and SatB1 sites are spaced more often than expected at a certain
1048 relative distance from each other), projection test (i.e., testing for significant overlap between these two
1049 positions assuming they represent single points points), and the Jaccard test (testing for correlation of
1050 these two positions assuming that they are not points but instead occupy some interval of the genome).
1051 To generate genome wide line plots of averages of intensities (relative score) of DamID and ChIP-seq
1052 peak data were generated over inter-LAD (10% of the size of the adjacent LAD)/border flanked LADs
1053 scaled to the same relative size using the Genomation R package(*141*). The average intensities were
1054 then normalized to fit a scale of -1 to 1 and plotted over the LADs (normalized relative score). To plot
1055 genomic features in the vicinity of enhancers, H3K4me1 peaks outside of LADs were filtered by
1056 subtracting away peaks that intersected LADs using the BEDTools (*142*). To plot genomic features in
1057 the vicinity DiPS in LADs, regions within LADs and DiPS were identified by LADetector. DiPS were then
1058 mapped as intervals and the method described above was applied to DiPS versus SATB1, CTCF, and
1059 chromatin modifications. Genome-wide averages of the respective ChIP-seq/DamID signal data were
1060 then generated within a +/- 3kb window centered at H3K4me1 peaks, using Genomation R package
1061 and plotted on a vertical scale ranging from -1 to 1.

1062

1063 **Figure legends**

1064 **Figure 1 Scheme of urea ChIP-seq and difference from standard ChIP-seq**

1065 A) An illustration for a BUR anchored to the high-salt extraction resistant SATB1 nuclear architecture
1066 (*39*). DNA-FISH signals (red dots) for a cloned SATB1-bound DNA in both alleles are shown in
1067 *Satb1*$^{+/+}$(WT) and *Satb1*$^{-/-}$(KO) thymocytes on slides treated with 2M NaCl solution to produce DNA
1068 halos around the nuclei (blue loops). SATB1 and the SATB1-bound DNA remain in the residual nucleus
1069 in WT thymocytes after salt treatment. However, in KO thymocytes the DNA regions normally bound by
1070 SATB1 are located in the DNA halos after the treatment. B) A comparative overview of the urea ChIP-
1071 seq and standard ChIP-seq protocols. In urea ChIP-seq, entire crosslinked chromatin purified by 8M
1072 urea ultracentrifugation is solubilized (see Materials and Methods) before chromatin
1073 immunoprecipitation. By contrast, in standard ChIP-seq, crosslinked chromatin in whole nuclei is
1074 sonicated, centrifuged and the soluble fraction is isolated for chromatin immunoprecipitation. These

1075 critical steps that are different between urea and standard ChIP-seq are highlighted in boxed texts. C)
1076 Differences in the profiles of the peaks generated from urea ChIP-seq versus standard ChIP-seq. A
1077 diagram is shown for ChIP-seq peaks using antibodies (α) against a DNA direct-binding protein (pink),
1078 a DNA indirect-binding protein (blue), and DNA direct-binding protein that resides in the inaccessible
1079 chromatin region (green) Note: This diagram illustrate a hypothetical scenario where some of the
1080 proteins (green) in the inaccessible chromatin region may also reside in the accessible chromatin
1081 binding indirectly to chromatin.

1082 **Figure 2. Identification of BURs as direct targets of SATB1 *in vivo* by urea ChIP-seq.**

1083 A) Contrasting distributions of SATB1-binding profiles determined by urea ChIP-seq (Urea) compared
1084 to standard ChIP-seq (Std) in mouse thymocytes. B) A zoomed-in view of the gray-highlighted region
1085 shown in (panel A). The track 3 (panels A and B) represents all potential BUR sites serving as a
1086 reference for BUR sites. For both panels A and B, two independent urea and standard ChIP-seq
1087 experiments show high reproducibility (tracks 1 and 2 and tracks 4 and 5). Tracks 6 and 7 [ENCODE,
1088 Bring Ren's Laboratory at the Ludwig Institute for Cancer Research (LICR)] and tracks 8 and 9
1089 (ENCODE, the University of Washington (UW) group]. C) The percentages of urea (Urea) and standard
1090 (Std) SATB1 ChIP-seq peaks that intersect with the BUR reference map (see *supplementary Table 1*).
1091 The significance (p values) of the overlap in each of the four cases (urea and standard ChIP-seq
1092 samples with two replicates each) with BURs is estimated as the fraction of the overlap counts greater
1093 than or equal to the observed count over 1000 random bootstrapped genomic features. $p<0.001$: none
1094 of 1000 random fragment showed greater overlap with BURs than observed in ChIP-seq samples, $p=1$
1095 means all 1000 random fragments showed greater overlap with BURs than observed in ChIP-seq,
1096 indicating avoidance of BURs (see Methods). D) Normalized genome-wide average intensity distribution
1097 profiles (normalized relative score) of SATB1 binding sites determined by standard ChIP-seq, urea
1098 ChIP-seq as well as BURs, over a ±3kb window centered at BUR peaks (top). Relative distance,
1099 projection, and Jaccard tests all indicate strong correlation ($p< 0.05$) between urea ChIP-seq peaks for
1100 SATB1 and BURs, but no overlap ($p< 0.05$) between standard ChIP-seq peaks for SATB1 and BUR
1101 peaks. E) (Left) Heatmaps showing SATB1 ChIP-seq signal intensity centered on all BUR elements.
1102 Signal is plotted within ±3 kb of each BUR center using 50 bp bins using EnrichedHeatmap package
1103 (v1.30.0). The line plots above the heatmaps display the average SATB1 signal across all regions. Only
1104 a subset of BURs exhibits strong SATB1 binding, consistent with selective occupancy. (Right)
1105 Heatmaps showing BUR signal intensity centered on SATB1-bound regions (from ChIP-seq peaks).
1106 The vast majority of SATB1 binding events are positioned within BURs, as evidenced by sharp, centered
1107 BUR signal at nearly all SATB1 peaks. Line plots reflect the average BUR signal profile across all
1108 SATB1 sites in each domain class. BUR intensities are derived from *in vitro* SATB1 BUR-binding
1109 assays.

1110 **Figure 3. Identical CTCF-binding profiles are produced by urea and standard ChIP-seq,**
1111 **independent of SATB1.**

1112 A) Urea ChIP-seq (Urea) profiles for CTCF in *Satb1*$^{+/+}$ (WT) thymocytes and *Satb1*$^{-/-}$ (KO) thymocytes
1113 (track 2 and 3), and for SATB1 in WT thymocytes (track 1). These binding patterns were compared
1114 against CTCF-binding profiles generated by standard ChIP-seq (Std) from ENCODE (tracks 4 and 5)
1115 for testis and thymocytes (ENCODE, LICR), respectively, along with the DNase1 HS profile from
1116 ENCODE, UW (track 6) as well as the SATB1-binding profile from standard ChIP-seq (track 7). B)
1117 Genome-wide average intensity distribution (relative score) of peaks from CTCF and SATB1 urea ChIP-
1118 seq for *Satb1*$^{+/+}$ thymocytes (WT), CTCF urea ChIP-seq for *Satb1*$^{-/-}$ thymocytes (KO), and SATB1
1119 standard ChIP-seq (WT) over a +/- 3kb window centered at CTCF peaks (WT). Relative distance,
1120 projection, and Jaccard tests all indicate strong correlation ($p< 0.05$) between CTCF urea ChIP-seq
1121 peaks for WT and KO thymocytes, between these peaks and standard ChIP-seq peaks for SATB1, but
1122 no overlap ($p< 0.05$) between SATB1 urea ChIP-seq peaks. C) Urea-ChIP-Western results for CTCF,
1123 RAD21, and SATB1, showing that SATB1 does not associate with CTCF nor RAD21 on chromatin.
1124 Also, CTCF and RAD21 co-binding to chromatin appears to be infrequent, suggested by the weak ChIP-
1125 Western signals. D) Hi-C interaction heatmaps for *Satb1*$^{+/+}$:*Cd4*-cre (WT) (top right triangle) and *Satb1*
1126 $^{F/F}$:*Cd4*-cre (KO) thymocytes (bottom left triangle) show essentially identical patterns. E) Genome-wide
1127 comparison of distributions of cis-Eigenvector 1 values shows no difference between WT and KO
1128 thymocytes (high correlation at r=0.998), indicating that genomic compartmentalization is unaffected in
1129 *Satb1* KO thymocytes. Experiments were done in two replicates each for WT and KO samples. The
1130 data shown in D and E were generated by combining data from the replicates for each condition.
1131

1132 **Figure 4. SATB1-bound sites identified by standard ChIP-seq at regulatory regions are SATB1**
1133 **dependent.**

1134 SATB1-binding profiles in immature thymocytes determined by urea ChIP-seq (Urea) and standard
1135 ChIP-seq (Std) covering three loci at *Rag1/Rag2* (top) *Foxp3* (middle), and *Runx3* (bottom) are shown.
1136 For each of the three loci, the standard SATB1 ChIP-seq generates peaks in *Satb1*$^{+/+}$ (WT) thymocytes
1137 (track 3), but not in *Satb1*$^{-/-}$ (KO) thymocytes (tracks 9 for *Rag 1/2* and *Runx3* and tracks 11 for *Foxp3*).
1138 Input chromatin for standard ChIP-seq in these regions did not produce any major peaks (track 10 in
1139 *Rag1/Rag2* and *Runx3* and track 12 in *Foxp3*). The SATB1 peaks from standard ChIP-seq in
1140 *Rag1/Rag2* and *Runx3* loci largely overlap with enhancers (marked by H3K4me1 and H3K27ac). At the
1141 *Foxp3* locus in immature thymocytes SATB1 peaks (track 3) appear in a region marked by low levels
1142 of H3K27ac and H3Kme1 (tracks 4 and 5) where super-enhancer is established upon differentiation
1143 into Treg cells (tracks 6 and 7)(*47*). SATB1-bound peaks produced by urea ChIP-seq (track 2) are
1144 consistently located in distinct positions from those peaks obtained by standard ChIP-seq in these gene
1145 loci. Urea ChIP-seq did not generate peaks in KO thymocytes with anti-SATB1 antibody. Input

1146 chromatin also did not produce any peaks. H3K27ac and H3Kme1 data (tracks 4 and 5) are from
1147 Encode, generated by Bing Ren's laboratory at LICR, and data for Treg shown in (tracks 6 and 7) are
1148 from Kitagawa(*47*).
1149

1150 **Figure 5. SATB1 mediates dense chromatin interactions over *Rag1/2*-containing gene-rich**
1151 **region.**

1152 A) Chromatin interactions detected by urea 4C-seq using a SATB1-bound BUR (BUR-1) and another
1153 site (BUR-2) as baits. These baits are mapped in an accessible chromatin and located at near the
1154 border of a gene-poor region and a gene-rich region containing SATB1-regulated *Rag1* and *Rag2* genes
1155 (pink vertical bar with arrowhead). BUR-2 was found to be one of the interacting sites of BUR-1.
1156 Therefore, it was used as a reciprocal control for BUR-1 to check the reproducibility of BUR-1
1157 interactions. We used *Satb1*$^{+/+}$ (WT) and *Satb1*$^{-/-}$ (KO) thymocytes from 2 weeks old mice for urea 4C-
1158 seq. BUR-1 and BUR-2 interacts with many sites within the ~5.8Mb gene-rich region, containing *Rag1*
1159 and *Rag2* (tracks WT-BUR1 and WT-BUR2). These interactions were greatly reduced upon SATB1
1160 deletion (track KO-BUR1). B) A zoom-in view, focusing on the *Rag1* and *Rag2* region, shows that BUR-
1161 1 interacts extensively over this region in WT thymocytes (shown by parabolas). Such interactions were
1162 virtually diminished in the absence of SATB1 (KO-BUR1 and KO-BUR2 tracks). The pink vertical bars
1163 with arrowheads indicate the positions of the BUR-1 and BUR-2 bait primers. Each of these primer
1164 sequences is located at the end of the *Hind*III fragment containing the primer. These *Hind*III fragments
1165 are marked by thick purple bars adjacent to pink arrowheads pointing primer positions. The map of
1166 *Hind*III fragments is shown for interacting regions (track *Hind*III sites). BUR-1 and BUR-2, along with
1167 other BURs bound by SATB1 (as confirmed by SATB1 urea ChIP-seq peaks and the BUR reference)
1168 that interact with BUR-1 or BUR-2 are marked by small red stars.

1169 Note: Reads to the *Hind*III fragment immediately adjacent to each of the bait primers (BUR-1 and
1170 BURs) were removed as they comprised more than 2% of the total reads, typically derived from re-
1171 ligation of digested chromatin fragments to their original neighboring sequences and/or from a small
1172 undigested chromatin fraction.
1173

1174 **Figure 6. SATB1 binds to BURs in a cell-type dependent manner.**

1175 A) SATB1-binding profiles in a ~2.4 Mb region in chromosome 6 containing *Cd4* in a gene-rich region
1176 from standard ChIP-seq (Std) (track 2) and urea ChIP-seq (Urea) (tracks 3-8). Urea ChIP-seq-derived
1177 SATB1 profiles in thymocytes (track 3), brain (track 4) and skin (track 5) show difference in peak
1178 numbers depending on cell type (see *supplementary* Table 1 and 2). This contrasts with mostly identical
1179 CTCF patterns in these cell types (tracks 11-13). B) SATB1-binding profiles in a 406kb region in
1180 chromosome 5 containing *Gabra2* and *Gabrg1*, highly expressed in brain, also shows much increased

1181 BUR binding in brain, compared to thymocytes and skin similar to A). In this region, there is no SATB1-
1182 binding site detected by standard ChIP-seq (track 2), and CTCF binding sites are mostly absent (track
1183 9). C) Percentages of SATB1 urea-ChIP-seq peaks in skin, thymocytes and brain intersecting with the
1184 BUR reference map, indicating that the majority of the peaks are BURs (*supplementary* Table 1). D)
1185 The percentage of BURs among all BURs identified in the BUR reference map that intersected with
1186 urea SATB1 ChIP-seq peaks identified in skin, thymocytes and brain. DNase1 HS data are from
1187 ENCODE (UW), the CTCF-binding profile and H3K27ac data from standard ChIP-seq are from
1188 ENCODE (LICR).

1189

1190 **Figure 7. BURs largely co-map with LADs**

1191 A) The BUR distribution (BUR reference map, track 2) was compared against Lamin B1-DAM-ID
1192 sites(*86*) (track 1) and SATB1-binding sites derived from urea-ChIP-seq (Urea) (track 3 and 4) over a
1193 8.97 Mb region in chromosome 5 containing neuronal genes, *Gabrg1*, *Gabra2, Gabra4,* and *Gabrb1*. In
1194 this region, co-mapping of BURs and Lamin B1-DAM-ID regions is confirmed. Among BURs, SATB1-
1195 bound BURs derived from urea ChIP-seq (Urea) show difference in the number of peaks depending on
1196 cell type (see *supplementary* Table 1 and 2). SATB1-binding sites derived from urea ChIP-seq avoid
1197 CTCF-binding sites, H3Kme1, H3K27ac sites (from Encode LICR). B) Average Lamin B1 DamID signal
1198 (black dotted), standard ChIP signal for SATB1 (black) and urea ChIP for SATB1 (blue) signal over
1199 LADs and flanking regions (interLAD sized at10% of adjacent LAD). C) Average Lamin B1 DamID signal
1200 (dotted black), BUR signal (red), and urea ChIP for CTCF (orange) signal over LADs (gray shaded) and
1201 flanking regions (interLAD sized at 10% of adjacent LAD). D) Average BUR signal (red), urea ChIP for
1202 SATB1 (blue) signal, Lamin B1 DamID (black, dotted), H3K4me1 (light green) and H3K27ac (light
1203 orange) signals over a +/- 3kb window centered at H3K4me1 peaks within LADs (LADs are gray shaded
1204 and DiPC that reside inside large LADs are unshaded, see text). E) Average BUR signal (red), urea
1205 ChIP for SATB1 (blue) signal, H3K4me1 (light green) and H3K27ac (light orange) signals over a
1206 ±3kbswindow centered at H3K4me1 peaks outside LADs. Relative distance, projection, and Jaccard
1207 tests all indicate strong correlation ($p < 0.05$) between urea ChIP-seq peaks for SATB1 and LADs,
1208 between BURs and LADs, but no overlap ($p<0.05$) between urea ChIP-seq SATB1 and H3K27ac and
1209 H3K4me3 peaks. The results in B to E represent normalized average intensities of signals.

1210

1211 **Figure 8. A model for SATB1-mediated chromatin organization with direct and indirect binding**
1212 **of SATB1 with chromatin.** This model is based on the chromatin-binding profile of SATB1 obtained
1213 from urea ChIP-seq, which shows direct binding of SATB1 to BURs, and from standard ChIP-seq, which
1214 indicates presumably indirect binding of SATB1 to gene-rich, accessible chromatin regions.
1215 Additionally, the model incorporates chromatin interactions of selected SATB1-bound BURs detected
1216 by urea 4C-seq in this study. These BURs are mapped within accessible chromatin. Once BURs are

1217 bound by SATB1, they are tightly anchored to the SATB1 subnuclear structure, which resists high salt
1218 extraction, as demonstrated in previous studies (*39, 40*). We propose that the direct binding of SATB1
1219 to BURs within the SATB1-rich subnuclear structure is stable and forms a chromatin scaffold. This
1220 chromatin scaffold interacts dynamically with active gene-rich regions through indirect binding, creating
1221 functional chromatin complexes (or hubs) that regulate gene expression depending on the cell type.
1222 Future studies are needed to determine the potential role of soluble SATB1 proteins and other
1223 regulatory factors in these interaction events.
1224

1225 # Acknowledgements

1226 We thank Dr. Aristotelis Tsirigos, Ziyan Lin, and Javier Rodriguez Hernaez at New York University
1227 School of Medicine for Hi-C and intersection analyses, Dr. Anthony Schmitt from Arima Genomics for
1228 help with Hi-C experiments. We also thank Dr. Elphege Nora for reviewing Hi-C results and providing
1229 critical comments on the manuscript and Ms. Bao Ho for providing technical assistance. We thank Dr.
1230 Minoree Kohwi for critical reviewing of the manuscript and Dr. Peter Krijger for kindly testing our samples
1231 and Dr. Elzo de Wit for discussion on the 4C-seq analysis.
1232 **Funding:**
1233 National Institute of Health grant R31CA39681 (TKS)
1234 National Institute of Health grant R01ES023854 (TKS)
1235 National Institute of Health grant R01GM132427 (KLR)
1236 National Institute of Health grant R01AR071727 (VAB and TKS)
1237 National Institute of Health grant R01 AR047364 (C-MC and TKS)
1238 **Author contribution:**
1239 Conceptualization: Terumi Kohwi-Shigematsu and Yoshinori Kohwi
1240 Method development and validation: Terumi Kohwi-Shigematsu and Yoshinori Kohwi
1241 Data production: Yoshinori Kohwi, assisted by Mari Grange
1242 Formal analyses and bioinformatic analyses: Terumi Kohwi-Shigematsu, Karen L. Reddy, Xianrong
1243 Wong, Thomas Sexton, Hunter W. Richards and Ya-Chen Liang (Karen L. Reddy and Xianrong Wong
1244 performed all bioinformatic and statistical analyses on LADs and Thomas Sexton conducted data
1245 processing and bioinformatic analysis for the urea 4C-seq data)
1246 Supervision: Terumi Kohwi-Shigematsu, Yoshinori Kohwi and Karen L. Reddy
1247 Materials: Ichiro Taniuchi provided thymocytes from *Satb1*$^{F/F}$: *Cd4-cre and Satb1*$^{+/+}$: *Cd4-cre* mice for
1248 the Hi-C study. Yohko Kitagawa and Shimon Sakaguchi provided modified histone H3 ChIP-seq data
1249 for different stages of thymocyte development. Vladimir A. Botchkarev provided mouse skin for the
1250 urea ChIP-seq studies.
1251 Funding acquisition: Terumi Kohwi-Shigematsu, Vladimir A. Botchkarev and Cheng-Ming Chuong
1252 Writing—original draft: Terumi Kohwi-Shigematsu, Karen L. Reddy and Yoshinori Kohwi

Writing—review, editing and/or discussion: Terumi Kohwi-Shigematsu, Karen L. Reddy, Xianrong Wong, Yoshinori Kohwi, Ichiro Taniuchi, Thomas Sexton, Yohko Kitagawa and Shimon Sakaguchi

Competing interests: The authors declare no competing interests

Data availability: All sequencing data for ChIP-seq and Hi-C in this study was uploaded to NCBI Gene Expression Omnibus (GEO) and is available under the accession GSE191146.

References

1. J. C. Politz, D. Scalzo, M. Groudine, Something silent this way forms: the functional organization of the repressive nuclear compartment. *Annu Rev Cell Dev Biol* **29**, 241-270 (2013). DOI: 10.1146/annurev-cellbio-101512-122317.
2. B. van Steensel, A. S. Belmont, Lamina-Associated Domains: Links with Chromosome Architecture, Heterochromatin, and Gene Repression. *Cell* **169**, 780-791 (2017). DOI: 10.1016/j.cell.2017.04.022.
3. S. Schoenfelder, P. Fraser, Long-range enhancer-promoter contacts in gene expression control. *Nat Rev Genet* **20**, 437-455 (2019). DOI: 10.1038/s41576-019-0128-0.
4. E. Bashkirova, S. Lomvardas, Olfactory receptor genes make the case for inter-chromosomal interactions. *Curr Opin Genet Dev* **55**, 106-113 (2019). DOI: 10.1016/j.gde.2019.07.004.
5. A. Gondor, R. Ohlsson, Enhancer functions in three dimensions: beyond the flat world perspective. *F1000Res* **7**, (2018). DOI: 10.12688/f1000research.13842.1.
6. V. Loubiere, G. L. Papadopoulos, Q. Szabo, A. M. Martinez, G. Cavalli, Widespread activation of developmental gene expression characterized by PRC1-dependent chromatin looping. *Sci Adv* **6**, eaax4001 (2020). DOI: 10.1126/sciadv.aax4001.
7. T. Misteli, The Self-Organizing Genome: Principles of Genome Architecture and Function. *Cell* **183**, 28-45 (2020). DOI: 10.1016/j.cell.2020.09.014.
8. E. Lieberman-Aiden, N. L. van Berkum, L. Williams, M. Imakaev, T. Ragoczy, A. Telling, I. Amit, B. R. Lajoie, P. J. Sabo, M. O. Dorschner, R. Sandstrom, B. Bernstein, M. A. Bender, M. Groudine, A. Gnirke, J. Stamatoyannopoulos, L. A. Mirny, E. S. Lander, J. Dekker, Comprehensive mapping of long-range interactions reveals folding principles of the human genome. *Science* **326**, 289-293 (2009). DOI: 10.1126/science.1181369.
9. L. Guelen, L. Pagie, E. Brasset, W. Meuleman, M. B. Faza, W. Talhout, B. H. Eussen, A. de Klein, L. Wessels, W. de Laat, B. van Steensel, Domain organization of human chromosomes revealed by mapping of nuclear lamina interactions. *Nature* **453**, 948-951 (2008). DOI: 10.1038/nature06947.
10. J. Kind, L. Pagie, S. S. de Vries, L. Nahidiazar, S. S. Dey, M. Bienko, Y. Zhan, B. Lajoie, C. A. de Graaf, M. Amendola, G. Fudenberg, M. Imakaev, L. A. Mirny, K. Jalink, J. Dekker, A. van Oudenaarden, B. van Steensel, Genome-wide maps of nuclear lamina interactions in single human cells. *Cell* **163**, 134-147 (2015). DOI: 10.1016/j.cell.2015.08.040.
11. B. van Steensel, J. Delrow, S. Henikoff, Chromatin profiling using targeted DNA adenine methyltransferase. *Nat Genet* **27**, 304-308 (2001). DOI: 10.1038/85871.
12. J. R. Dixon, S. Selvaraj, F. Yue, A. Kim, Y. Li, Y. Shen, M. Hu, J. S. Liu, B. Ren, Topological domains in mammalian genomes identified by analysis of chromatin interactions. *Nature* **485**, 376-380 (2012). DOI: 10.1038/nature11082.
13. E. P. Nora, B. R. Lajoie, E. G. Schulz, L. Giorgetti, I. Okamoto, N. Servant, T. Piolot, N. L. van Berkum, J. Meisig, J. Sedat, J. Gribnau, E. Barillot, N. Bluthgen, J. Dekker, E. Heard, Spatial partitioning of the regulatory landscape of the X-inactivation centre. *Nature* **485**, 381-385 (2012). DOI: 10.1038/nature11049.
14. T. Sexton, E. Yaffe, E. Kenigsberg, F. Bantignies, B. Leblanc, M. Hoichman, H. Parrinello, A. Tanay, G. Cavalli, Three-dimensional folding and functional organization principles of the Drosophila genome. *Cell* **148**, 458-472 (2012). DOI: 10.1016/j.cell.2012.01.010.

15. A. L. Sanborn, S. S. Rao, S. C. Huang, N. C. Durand, M. H. Huntley, A. I. Jewett, I. D. Bochkov, D. Chinnappan, A. Cutkosky, J. Li, K. P. Geeting, A. Gnirke, A. Melnikov, D. McKenna, E. K. Stamenova, E. S. Lander, E. L. Aiden, Chromatin extrusion explains key features of loop and domain formation in wild-type and engineered genomes. *Proc Natl Acad Sci U S A* **112**, E6456-6465 (2015). DOI: 10.1073/pnas.1518552112.
16. G. Fudenberg, M. Imakaev, C. Lu, A. Goloborodko, N. Abdennur, L. A. Mirny, Formation of Chromosomal Domains by Loop Extrusion. *Cell Rep* **15**, 2038-2049 (2016). DOI: 10.1016/j.celrep.2016.04.085.
17. S. S. Rao, M. H. Huntley, N. C. Durand, E. K. Stamenova, I. D. Bochkov, J. T. Robinson, A. L. Sanborn, I. Machol, A. D. Omer, E. S. Lander, E. L. Aiden, A 3D Map of the Human Genome at Kilobase Resolution Reveals Principles of Chromatin Looping. *Cell* **159**, 1665-1680 (2014). DOI: 10.1016/j.cell.2014.11.021.
18. E. P. Nora, A. Goloborodko, A. L. Valton, J. H. Gibcus, A. Uebersohn, N. Abdennur, J. Dekker, L. A. Mirny, B. G. Bruneau, Targeted Degradation of CTCF Decouples Local Insulation of Chromosome Domains from Genomic Compartmentalization. *Cell* **169**, 930-944 e922 (2017). DOI: 10.1016/j.cell.2017.05.004.
19. S. S. P. Rao, S. C. Huang, B. Glenn St Hilaire, J. M. Engreitz, E. M. Perez, K. R. Kieffer-Kwon, A. L. Sanborn, S. E. Johnstone, G. D. Bascom, I. D. Bochkov, X. Huang, M. S. Shamim, J. Shin, D. Turner, Z. Ye, A. D. Omer, J. T. Robinson, T. Schlick, B. E. Bernstein, R. Casellas, E. S. Lander, E. L. Aiden, Cohesin Loss Eliminates All Loop Domains. *Cell* **171**, 305-320 e324 (2017). DOI: 10.1016/j.cell.2017.09.026.
20. G. Wutz, C. Varnai, K. Nagasaka, D. A. Cisneros, R. R. Stocsits, W. Tang, S. Schoenfelder, G. Jessberger, M. Muhar, M. J. Hossain, N. Walther, B. Koch, M. Kueblbeck, J. Ellenberg, J. Zuber, P. Fraser, J. M. Peters, Topologically associating domains and chromatin loops depend on cohesin and are regulated by CTCF, WAPL, and PDS5 proteins. *EMBO J* **36**, 3573-3599 (2017). DOI: 10.15252/embj.201798004.
21. W. Schwarzer, N. Abdennur, A. Goloborodko, A. Pekowska, G. Fudenberg, Y. Loe-Mie, N. A. Fonseca, W. Huber, C. H. Haering, L. Mirny, F. Spitz, Two independent modes of chromatin organization revealed by cohesin removal. *Nature* **551**, 51-56 (2017). DOI: 10.1038/nature24281.
22. D. I. Cattoni, A. M. Cardozo Gizzi, M. Georgieva, M. Di Stefano, A. Valeri, D. Chamousset, C. Houbron, S. Dejardin, J. B. Fiche, I. Gonzalez, J. M. Chang, T. Sexton, M. A. Marti-Renom, F. Bantignies, G. Cavalli, M. Nollmann, Single-cell absolute contact probability detection reveals chromosomes are organized by multiple low-frequency yet specific interactions. *Nat Commun* **8**, 1753 (2017). DOI: 10.1038/s41467-017-01962-x.
23. B. Bintu, L. J. Mateo, J. H. Su, N. A. Sinnott-Armstrong, M. Parker, S. Kinrot, K. Yamaya, A. N. Boettiger, X. Zhuang, Super-resolution chromatin tracing reveals domains and cooperative interactions in single cells. *Science* **362**, (2018). DOI: 10.1126/science.aau1783.
24. E. H. Finn, G. Pegoraro, H. B. Brandao, A. L. Valton, M. E. Oomen, J. Dekker, L. Mirny, T. Misteli, Extensive Heterogeneity and Intrinsic Variation in Spatial Genome Organization. *Cell* **176**, 1502-1515 e1510 (2019). DOI: 10.1016/j.cell.2019.01.020.
25. M. Gabriele, H. B. Brandao, S. Grosse-Holz, A. Jha, G. M. Dailey, C. Cattoglio, T. S. Hsieh, L. Mirny, C. Zechner, A. S. Hansen, Dynamics of CTCF- and cohesin-mediated chromatin looping revealed by live-cell imaging. *Science* **376**, 496-501 (2022). DOI: 10.1126/science.abn6583.
26. P. Mach, P. I. Kos, Y. Zhan, J. Cramard, S. Gaudin, J. Tunnermann, E. Marchi, J. Eglinger, J. Zuin, M. Kryzhanovska, S. Smallwood, L. Gelman, G. Roth, E. P. Nora, G. Tiana, L. Giorgetti, Cohesin and CTCF control the dynamics of chromosome folding. *Nat Genet* **54**, 1907-1918 (2022). DOI: 10.1038/s41588-022-01232-7.
27. Y. Chi, J. Shi, D. Xing, L. Tan, Every gene everywhere all at once: High-precision measurement of 3D chromosome architecture with single-cell Hi-C. *Front Mol Biosci* **9**, 959688 (2022). DOI: 10.3389/fmolb.2022.959688.
28. L. F. Chen, J. Lee, A. Boettiger, Recent progress and challenges in single-cell imaging of enhancer-promoter interaction. *Curr Opin Genet Dev* **79**, 102023 (2023). DOI: 10.1016/j.gde.2023.102023.

29. A. Hafner, M. Park, S. E. Berger, S. E. Murphy, E. P. Nora, A. N. Boettiger, Loop stacking organizes genome folding from TADs to chromosomes. *Mol Cell* **83**, 1377-1392 e1376 (2023). DOI: 10.1016/j.molcel.2023.04.008.
30. T. Kohwi-Shigematsu, Y. Kohwi, Torsional stress stabilizes extended base unpairing in suppressor sites flanking immunoglobulin heavy chain enhancer. *Biochemistry* **29**, 9551-9560. (1990). DOI:
31. J. Bode, Y. Kohwi, L. Dickinson, T. Joh, D. Klehr, C. Mielke, T. Kohwi-Shigematsu, Biological significance of unwinding capability of nuclear matrix-associating DNAs. *Science* **255**, 195-197 (1992). DOI: 10.1126/science.1553545.
32. L. A. Dickinson, T. Joh, Y. Kohwi, T. Kohwi-Shigematsu, A tissue-specific MAR/SAR DNA-binding protein with unusual binding site recognition. *Cell* **70**, 631-645. (1992). DOI:
33. T. Kohwi-Shigematsu, Y. Kohwi, Detection of non-B-DNA structures at specific sites in supercoiled plasmid DNA and chromatin with haloacetaldehyde and diethyl pyrocarbonate. *Methods Enzymol* **212**, 155-180 (1992). DOI:
34. J. D. Alvarez, D. H. Yasui, H. Niida, T. Joh, D. Y. Loh, T. Kohwi-Shigematsu, The MAR-binding protein SATB1 orchestrates temporal and spatial expression of multiple genes during T-cell development. *Genes Dev* **14**, 521-535 (2000). DOI:
35. Y. Zhang, L. Zheng, M. Le, Y. Nakano, B. Chan, Y. Huang, P. M. Torbaty, Y. Kohwi, R. Marcucio, S. Habelitz, P. K. Den Besten, T. Kohwi-Shigematsu, SATB1 establishes ameloblast cell polarity and regulates directional amelogenin secretion for enamel formation. *BMC Biol* **17**, 104 (2019). DOI: 10.1186/s12915-019-0722-9.
36. M. Y. Fessing, A. N. Mardaryev, M. R. Gdula, A. A. Sharov, T. Y. Sharova, V. Rapisarda, K. B. Gordon, A. D. Smorodchenko, K. Poterlowicz, G. Ferone, Y. Kohwi, C. Missero, T. Kohwi-Shigematsu, V. A. Botchkarev, p63 regulates Satb1 to control tissue-specific chromatin remodeling during development of the epidermis. *J Cell Biol* **194**, 825-839 (2011). DOI: jcb.201101148 [pii] 10.1083/jcb.201101148.
37. M. A. Balamotis, N. Tamberg, Y. J. Woo, J. Li, B. Davy, T. Kohwi-Shigematsu, Y. Kohwi, Satb1 ablation alters temporal expression of immediate early genes and reduces dendritic spine density during postnatal brain development. *Mol Cell Biol* **32**, 333-347 (2012). DOI: 10.1128/MCB.05917-11.
38. Y. Huang, L. Zhang, N. N. Song, Z. L. Hu, J. Y. Chen, Y. Q. Ding, Distribution of Satb1 in the central nervous system of adult mice. *Neurosci Res* **71**, 12-21 (2011). DOI: 10.1016/j.neures.2011.05.015.
39. S. Cai, H. J. Han, T. Kohwi-Shigematsu, Tissue-specific nuclear architecture and gene expression regulated by SATB1. *Nat Genet* **34**, 42-51 (2003). DOI: 10.1038/ng1146.
40. I. de Belle, S. Cai, T. Kohwi-Shigematsu, The genomic sequences bound to special AT-rich sequence-binding protein 1 (SATB1) in vivo in Jurkat T cells are tightly associated with the nuclear matrix at the bases of the chromatin loops. *J Cell Biol* **141**, 335-348 (1998). DOI: 10.1083/jcb.141.2.335.
41. T. Kohwi-Shigematsu, K. Poterlowicz, E. Ordinario, H. J. Han, V. A. Botchkarev, Y. Kohwi, Genome organizing function of SATB1 in tumor progression. *Semin Cancer Biol*, (2013). DOI: S1044-579X(12)00101-0 [pii] 10.1016/j.semcancer.2012.06.009.
42. S. Cai, C. C. Lee, T. Kohwi-Shigematsu, SATB1 packages densely looped, transcriptionally active chromatin for coordinated expression of cytokine genes. *Nat Genet* **38**, 1278-1288 (2006). DOI:
43. Y. Satoh, T. Yokota, T. Sudo, M. Kondo, A. Lai, P. W. Kincade, T. Kouro, R. Iida, K. Kokame, T. Miyata, Y. Habuchi, K. Matsui, H. Tanaka, I. Matsumura, K. Oritani, T. Kohwi-Shigematsu, Y. Kanakura, The Satb1 protein directs hematopoietic stem cell differentiation toward lymphoid lineages. *Immunity* **38**, 1105-1115 (2013). DOI: 10.1016/j.immuni.2013.05.014.
44. D. Skowronska-Krawczyk, Q. Ma, M. Schwartz, K. Scully, W. Li, Z. Liu, H. Taylor, J. Tollkuhn, K. A. Ohgi, D. Notani, Y. Kohwi, T. Kohwi-Shigematsu, M. G. Rosenfeld, Required enhancer-matrin-3 network interactions for a homeodomain transcription program. *Nature* **514**, 257-261 (2014). DOI: 10.1038/nature13573.
45. B. Hao, A. K. Naik, A. Watanabe, H. Tanaka, L. Chen, H. W. Richards, M. Kondo, I. Taniuchi, Y. Kohwi, T. Kohwi-Shigematsu, M. S. Krangel, An anti-silencer- and SATB1-dependent

chromatin hub regulates Rag1 and Rag2 gene expression during thymocyte development. *J Exp Med* **212**, 809-824 (2015). DOI: 10.1084/jem.20142207.

46. K. Kakugawa, S. Kojo, H. Tanaka, W. Seo, T. A. Endo, Y. Kitagawa, S. Muroi, M. Tenno, N. Yasmin, Y. Kohwi, S. Sakaguchi, T. Kowhi-Shigematsu, I. Taniuchi, Essential Roles of SATB1 in Specifying T Lymphocyte Subsets. *Cell Rep* **19**, 1176-1188 (2017). DOI: 10.1016/j.celrep.2017.04.038.
47. Y. Kitagawa, N. Ohkura, Y. Kidani, A. Vandenbon, K. Hirota, R. Kawakami, K. Yasuda, D. Motooka, S. Nakamura, M. Kondo, I. Taniuchi, T. Kohwi-Shigematsu, S. Sakaguchi, Guidance of regulatory T cell development by Satb1-dependent super-enhancer establishment. *Nat Immunol* **18**, 173-183 (2017). DOI: 10.1038/ni.3646.
48. K. Yasuda, Y. Kitagawa, R. Kawakami, Y. Isaka, H. Watanabe, G. Kondoh, T. Kohwi-Shigematsu, S. Sakaguchi, K. Hirota, Satb1 regulates the effector program of encephalitogenic tissue Th17 cells in chronic inflammation. *Nat Commun* **10**, 549 (2019). DOI: 10.1038/s41467-019-08404-w.
49. M. Goolam, M. Zernicka-Goetz, The chromatin modifier Satb1 regulates cell fate through Fgf signalling in the early mouse embryo. *Development* **144**, 1450-1461 (2017). DOI: 10.1242/dev.144139.
50. H. J. Han, J. Russo, Y. Kohwi, T. Kohwi-Shigematsu, SATB1 reprogrammes gene expression to promote breast tumour growth and metastasis. *Nature* **452**, 187-193 (2008). DOI:
51. A. Fromberg, K. Engeland, A. Aigner, The Special AT-rich Sequence Binding Protein 1 (SATB1) and its role in solid tumors. *Cancer Lett* **417**, 96-111 (2018). DOI: 10.1016/j.canlet.2017.12.031.
52. E. Ordinario, H. J. Han, S. Furuta, L. M. Heiser, L. R. Jakkula, F. Rodier, P. T. Spellman, J. Campisi, J. W. Gray, M. J. Bissell, Y. Kohwi, T. Kohwi-Shigematsu, ATM suppresses SATB1-induced malignant progression in breast epithelial cells. *PLoS One* **7**, e51786 (2012). DOI: 10.1371/journal.pone.0051786.
53. D. Feng, Y. Chen, R. Dai, S. Bian, W. Xue, Y. Zhu, Z. Li, Y. Yang, Y. Zhang, J. Zhang, J. Bai, L. Qin, Y. Kohwi, W. Shi, T. Kohwi-Shigematsu, J. Ma, S. Liao, B. Hao, Chromatin organizer SATB1 controls the cell identity of CD4(+) CD8(+) double-positive thymocytes by regulating the activity of super-enhancers. *Nat Commun* **13**, 5554 (2022). DOI: 10.1038/s41467-022-33333-6.
54. T. Zelenka, A. Klonizakis, D. Tsoukatou, D. A. Papamatheakis, S. Franzenburg, P. Tzerpos, I. R. Tzonevrakis, G. Papadogkonas, M. Kapsetaki, C. Nikolaou, D. Plewczynski, C. Spilianakis, The 3D enhancer network of the developing T cell genome is shaped by SATB1. *Nat Commun* **13**, 6954 (2022). DOI: 10.1038/s41467-022-34345-y.
55. B. Wang, L. Ji, Q. Bian, SATB1 regulates 3D genome architecture in T cells by constraining chromatin interactions surrounding CTCF-binding sites. *Cell Rep* **42**, 112323 (2023). DOI: 10.1016/j.celrep.2023.112323.
56. D. Jain, S. Baldi, A. Zabel, T. Straub, P. B. Becker, Active promoters give rise to false positive 'Phantom Peaks' in ChIP-seq experiments. *Nucleic Acids Res* **43**, 6959-6968 (2015). DOI: 10.1093/nar/gkv637.
57. D. Park, Y. Lee, G. Bhupindersingh, V. R. Iyer, Widespread misinterpretable ChIP-seq bias in yeast. *PLoS One* **8**, e83506 (2013). DOI: 10.1371/journal.pone.0083506.
58. L. Teytelman, D. M. Thurtle, J. Rine, A. van Oudenaarden, Highly expressed loci are vulnerable to misleading ChIP localization of multiple unrelated proteins. *Proc Natl Acad Sci U S A* **110**, 18602-18607 (2013). DOI: 10.1073/pnas.1316064110.
59. C. A. Meyer, X. S. Liu, Identifying and mitigating bias in next-generation sequencing methods for chromatin biology. *Nat Rev Genet* **15**, 709-721 (2014). DOI: 10.1038/nrg3788.
60. S. Baumgarten, J. Bryant, Chromatin structure can introduce systematic biases in genome-wide analyses of Plasmodium falciparum. *Open Res Eur* **2**, 75 (2022). DOI: 10.12688/openreseurope.14836.2.
61. K. Gesson, P. Rescheneder, M. P. Skoruppa, A. von Haeseler, T. Dechat, R. Foisner, A-type lamins bind both hetero- and euchromatin, the latter being regulated by lamina-associated polypeptide 2 alpha. *Genome Res* **26**, 462-473 (2016). DOI: 10.1101/gr.196220.115.

1468 62. T. Kohwi-Shigematsu, I. deBelle, L. A. Dickinson, S. Galande, Y. Kohwi, Identification of base-
1469 unpairing region-binding proteins and characterization of their in vivo binding sequences.
1470 *Methods Cell Biol* **53**, 323-354 (1998). DOI:
1471 63. E. A. Oprzeska-Zingrebe, J. Smiatek, Preferential Binding of Urea to Single-Stranded DNA
1472 Structures: A Molecular Dynamics Study. *Biophys J* **114**, 1551-1562 (2018). DOI:
1473 10.1016/j.bpj.2018.02.013.
1474 64. A. Das, C. Mukhopadhyay, Urea-mediated protein denaturation: a consensus view. *J Phys*
1475 *Chem B* **113**, 12816-12824 (2009). DOI: 10.1021/jp906350s.
1476 65. S. Raghunathan, T. Jaganade, U. D. Priyakumar, Urea-aromatic interactions in biology.
1477 *Biophys Rev* **12**, 65-84 (2020). DOI: 10.1007/s12551-020-00620-9.
1478 66. T. Kohwi-Shigematsu, Y. Kohwi, K. Takahashi, H. W. Richards, S. D. Ayers, H. J. Han, S. Cai,
1479 SATB1-mediated functional packaging of chromatin into loops. *Methods* **58**, 243-254 (2012).
1480 DOI: 10.1016/j.ymeth.2012.06.019.
1481 67. P. Kourilsky, S. Manteuil, M. H. Zamansky, F. Gros, DNA-RNA hybridization at low
1482 temperature in the presence of urea. *Biochem Biophys Res Commun* **41**, 1080-1087 (1970).
1483 DOI: 10.1016/0006-291x(70)90196-8.
1484 68. P. Kourilsky, J. Leidner, G. Y. Tremblay, DNA-DNA hybridization on filters at low temperature
1485 in the presence of formamide or urea. *Biochimie* **53**, 1111-1114 (1971). DOI: 10.1016/s0300-
1486 9084(71)80201-8.
1487 69. E. Hegedus, E. Kokai, A. Kotlyar, V. Dombradi, G. Szabo, Separation of 1-23-kb
1488 complementary DNA strands by urea-agarose gel electrophoresis. *Nucleic Acids Res* **37**, e112
1489 (2009). DOI: 10.1093/nar/gkp539.
1490 70. H. Summer, R. Gramer, P. Droge, Denaturing urea polyacrylamide gel electrophoresis (Urea
1491 PAGE). *J Vis Exp*, (2009). DOI: 10.3791/1485.
1492 71. W. Mu, E. S. Davis, S. Lee, M. G. Dozmorov, D. H. Phanstiel, M. I. Love, bootRanges: flexible
1493 generation of null sets of genomic ranges for hypothesis testing. *Bioinformatics* **39**, (2023).
1494 DOI: 10.1093/bioinformatics/btad190.
1495 72. C. A. Davis, B. C. Hitz, C. A. Sloan, E. T. Chan, J. M. Davidson, I. Gabdank, J. A. Hilton, K.
1496 Jain, U. K. Baymuradov, A. K. Narayanan, K. C. Onate, K. Graham, S. R. Miyasato, T. R.
1497 Dreszer, J. S. Strattan, O. Jolanki, F. Y. Tanaka, J. M. Cherry, The Encyclopedia of DNA
1498 elements (ENCODE): data portal update. *Nucleic Acids Res* **46**, D794-D801 (2018). DOI:
1499 10.1093/nar/gkx1081.
1500 73. J. C. Peng, A. Valouev, T. Swigut, J. Zhang, Y. Zhao, A. Sidow, J. Wysocka, Jarid2/Jumonji
1501 coordinates control of PRC2 enzymatic activity and target gene occupancy in pluripotent cells.
1502 *Cell* **139**, 1290-1302 (2009). DOI: 10.1016/j.cell.2009.12.002.
1503 74. Y. Tanaka, T. Sotome, A. Inoue, T. Mukozu, T. Kuwabara, T. Mikami, T. Kowhi-Shigematsu,
1504 M. Kondo, SATB1 Conditional Knockout Results in Sjogren's Syndrome in Mice. *J Immunol*
1505 **199**, 4016-4022 (2017). DOI: 10.4049/jimmunol.1700550.
1506 75. M. Kondo, Y. Tanaka, T. Kuwabara, T. Naito, T. Kohwi-Shigematsu, A. Watanabe, SATB1
1507 Plays a Critical Role in Establishment of Immune Tolerance. *J Immunol* **196**, 563-572 (2016).
1508 DOI: 10.4049/jimmunol.1501429.
1509 76. N. Yannoutsos, V. Barreto, Z. Misulovin, A. Gazumyan, W. Yu, N. Rajewsky, B. R. Peixoto, T.
1510 Eisenreich, M. C. Nussenzweig, A cis element in the recombination activating gene locus
1511 regulates gene expression by counteracting a distant silencer. *Nat Immunol* **5**, 443-450 (2004).
1512 DOI: 10.1038/ni1053.
1513 77. Y. Ben Zouari, A. Platania, A. M. Molitor, T. Sexton, 4See: A Flexible Browser to Explore 4C
1514 Data. *Front Genet* **10**, 1372 (2019). DOI: 10.3389/fgene.2019.01372.
1515 78. E. de Wit, B. A. Bouwman, Y. Zhu, P. Klous, E. Splinter, M. J. Verstegen, P. H. Krijger, N.
1516 Festuccia, E. P. Nora, M. Welling, E. Heard, N. Geijsen, R. A. Poot, I. Chambers, W. de Laat,
1517 The pluripotent genome in three dimensions is shaped around pluripotency factors. *Nature*
1518 **501**, 227-231 (2013). DOI: 10.1038/nature12420.
1519 79. G. Geeven, H. Teunissen, W. de Laat, E. de Wit, peakC: a flexible, non-parametric peak
1520 calling package for 4C and Capture-C data. *Nucleic Acids Res* **46**, e91 (2018). DOI:
1521 10.1093/nar/gky443.

1522 80. P. H. L. Krijger, G. Geeven, V. Bianchi, C. R. E. Hilvering, W. de Laat, 4C-seq from beginning
1523 to end: A detailed protocol for sample preparation and data analysis. *Methods* **170**, 17-32
1524 (2020). DOI: 10.1016/j.ymeth.2019.07.014.
1525 81. D. Noordermeer, M. Leleu, E. Splinter, J. Rougemont, W. De Laat, D. Duboule, The dynamic
1526 architecture of Hox gene clusters. *Science* **334**, 222-225 (2011). DOI:
1527 10.1126/science.1207194.
1528 82. P. J. Wijchers, P. H. L. Krijger, G. Geeven, Y. Zhu, A. Denker, M. Verstegen, C. Valdes-
1529 Quezada, C. Vermeulen, M. Janssen, H. Teunissen, L. C. M. Anink-Groenen, P. J. Verschure,
1530 W. de Laat, Cause and Consequence of Tethering a SubTAD to Different Nuclear
1531 Compartments. *Mol Cell* **61**, 461-473 (2016). DOI: 10.1016/j.molcel.2016.01.001.
1532 83. F. Ramirez, D. P. Ryan, B. Gruning, V. Bhardwaj, F. Kilpert, A. S. Richter, S. Heyne, F.
1533 Dundar, T. Manke, deepTools2: a next generation web server for deep-sequencing data
1534 analysis. *Nucleic Acids Res* **44**, W160-165 (2016). DOI: 10.1093/nar/gkw257.
1535 84. L. A. Dickinson, T. Kohwi-Shigematsu, Nucleolin is a matrix attachment region DNA-binding
1536 protein that specifically recognizes a region with high base-unpairing potential. *Mol Cell Biol*
1537 **15**, 456-465 (1995). DOI: 10.1128/MCB.15.1.456.
1538 85. W. Meuleman, D. Peric-Hupkes, J. Kind, J. B. Beaudry, L. Pagie, M. Kellis, M. Reinders, L.
1539 Wessels, B. van Steensel, Constitutive nuclear lamina-genome interactions are highly
1540 conserved and associated with A/T-rich sequence. *Genome Res* **23**, 270-280 (2013). DOI:
1541 10.1101/gr.141028.112.
1542 86. S. Chen, T. R. Luperchio, X. Wong, E. B. Doan, A. T. Byrd, K. Roy Choudhury, K. L. Reddy,
1543 M. S. Krangel, A Lamina-Associated Domain Border Governs Nuclear Lamina Interactions,
1544 Transcription, and Recombination of the Tcrb Locus. *Cell Rep* **25**, 1729-1740 e1726 (2018).
1545 DOI: 10.1016/j.celrep.2018.10.052.
1546 87. M. J. Vogel, D. Peric-Hupkes, B. van Steensel, Detection of in vivo protein-DNA interactions
1547 using DamID in mammalian cells. *Nat Protoc* **2**, 1467-1478 (2007). DOI:
1548 10.1038/nprot.2007.148.
1549 88. K. L. Reddy, X. Wong, An Optimized Adaptation of DamID for NGS Applications. *Methods Mol*
1550 *Biol* **2866**, 245-262 (2025). DOI: 10.1007/978-1-0716-4192-7_14.
1551 89. B. Wen, H. Wu, Y. H. Loh, E. Briem, G. Q. Daley, A. P. Feinberg, Euchromatin islands in large
1552 heterochromatin domains are enriched for CTCF binding and differentially DNA-methylated
1553 regions. *BMC Genomics* **13**, 566 (2012). DOI: 10.1186/1471-2164-13-566.
1554 90. C. Leemans, M. C. H. van der Zwalm, L. Brueckner, F. Comoglio, T. van Schaik, L. Pagie, J.
1555 van Arensbergen, B. van Steensel, Promoter-Intrinsic and Local Chromatin Features
1556 Determine Gene Repression in LADs. *Cell* **177**, 852-864 e814 (2019). DOI:
1557 10.1016/j.cell.2019.03.009.
1558 91. T. R. Luperchio, Sauria, M. EG., Wong, X., Gaillard, M-C., Tsang, P., Pekrun, K., Ach, R.A.,
1559 Yamada, N.A., Taylor, J., Reddy, K.L., Chromosome Conformation Paints Reveal the Role of
1560 Lamina Association in Genome Organization and Regulation. *bioRxiv*. DOI:
1561 https://doi.org/10.1101/122226.
1562 92. S. Galande, L. A. Dickinson, I. S. Mian, M. Sikorska, T. Kohwi-Shigematsu, SATB1 cleavage
1563 by caspase 6 disrupts PDZ domain-mediated dimerization, causing detachment from
1564 chromatin early in T-cell apoptosis. *Mol Cell Biol* **21**, 5591-5604. (2001). DOI:
1565 93. L. A. Dickinson, C. D. Dickinson, T. Kohwi-Shigematsu, An atypical homeodomain in SATB1
1566 promotes specific recognition of the key structural element in a matrix attachment region. *J*
1567 *Biol Chem* **272**, 11463-11470. (1997). DOI:
1568 94. K. Nakagomi, Y. Kohwi, L. A. Dickinson, T. Kohwi-Shigematsu, A novel DNA-binding motif in
1569 the nuclear matrix attachment DNA-binding protein SATB1. *Mol Cell Biol* **14**, 1852-1860.
1570 (1994). DOI:
1571 95. Z. Wang, X. Yang, S. Guo, Y. Yang, X. C. Su, Y. Shen, J. Long, Crystal structure of the
1572 ubiquitin-like domain-CUT repeat-like tandem of special AT-rich sequence binding protein 1
1573 (SATB1) reveals a coordinating DNA-binding mechanism. *J Biol Chem* **289**, 27376-27385
1574 (2014). DOI: 10.1074/jbc.M114.562314.

1575 96. P. Pavan Kumar, P. K. Purbey, C. K. Sinha, D. Notani, A. Limaye, R. S. Jayani, S. Galande,
1576 Phosphorylation of SATB1, a global gene regulator, acts as a molecular switch regulating its
1577 transcriptional activity in vivo. *Mol Cell* **22**, 231-243 (2006). DOI:
1578 97. D. Notani, K. P. Gottimukkala, R. S. Jayani, A. S. Limaye, M. V. Damle, S. Mehta, P. K.
1579 Purbey, J. Joseph, S. Galande, Global regulator SATB1 recruits beta-catenin and regulates
1580 T(H)2 differentiation in Wnt-dependent manner. *PLoS Biol* **8**, e1000296 (2010). DOI:
1581 10.1371/journal.pbio.1000296.
1582 98. D. Notani, P. L. Ramanujam, P. P. Kumar, K. P. Gottimukkala, C. Kumar-Sinha, S. Galande,
1583 N-terminal PDZ-like domain of chromatin organizer SATB1 contributes towards its function as
1584 transcription regulator. *J Biosci* **36**, 461-469 (2011). DOI: 10.1007/s12038-011-9091-4.
1585 99. T. L. Stephen, K. K. Payne, R. A. Chaurio, M. J. Allegrezza, H. Zhu, J. Perez-Sanz, A.
1586 Perales-Puchalt, J. M. Nguyen, A. E. Vara-Ailor, E. B. Eruslanov, M. E. Borowsky, R. Zhang,
1587 T. M. Laufer, J. R. Conejo-Garcia, SATB1 Expression Governs Epigenetic Repression of PD-1
1588 in Tumor-Reactive T Cells. *Immunity* **46**, 51-64 (2017). DOI: 10.1016/j.immuni.2016.12.015.
1589 100. D. Yasui, M. Miyano, S. Cai, P. Varga-Weisz, T. Kohwi-Shigematsu, SATB1 targets chromatin
1590 remodelling to regulate genes over long distances. *Nature* **419**, 641-645. (2002). DOI:
1591 101. T. Zhan, N. Rindtorff, M. Boutros, Wnt signaling in cancer. *Oncogene* **36**, 1461-1473 (2017).
1592 DOI: 10.1038/onc.2016.304.
1593 102. P. Song, Z. Gao, Y. Bao, L. Chen, Y. Huang, Y. Liu, Q. Dong, X. Wei, Wnt/beta-catenin
1594 signaling pathway in carcinogenesis and cancer therapy. *Journal of hematology & oncology*
1595 **17**, 46 (2024). DOI: 10.1186/s13045-024-01563-4.
1596 103. J. A. Nickerson, G. Krochmalnic, K. M. Wan, S. Penman, Chromatin architecture and nuclear
1597 RNA. *Proc Natl Acad Sci U S A* **86**, 177-181 (1989). DOI: 10.1073/pnas.86.1.177.
1598 104. J. A. Nickerson, The ribonucleoprotein network of the nucleus: a historical perspective. *Curr*
1599 *Opin Genet Dev* **75**, 101940 (2022). DOI: 10.1016/j.gde.2022.101940.
1600 105. J. Thakur, S. Henikoff, Architectural RNA in chromatin organization. *Biochem Soc Trans* **48**,
1601 1967-1978 (2020). DOI: 10.1042/BST20191226.
1602 106. D. Michieletto, N. Gilbert, Role of nuclear RNA in regulating chromatin structure and
1603 transcription. *Curr Opin Cell Biol* **58**, 120-125 (2019). DOI: 10.1016/j.ceb.2019.03.007.
1604 107. D. Peric-Hupkes, W. Meuleman, L. Pagie, S. W. Bruggeman, I. Solovei, W. Brugman, S. Graf,
1605 P. Flicek, R. M. Kerkhoven, M. van Lohuizen, M. Reinders, L. Wessels, B. van Steensel,
1606 Molecular maps of the reorganization of genome-nuclear lamina interactions during
1607 differentiation. *Mol Cell* **38**, 603-613 (2010). DOI: 10.1016/j.molcel.2010.03.016.
1608 108. H. Zhao, E. G. Sifakis, N. Sumida, L. Millan-Arino, B. A. Scholz, J. P. Svensson, X. Chen, A. L.
1609 Ronnegren, C. D. Mallet de Lima, F. S. Varnoosfaderani, C. Shi, O. Loseva, S. Yammine, M.
1610 Israelsson, L. S. Rathje, B. Nemeti, E. Fredlund, T. Helleday, M. P. Imreh, A. Gondor, PARP1-
1611 and CTCF-Mediated Interactions between Active and Repressed Chromatin at the Lamina
1612 Promote Oscillating Transcription. *Mol Cell* **59**, 984-997 (2015). DOI:
1613 10.1016/j.molcel.2015.07.019.
1614 109. T. Lucas, T. L. Hafer, H. G. Zhang, N. Molotkova, M. Kohwi, Discrete cis-acting element
1615 regulates developmentally timed gene-lamina relocation and neural progenitor competence in
1616 vivo. *Dev Cell* **56**, 2649-2663 e2646 (2021). DOI: 10.1016/j.devcel.2021.08.020.
1617 110. I. Solovei, M. Kreysing, C. Lanctot, S. Kosem, L. Peichl, T. Cremer, J. Guck, B. Joffe, Nuclear
1618 architecture of rod photoreceptor cells adapts to vision in mammalian evolution. *Cell* **137**, 356-
1619 368 (2009). DOI: 10.1016/j.cell.2009.01.052.
1620 111. J. Kind, L. Pagie, H. Ortabozkoyun, S. Boyle, S. S. de Vries, H. Janssen, M. Amendola, L. D.
1621 Nolen, W. A. Bickmore, B. van Steensel, Single-cell dynamics of genome-nuclear lamina
1622 interactions. *Cell* **153**, 178-192 (2013). DOI: 10.1016/j.cell.2013.02.028.
1623 112. Q. Bian, N. Khanna, J. Alvikas, A. S. Belmont, beta-Globin cis-elements determine differential
1624 nuclear targeting through epigenetic modifications. *J Cell Biol* **203**, 767-783 (2013). DOI:
1625 10.1083/jcb.201305027.
1626 113. X. Wong, T. R. Luperchio, K. L. Reddy, NET gains and losses: the role of changing nuclear
1627 envelope proteomes in genome regulation. *Curr Opin Cell Biol* **28**, 105-120 (2014). DOI:
1628 10.1016/j.ceb.2014.04.005.

114. J. C. Harr, T. R. Luperchio, X. Wong, E. Cohen, S. J. Wheelan, K. L. Reddy, Directed targeting of chromatin to the nuclear lamina is mediated by chromatin state and A-type lamins. *J Cell Biol* **208**, 33-52 (2015). DOI: 10.1083/jcb.201405110.
115. X. Wong, V. E. Hoskins, A. J. Melendez-Perez, J. C. Harr, M. Gordon, K. L. Reddy, Lamin C is required to establish genome organization after mitosis. *Genome Biol* **22**, 305 (2021). DOI: 10.1186/s13059-021-02516-7.
116. L. A. Watson, L. H. Tsai, In the loop: how chromatin topology links genome structure to function in mechanisms underlying learning and memory. *Curr Opin Neurobiol* **43**, 48-55 (2017). DOI: 10.1016/j.conb.2016.12.002.
117. J. Close, H. Xu, N. De Marco Garcia, R. Batista-Brito, E. Rossignol, B. Rudy, G. Fishell, Satb1 is an activity-modulated transcription factor required for the terminal differentiation and connectivity of medial ganglionic eminence-derived cortical interneurons. *J Neurosci* **32**, 17690-17705 (2012). DOI: 10.1523/JNEUROSCI.3583-12.2012.
118. S. Galande, T. Kohwi-Shigematsu, Poly(ADP-ribose) polymerase and Ku autoantigen form a complex and synergistically bind to matrix attachment sequences. *J Biol Chem* **274**, 20521-20528. (1999). DOI:
119. W. M. Liu, F. K. Guerra-Vladusic, S. Kurakata, R. Lupu, T. Kohwi-Shigematsu, HMG-I(Y) recognizes base-unpairing regions of matrix attachment sequences and its increased expression is directly linked to metastatic breast cancer phenotype. *Cancer Res* **59**, 5695-5703. (1999). DOI:
120. M. Levo, J. Raimundo, X. Y. Bing, Z. Sisco, P. J. Batut, S. Ryabichko, T. Gregor, M. S. Levine, Transcriptional coupling of distant regulatory genes in living embryos. *Nature* **605**, 754-760 (2022). DOI: 10.1038/s41586-022-04680-7.
121. P. J. Batut, X. Y. Bing, Z. Sisco, J. Raimundo, M. Levo, M. S. Levine, Genome organization controls transcriptional dynamics during development. *Science* **375**, 566-570 (2022). DOI: 10.1126/science.abi7178.
122. G. Mohana, J. Dorier, X. Li, M. Mouginot, R. C. Smith, H. Malek, M. Leleu, D. Rodriguez, J. Khadka, P. Rosa, P. Cousin, C. Iseli, S. Restrepo, N. Guex, B. D. McCabe, A. Jankowski, M. S. Levine, M. C. Gambetta, Chromosome-level organization of the regulatory genome in the Drosophila nervous system. *Cell* **186**, 3826-3844 e3826 (2023). DOI: 10.1016/j.cell.2023.07.008.
123. L. Lizana, Y. B. Schwartz, The scales, mechanisms, and dynamics of the genome architecture. *Sci Adv* **10**, eadm8167 (2024). DOI: 10.1126/sciadv.adm8167.
124. W. Huber, V. J. Carey, R. Gentleman, S. Anders, M. Carlson, B. S. Carvalho, H. C. Bravo, S. Davis, L. Gatto, T. Girke, R. Gottardo, F. Hahne, K. D. Hansen, R. A. Irizarry, M. Lawrence, M. I. Love, J. MacDonald, V. Obenchain, A. K. Oles, H. Pages, A. Reyes, P. Shannon, G. K. Smyth, D. Tenenbaum, L. Waldron, M. Morgan, Orchestrating high-throughput genomic analysis with Bioconductor. *Nat Methods* **12**, 115-121 (2015). DOI: 10.1038/nmeth.3252.
125. A. B. Olshen, E. S. Venkatraman, R. Lucito, M. Wigler, Circular binary segmentation for the analysis of array-based DNA copy number data. *Biostatistics* **5**, 557-572 (2004). DOI: 10.1093/biostatistics/kxh008.
126. B. Gel, A. Diez-Villanueva, E. Serra, M. Buschbeck, M. A. Peinado, R. Malinverni, regioneR: an R/Bioconductor package for the association analysis of genomic regions based on permutation tests. *Bioinformatics* **32**, 289-291 (2016). DOI: 10.1093/bioinformatics/btv562.
127. Z. Gu, R. Eils, M. Schlesner, N. Ishaque, EnrichedHeatmap: an R/Bioconductor package for comprehensive visualization of genomic signal associations. *BMC Genomics* **19**, 234 (2018). DOI: 10.1186/s12864-018-4625-x.
128. Z. Gu, L. Gu, R. Eils, M. Schlesner, B. Brors, circlize Implements and enhances circular visualization in R. *Bioinformatics* **30**, 2811-2812 (2014). DOI: 10.1093/bioinformatics/btu393.
129. C. Lazaris, S. Kelly, P. Ntziachristos, I. Aifantis, A. Tsirigos, HiC-bench: comprehensive and reproducible Hi-C data analysis designed for parameter exploration and benchmarking. *BMC Genomics* **18**, 22 (2017). DOI: 10.1186/s12864-016-3387-6.
130. A. Kloetgen, P. Thandapani, P. Ntziachristos, Y. Ghebrechristos, S. Nomikou, C. Lazaris, X. Chen, H. Hu, S. Bakogianni, J. Wang, Y. Fu, F. Boccalatte, H. Zhong, E. Paietta, T. Trimarchi, Y. Zhu, P. Van Vlierberghe, G. G. Inghirami, T. Lionnet, I. Aifantis, A. Tsirigos, Three-

1684 dimensional chromatin landscapes in T cell acute lymphoblastic leukemia. *Nat Genet* **52**, 388-
1685 400 (2020). DOI: 10.1038/s41588-020-0602-9.
1686 131. B. Langmead, S. L. Salzberg, Fast gapped-read alignment with Bowtie 2. *Nat Methods* **9**, 357-
1687 359 (2012). DOI: 10.1038/nmeth.1923.
1688 132. A. Tsirigos, N. Haiminen, E. Bilal, F. Utro, GenomicTools: a computational platform for
1689 developing high-throughput analytics in genomics. *Bioinformatics* **28**, 282-283 (2012). DOI:
1690 10.1093/bioinformatics/btr646.
1691 133. M. Imakaev, G. Fudenberg, R. P. McCord, N. Naumova, A. Goloborodko, B. R. Lajoie, J.
1692 Dekker, L. A. Mirny, Iterative correction of Hi-C data reveals hallmarks of chromosome
1693 organization. *Nat Methods* **9**, 999-1003 (2012). DOI: 10.1038/nmeth.2148.
1694 134. Y. Gong, C. Lazaris, T. Sakellaropoulos, A. Lozano, P. Kambadur, P. Ntziachristos, I. Aifantis,
1695 A. Tsirigos, Stratification of TAD boundaries reveals preferential insulation of super-enhancers
1696 by strong boundaries. *Nat Commun* **9**, 542 (2018). DOI: 10.1038/s41467-018-03017-1.
1697 135. N. C. Durand, M. S. Shamim, I. Machol, S. S. Rao, M. H. Huntley, E. S. Lander, E. L. Aiden,
1698 Juicer Provides a One-Click System for Analyzing Loop-Resolution Hi-C Experiments. *Cell*
1699 *Syst* **3**, 95-98 (2016). DOI: 10.1016/j.cels.2016.07.002.
1700 136. S. Heinz, C. Benner, N. Spann, E. Bertolino, Y. C. Lin, P. Laslo, J. X. Cheng, C. Murre, H.
1701 Singh, C. K. Glass, Simple combinations of lineage-determining transcription factors prime cis-
1702 regulatory elements required for macrophage and B cell identities. *Mol Cell* **38**, 576-589
1703 (2010). DOI: 10.1016/j.molcel.2010.05.004.
1704 137. Y. Zhang, T. Liu, C. A. Meyer, J. Eeckhoute, D. S. Johnson, B. E. Bernstein, C. Nusbaum, R.
1705 M. Myers, M. Brown, W. Li, X. S. Liu, Model-based analysis of ChIP-Seq (MACS). *Genome*
1706 *Biol* **9**, R137 (2008). DOI: gb-2008-9-9-r137 [pii] 10.1186/gb-2008-9-9-r137.
1707 138. W. J. Kent, A. S. Zweig, G. Barber, A. S. Hinrichs, D. Karolchik, BigWig and BigBed: enabling
1708 browsing of large distributed datasets. *Bioinformatics* **26**, 2204-2207 (2010). DOI:
1709 10.1093/bioinformatics/btq351.
1710 139. J. M. Zullo, I. A. Demarco, R. Pique-Regi, D. J. Gaffney, C. B. Epstein, C. J. Spooner, T. R.
1711 Luperchio, B. E. Bernstein, J. K. Pritchard, K. L. Reddy, H. Singh, DNA sequence-dependent
1712 compartmentalization and silencing of chromatin at the nuclear lamina. *Cell* **149**, 1474-1487
1713 (2012). DOI: 10.1016/j.cell.2012.04.035.
1714 140. A. Favorov, L. Mularoni, L. M. Cope, Y. Medvedeva, A. A. Mironov, V. J. Makeev, S. J.
1715 Wheelan, Exploring massive, genome scale datasets with the GenometriCorr package. *PLoS*
1716 *Comput Biol* **8**, e1002529 (2012). DOI: 10.1371/journal.pcbi.1002529.
1717 141. A. Akalin, V. Franke, K. Vlahovicek, C. E. Mason, D. Schubeler, Genomation: a toolkit to
1718 summarize, annotate and visualize genomic intervals. *Bioinformatics* **31**, 1127-1129 (2015).
1719 DOI: 10.1093/bioinformatics/btu775.
1720 142. A. R. Quinlan, I. M. Hall, BEDTools: a flexible suite of utilities for comparing genomic features.
1721 *Bioinformatics* **26**, 841-842 (2010). DOI: 10.1093/bioinformatics/btq033.
1722

FIGURE 1

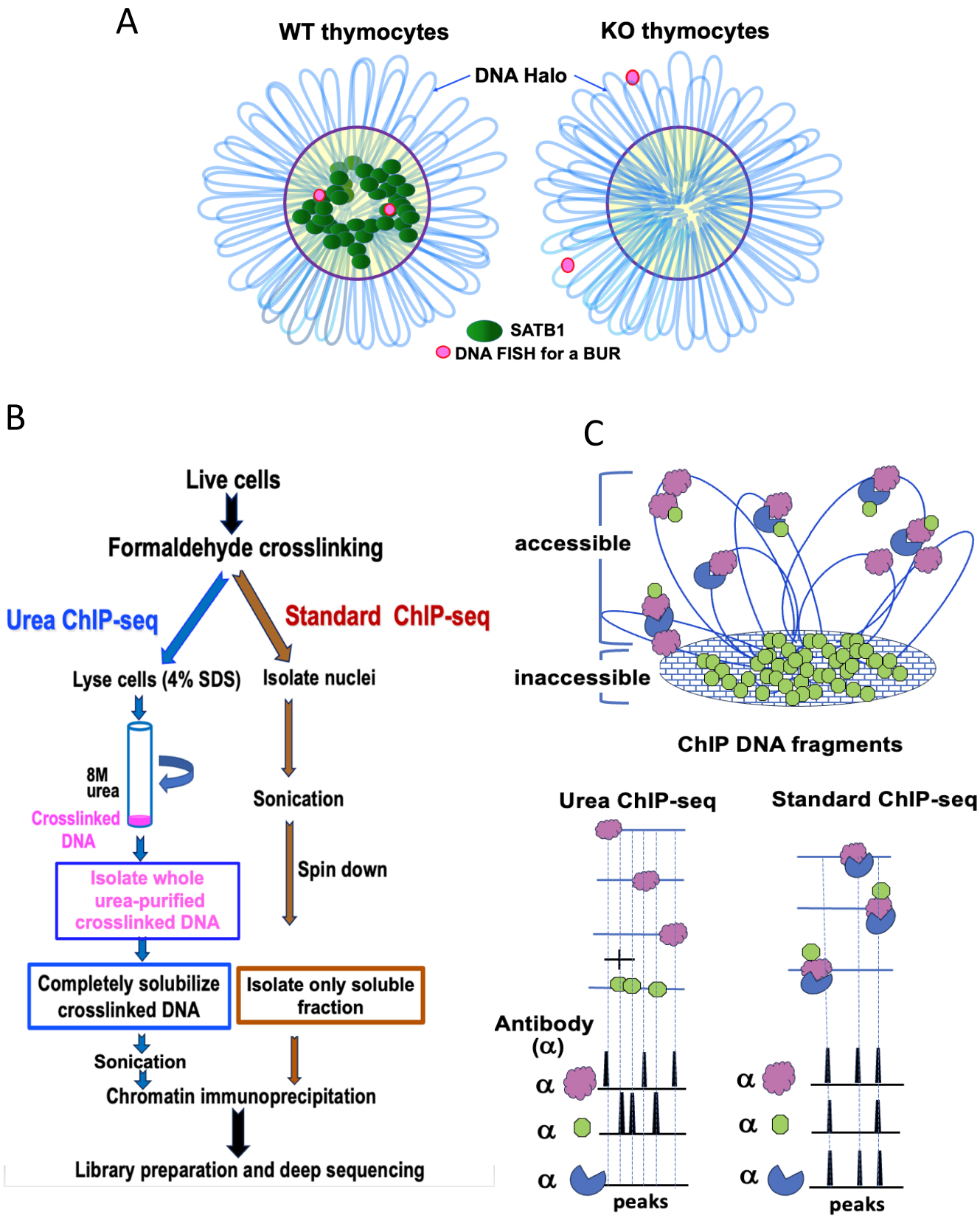
A
WT thymocytes
KO thymocytes
DNA Halo
SATB1
DNA FISH for a BUR
B
Live cells
Formaldehyde crosslinking
Urea ChIP-seq
Standard ChIP-seq
Lyse cells (4% SDS)
Isolate nuclei
8M urea
Crosslinked DNA
Sonication
Spin down
Isolate whole urea-purified crosslinked DNA
Completely solubilize crosslinked DNA
Isolate only soluble fraction
Sonication
Chromatin immunoprecipitation
Library preparation and deep sequencing
C
accessible
inaccessible
ChIP DNA fragments
Urea ChIP-seq
Standard ChIP-seq
Antibody (α)
α
α
α
peaks
α
α
α
peaks

FIGURE 2

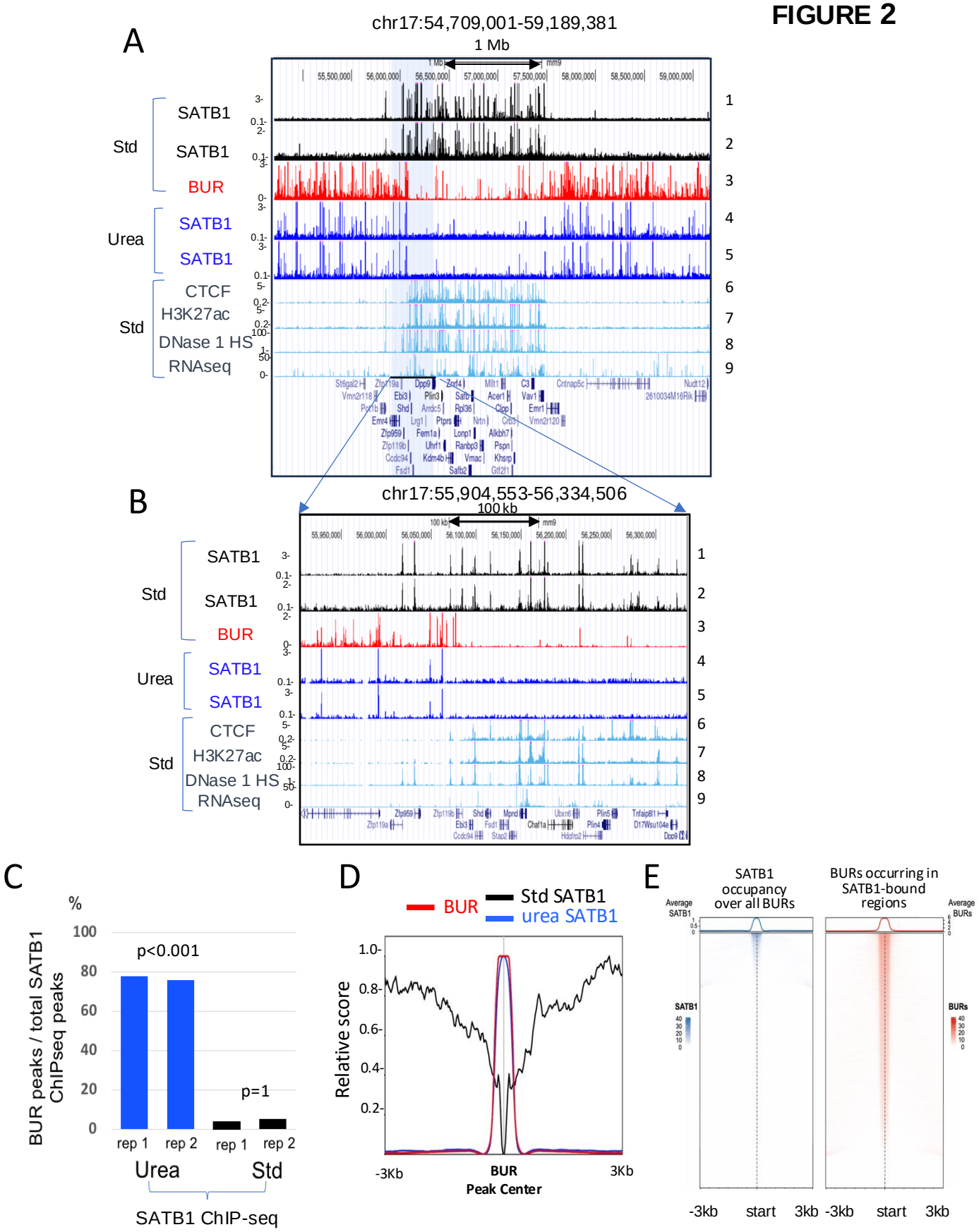
A
chr17:54,709,001-59,189,381
1 Mb
Std
SATB1
SATB1
BUR
Urea
SATB1
SATB1
Std
CTCF
H3K27ac
DNase 1 HS
RNAseq
B
chr17:55,904,553-56,334,506
100 kb
C
BUR peaks / total SATB1 ChIPseq peaks
%
p<0.001
p=1
rep 1
rep 2
rep 1
rep 2
Urea
Std
SATB1 ChIP-seq
D
BUR
Std SATB1
urea SATB1
Relative score
-3Kb
BUR
Peak Center
3Kb
E
SATB1 occupancy over all BURs
BURs occurring in SATB1-bound regions
Average SATB1
Average BURs
SATB1
BURs
-3kb
start
3kb
-3kb
start
3kb

FIGURE 3

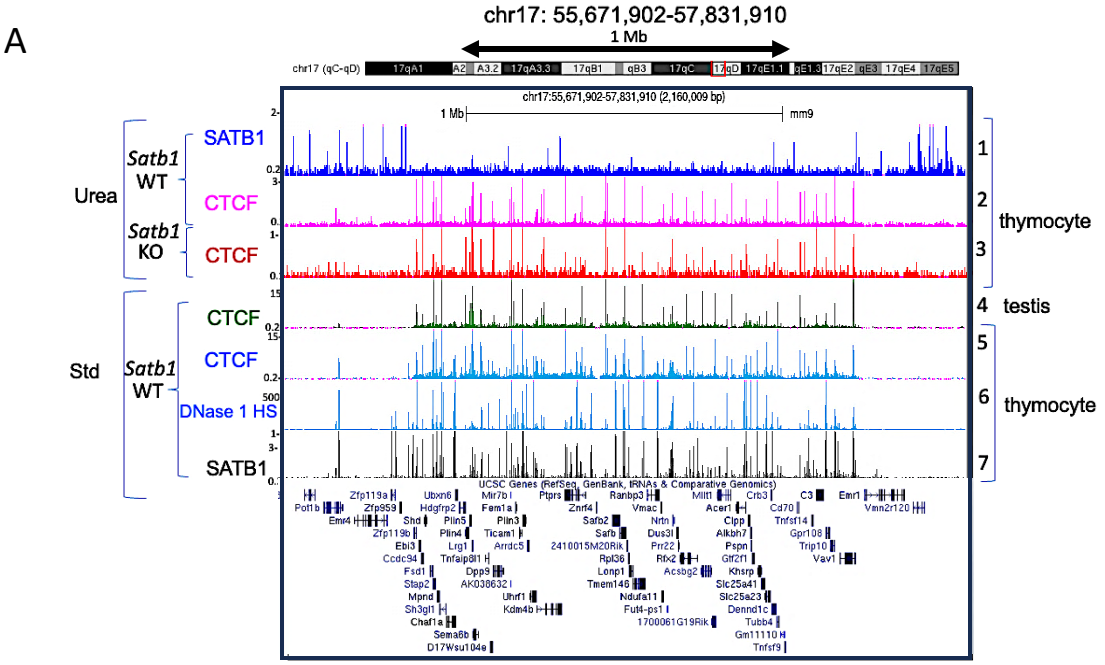
A
chr17: 55,671,902-57,831,910
1 Mb
Urea
Satb1 WT
SATB1
CTCF
Satb1 KO
CTCF
Std
Satb1 WT
CTCF
CTCF
DNase 1 HS
SATB1
thymocyte
testis
thymocyte

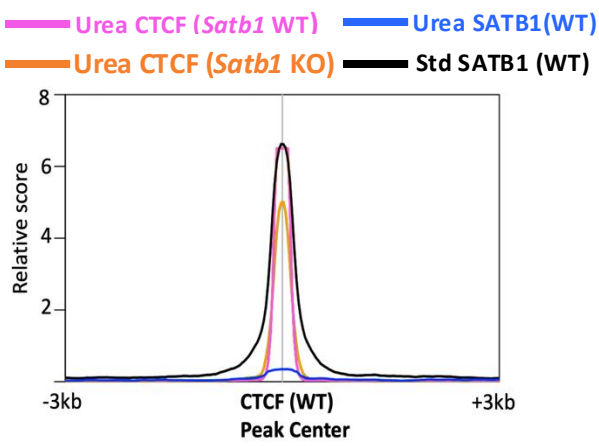
B
Urea CTCF (Satb1 WT)
Urea SATB1(WT)
Urea CTCF (Satb1 KO)
Std SATB1 (WT)
Relative score
-3kb
CTCF (WT)
Peak Center
+3kb

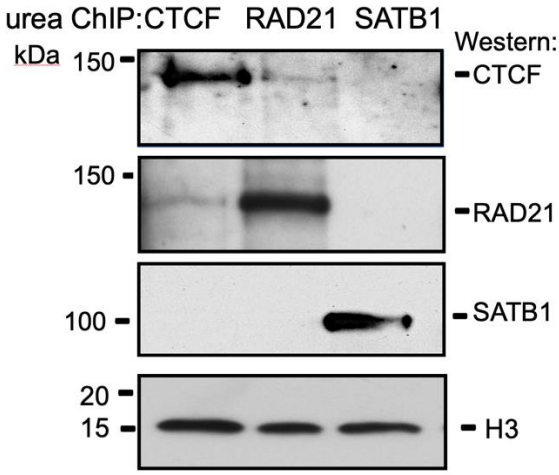
C
urea ChIP:CTCF RAD21 SATB1
kDa
Western:
CTCF
RAD21
SATB1
H3

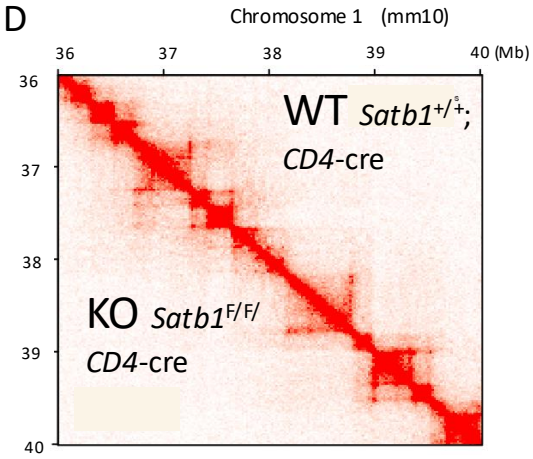
D
Chromosome 1 (mm10)
40 (Mb)
WT Satb1+/+;
CD4-cre
KO Satb1F/F/
CD4-cre

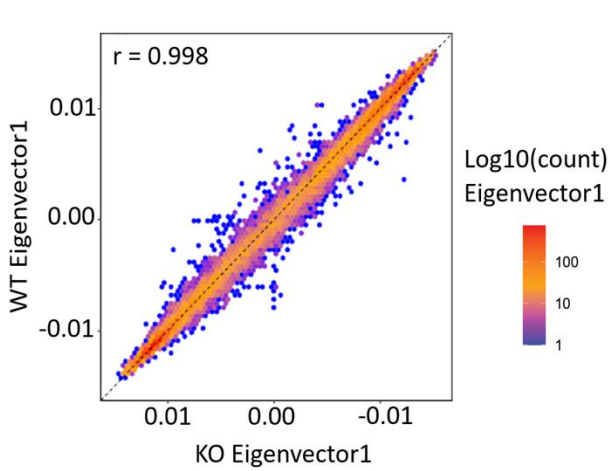
E
r = 0.998
WT Eigenvector1
KO Eigenvector1
Log10(count)
Eigenvector1

FIGURE 4

Rag1/Rag2 locus

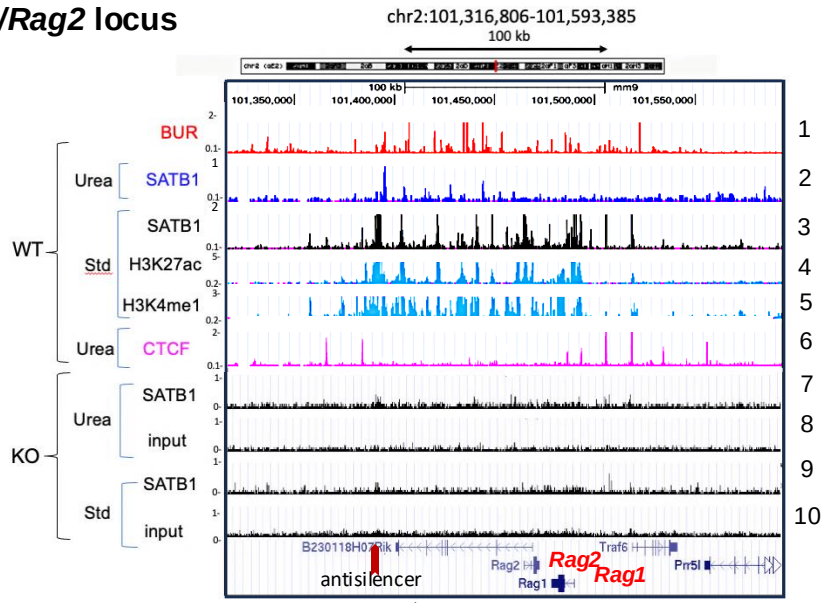

Foxp3 locus

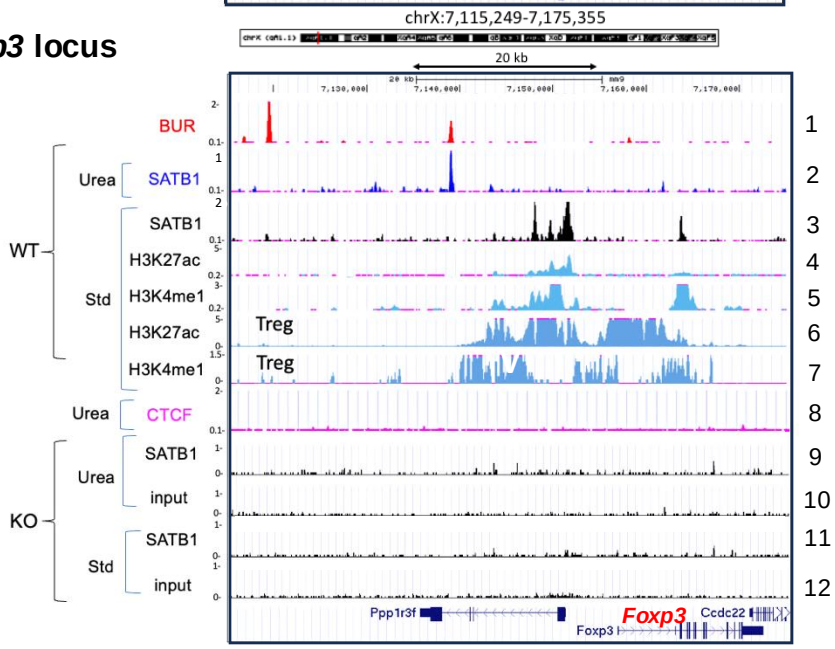

Runx3 locus

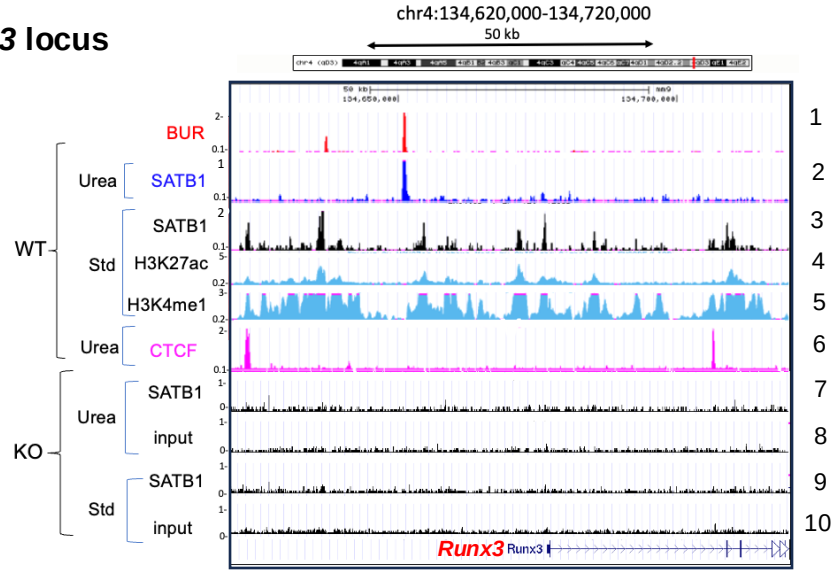

FIGURE 5

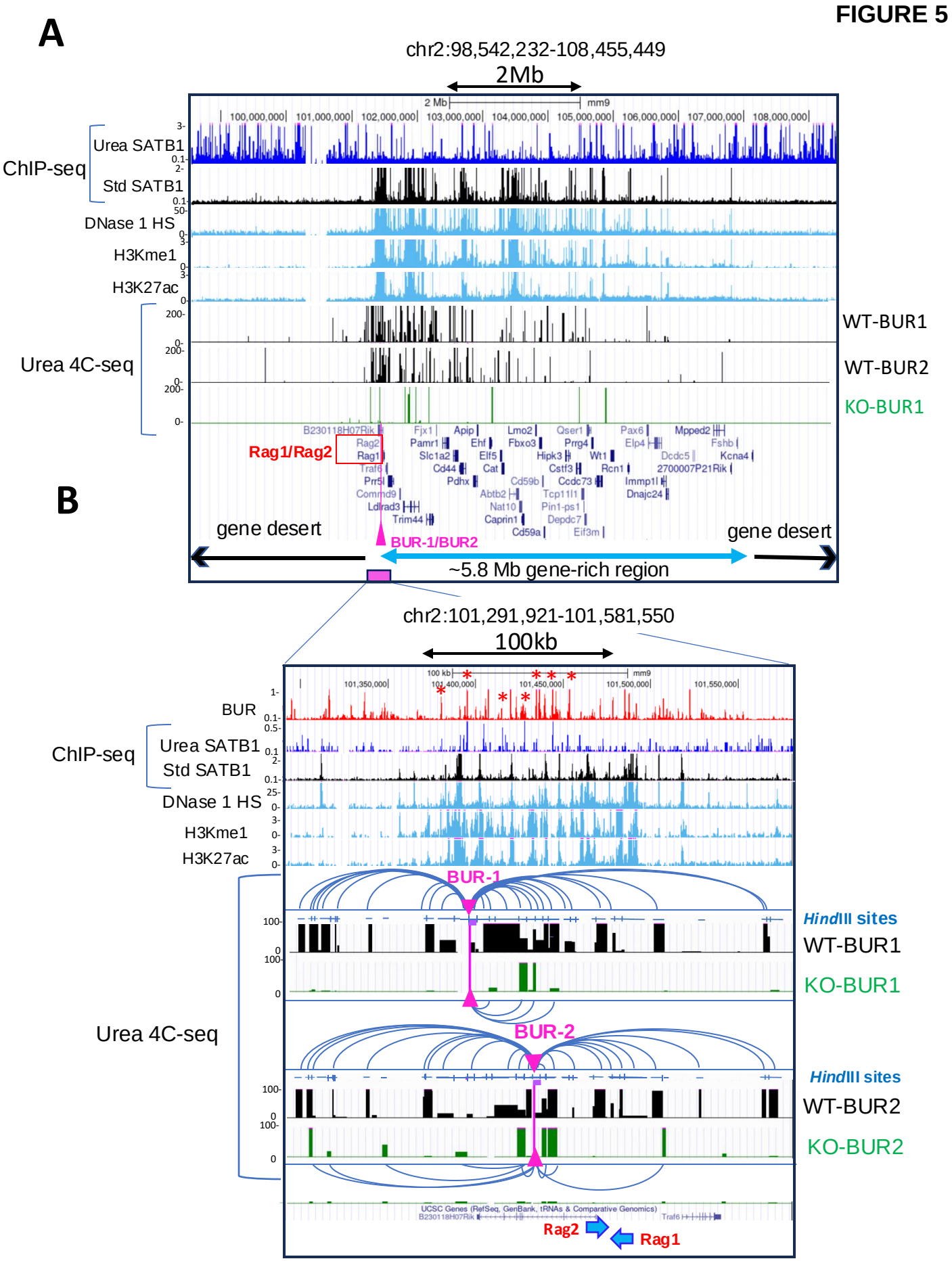
A
chr2:98,542,232-108,455,449
2Mb
ChIP-seq
Urea SATB1
Std SATB1
DNase 1 HS
H3Kme1
H3K27ac
Urea 4C-seq
WT-BUR1
WT-BUR2
KO-BUR1
Rag1/Rag2
gene desert
BUR-1/BUR2
gene desert
~5.8 Mb gene-rich region
B
chr2:101,291,921-101,581,550
100kb
BUR
ChIP-seq
Urea SATB1
Std SATB1
DNase 1 HS
H3Kme1
H3K27ac
BUR-1
HindIII sites
WT-BUR1
KO-BUR1
Urea 4C-seq
BUR-2
HindIII sites
WT-BUR2
KO-BUR2
Rag2
Rag1

FIGURE 6

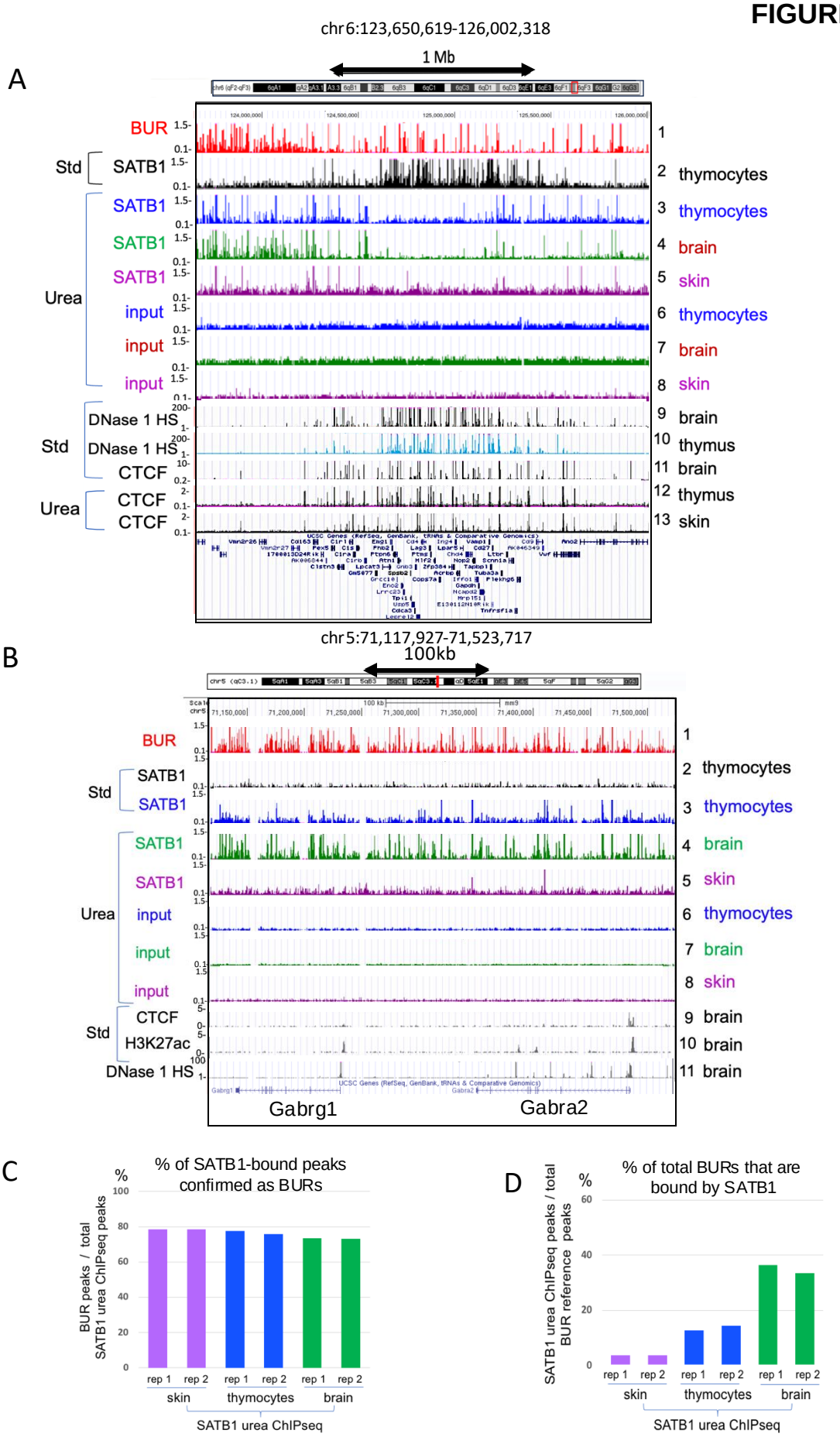
A
chr6:123,650,619-126,002,318
1 Mb
BUR
Std
SATB1
Urea
input
DNase 1 HS
CTCF
1 2 3 4 5 6 7 8 9 10 11 12 13
thymocytes
brain
skin
thymus
B
chr5:71,117,927-71,523,717
100kb
H3K27ac
Gabrg1
Gabra2
C
% of SATB1-bound peaks confirmed as BURs
BUR peaks / total SATB1 urea ChIPseq peaks
rep 1
rep 2
SATB1 urea ChIPseq
D
% of total BURs that are bound by SATB1
SATB1 urea ChIPseq peaks / total BUR reference peaks

FIGURE 7

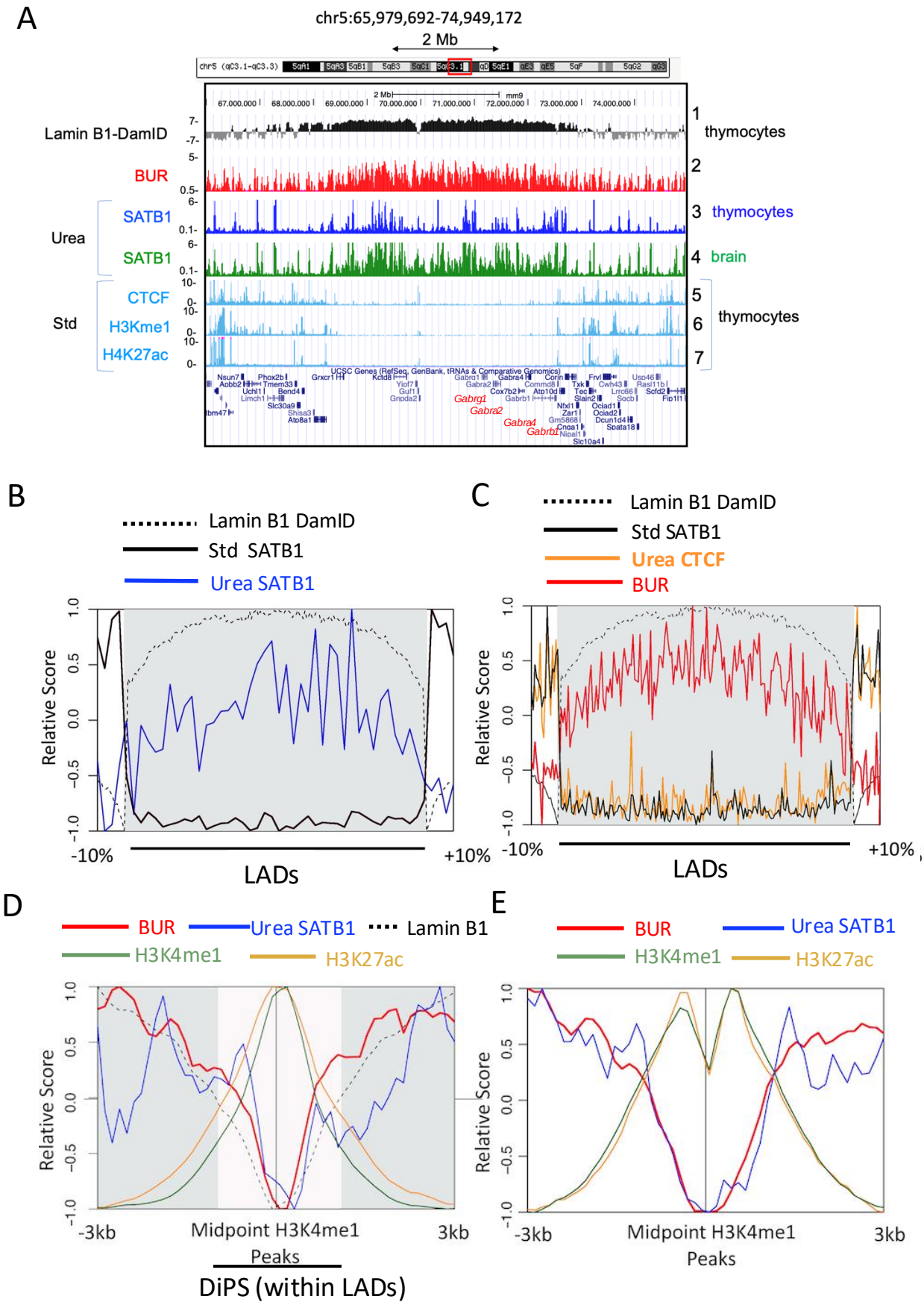
A
chr5:65,979,692-74,949,172
2 Mb
Lamin B1-DamID
BUR
Urea
SATB1
SATB1
Std
CTCF
H3Kme1
H4K27ac
1 thymocytes
2
3 thymocytes
4 brain
5
6 thymocytes
7
B
Lamin B1 DamID
Std SATB1
Urea SATB1
Relative Score
-10%
+10%
LADs
C
Lamin B1 DamID
Std SATB1
Urea CTCF
BUR
Relative Score
-10%
+10%
LADs
D
BUR
Urea SATB1
Lamin B1
H3K4me1
H3K27ac
Relative Score
-3kb
Midpoint H3K4me1
3kb
Peaks
DiPS (within LADs)
E
BUR
Urea SATB1
H3K4me1
H3K27ac
Relative Score
-3kb
Midpoint H3K4me1
3kb
Peaks

FIGURE 8

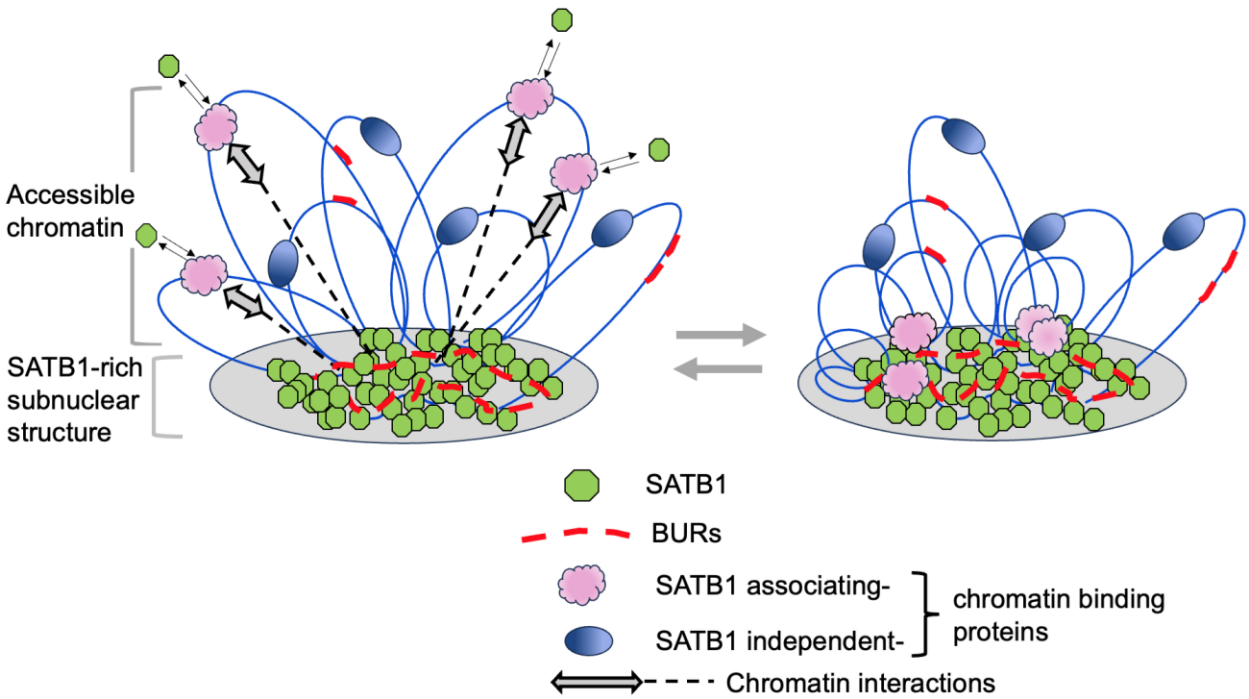
Accessible chromatin
SATB1-rich subnuclear structure
SATB1
BURs
SATB1 associating-
SATB1 independent-
chromatin binding proteins
Chromatin interactions

Figure Supplements and Supplementary Tables

Identification	Title	Page Index 1
Figure 2—figure supplement 1	Zoomed-in view of Figure 2B showing precise coincidence of SATB1 urea ChIP-seq peaks with a subset of BURs	2
Figure 3—figure supplement 1	Similar DNA binding profiles for PRC2 core subunits obtained by standard ChIP-seq and Urea ChIP-seq	3
Figure 3—figure supplement 2	SATB1 does not directly co-bind chromatin with CTCF and RAD21 or has a role in TAD formation	4
Figure 4—figure supplement 1	Standard ChIP-seq for SATB1 produces non-specific peaks in *Satb1*$^{-/-}$ thymocytes	5
Figure 5—figure supplement 1	Urea 4C-seq protocol	6
Figure 5—figure supplement 2	Long-range chromatin interactions from BUR-1 traverse TADs	7
Figure 5—figure supplement 3	Long-distance interactions covering distal gene-rich regions by BUR-1	8
Figure 5—figure supplement 4	Genes within the gene-rich region (chr2:98,542,232-108,455,449) that exhibit SATB1-dependent expression	9
Figure 7—figure supplement 1	BURs and BUR-bound SATB1 largely co-map with LaminB1-DamID	10
Figure 7—figure supplement 2	Some SATB1-bound BURs located in SATB1-dependent gene loci are outside of LADs	11
Figure 7—figure supplement 3	SATB1 occupancy relative to BURs, and BUR signal relative to SATB1-bound loci	12
Figure 7—figure supplement 4	Interaction sites from BUR-1 or BUR-2 are mostly confined to the inter-LAD region	13
Supplementary Table 1 and Table 2	Supplementary Table 1. Intersection analysis of ChIP-seq samples Supplement Table 2. ChIP-seq sample ID and peak number	14
Supplementary Table 3 and Table 4	Supplementary Table 3. Intersection analysis of WT and KO ChIP-seq samples Supplementary Table 4. WT and KO ChIP-seq sample ID and total peak number	15

Figure 2—figure supplement 1

A

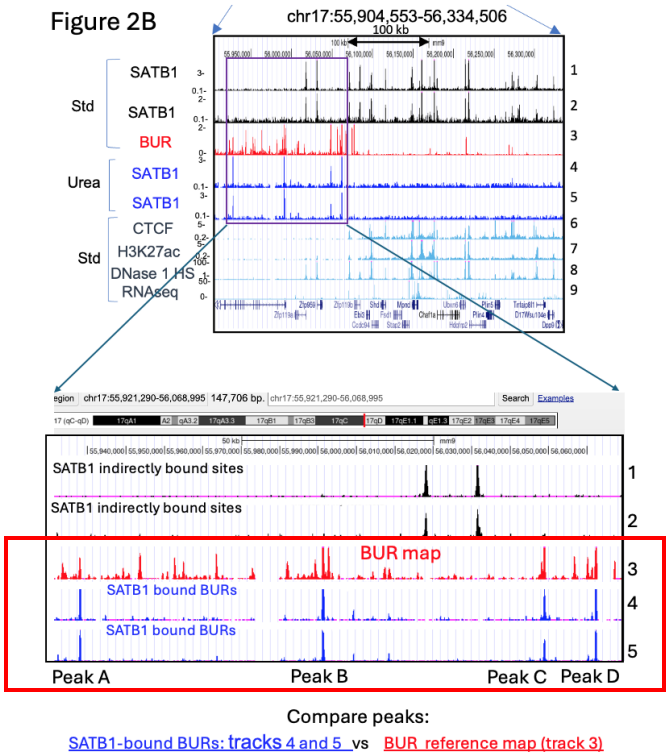

B

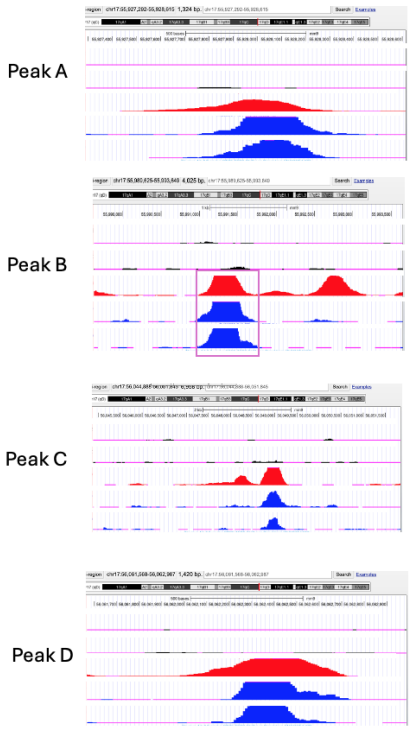

C

Peak B BUR

```
mm9_dna range=chr17:55991036-55991629
TACACGGCAGGCAGGCAAGAGCAGGACCAAATCTGGCTATCCTGACCGCA
CTCATGTCTGCCATAAGGATGGCTCACTCACAGTGTCCGTATTCAGGGCC
AGCCCTACTATGCTATCCAGGTGCACATCTCACAAGTTTTGTAATTCCCA
TGTCTATAGGTAGCCAAGGGATTTATTTGCATTAATTGTGATTTTGAATG
GACTTGTTTGACCTTTATCAATCATATTTTATTTGAGCTTCAATATACAA
TTTGTGTTATTATTGAGTATGTATTTTGTATTATTATTTAGTTTTAAGTG
TATTATTAGTAGTAGTATTAGTATTATTATTATGTGTATTTGTGGTATTA
TATGTCATATATGTGCCCATGAGCATATTCATGAAGATGCTAGAATTAAA
TGTTGGATATTCTGCTCTCTCATTGTCTTGACACAGGGTCTTTCTCTGAA
CCTGGAAAATTTCTGCCCAACAGGAAACCTCCATGATCCTTCTGACTCCA
TCCTTCCAAGTACTGAAGTAGCAGGTGTATATCTAAGCACACCCAGGTCT
CACATGGGTGCTGAGGATGTGAACTCAGGTACTCACGCTTACTG
```

ATC sequence stretch

ATG sequence stretch

Figure 2—figure supplement 1. **Zoomed-in view of Figure 2B showing precise coincidence of SATB1 urea ChIP-seq peaks with a subset of BURs.**

A) Peak A, Peak B, Peak C, and Peak D shown in tracks 4 and 5 overlap with BURs in track 3. The bottom panel is a zoom-in view of the top panel (from Figure 2B). B) High-resolution views of each peak region showing precise co-mapping of BUR (red peak) and SATB1 peak (blue peak).

C) A representative BUR sequence (a cluster of ATC/ATC sequences) from Peak B.

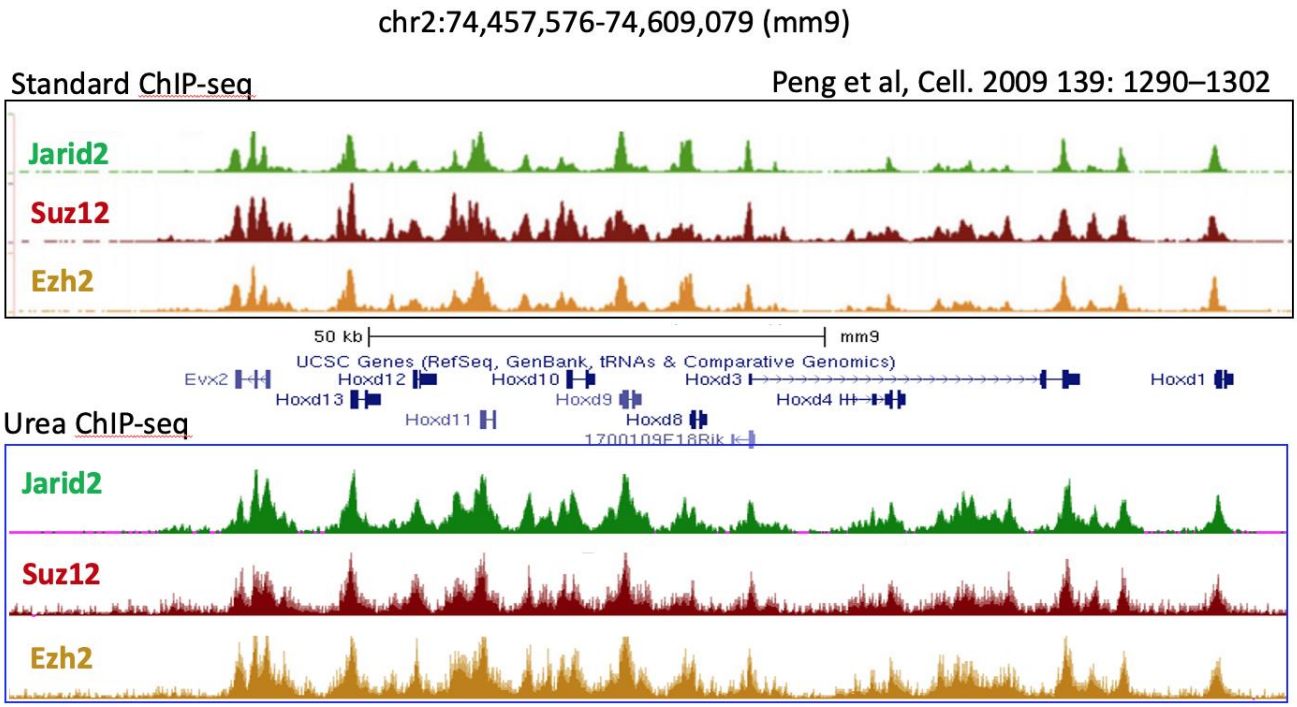

Figure 3—figure supplement 1. **Similar DNA binding profiles for PRC2 core subunits obtained by standard ChIP-seq and Urea ChIP-seq**

The DNA binding profiles of PRC2 core subunits, Jarid2, Suz12, and Ezh2 obtained by standard ChIP-seq (Ref 73) [Peng et al., Cell, 2009, GEO repository (GSE18776)] were compared against the DNA binding profiles of these proteins by urea ChIP-seq. Their binding profiles in the *Hoxd* cluster region on chromosome 2 (mm9) are shown. Their DNA binding profiles by urea ChIP-seq and by standard ChIP-seq are very similar.

Figure 3—figure supplement 2

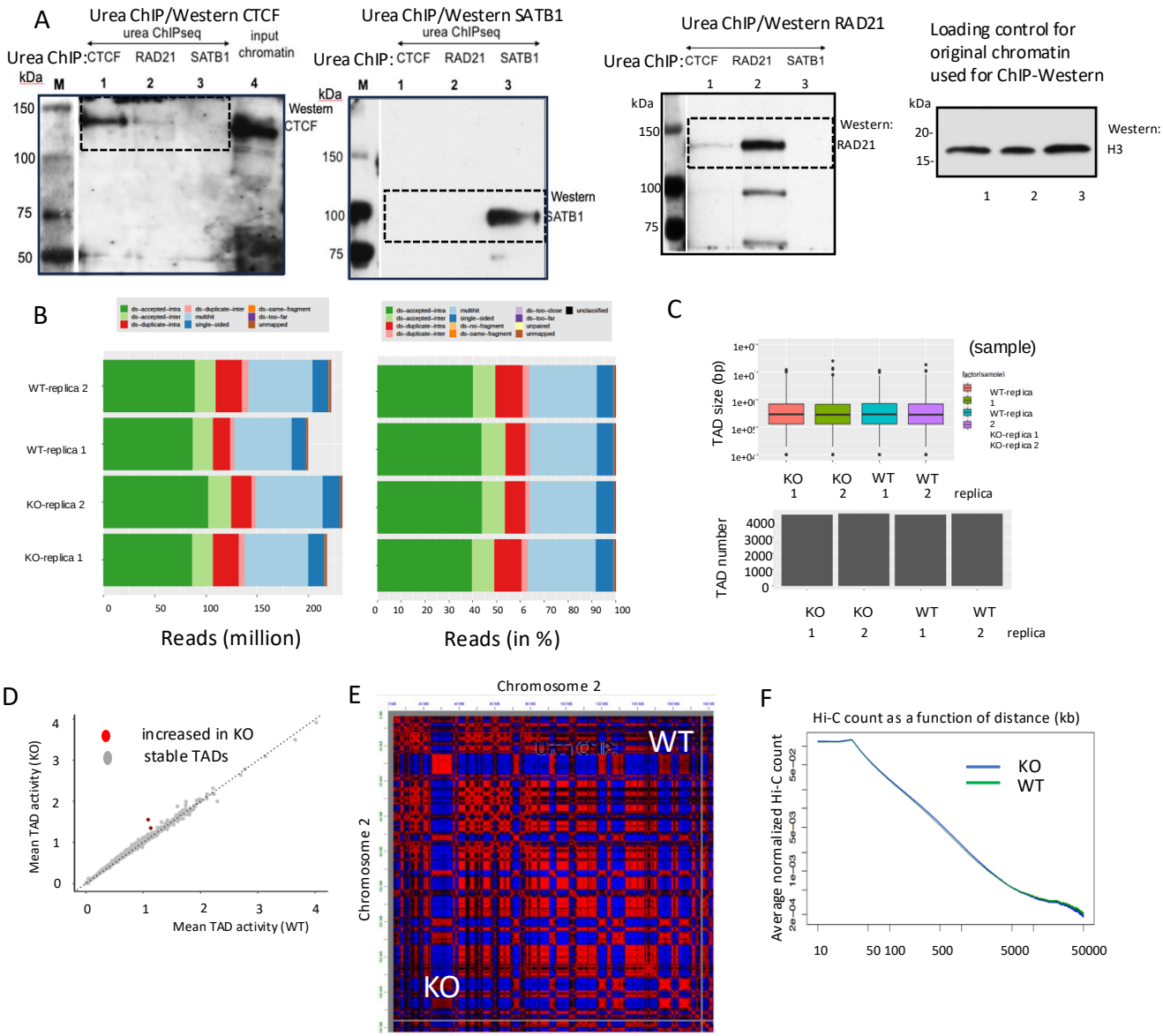

Figure 3—figure supplement 2. **SATB1 does not directly co-bind chromatin with CTCF and RAD21 or has a role in TAD formation.**

(A) Urea ChIP-Western studies for CTCF, RAD21 and SATB1. Original data for Figure 2C is shown. The excised areas are indicated by dotted boxes (first three panels). Western blot with the anti-H3 antibody shows that the original urea-purified chromatin samples before ChIP were similar in amount (right panel). **(B)** Read alignment statistics for Hi-C datasets, as absolute reads (left) and relative reads (in %, right). "ds.accepted.intra" are all intra-chromosomal reads used for all downstream analyses. **(C)** Distribution of TAD sizes and number of TAD calls per sample using hic-ratio TAD caller at 10kb bin resolution and the insulation score of 100kb windows. **(D)** Scatter plot of pair-wise comparisons of TAD activities (the sum of normalized Hi-C chromatin contacts inside the TAD in WT) between WT and KO thymocyte samples, showing well-conserved intra-TAD activity in KO thymocytes. **(E)** The Pearson correlation estimates computed between the counts for every pair of 10kb bins on chromosome 2 shows that WT (control: upper right triangle) and KO (observed: lower left triangle) thymocytes have no difference in compartmentalization. The compartment A (red) and compartment B (blue). **(F)** The scaling plots displaying how the Hi-C contacts decrease as a function of genomic distance.

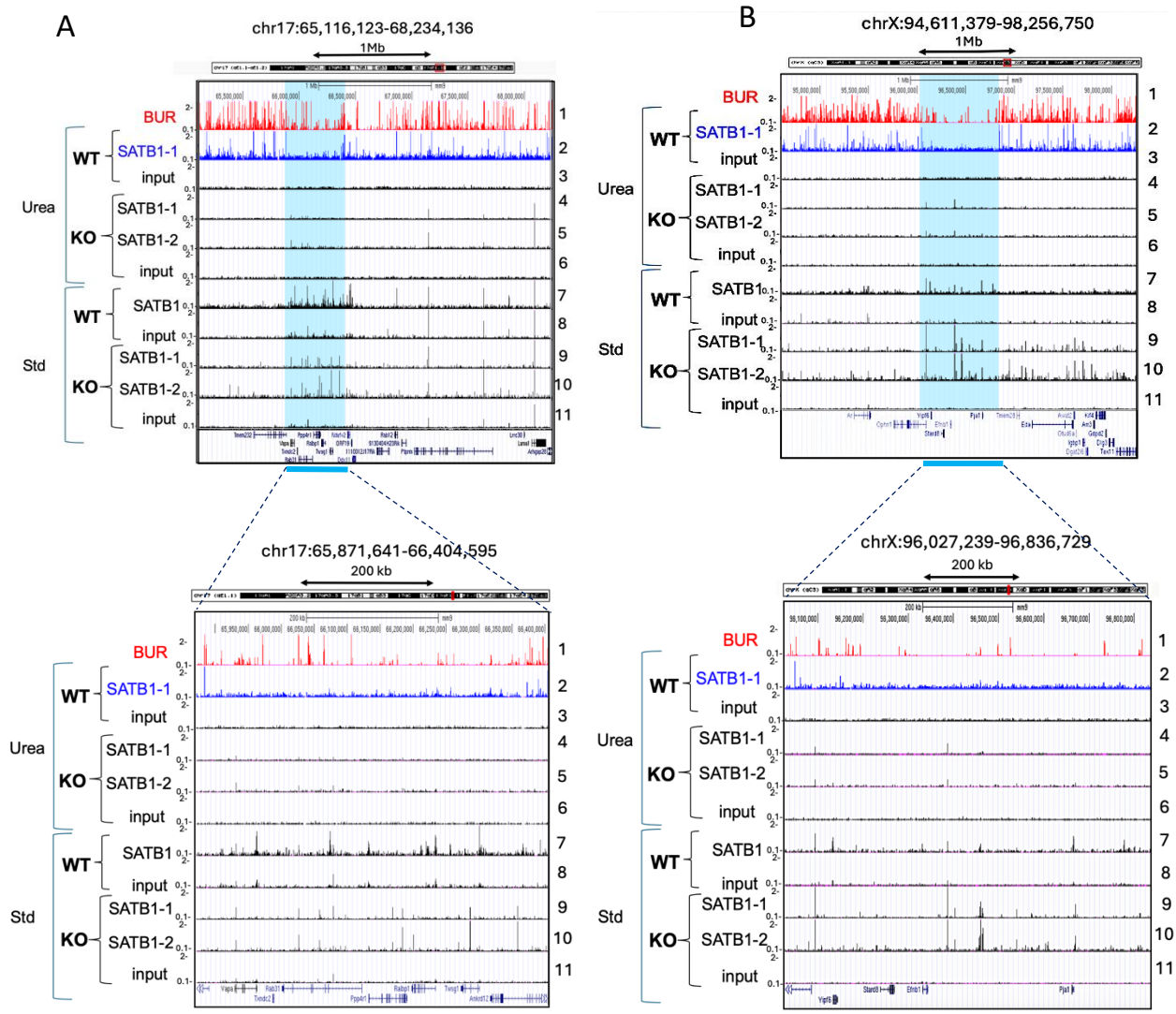

***Figure 4—figure supplement 1*. Standard ChIP-seq for SATB1 produces non-specific peaks in *Satb1*$^{-/-}$ thymocytes. (A)** Urea ChIP-seq (Urea) and std ChIP-seq (Std) profiles for SATB1 and input chromatin in a randomly chosen, 3.12 Mb region in chromosome 17 shows appearance of some peaks in input chromatin from std ChIP-seq that match with peaks for SATB1 in std ChIP-seq (top). For *Satb1*$^{-/-}$ thymocytes (KO), using either anti-SATB1 antibody 1583 (rabbit polyclonal, SATB1-1) or rabbit monoclonal ab109122 (SATB1-2), urea and std ChIP-seq experiments for SATB1 were performed. With std ChIP-seq, multiple peaks were generated in KO thymocytes in the similar regions observed in WT thymocytes (panel A track 7 versus 9 and 10), while urea ChIP-seq produced only few peaks (panel A top, track 2 versus 4 and 5). A zoomed-in view of the blue-highlighted SATB1-clustered regions (bottom) shows that in standard ChIP-seq, multiple peaks in KO thymocytes co-mapped with peaks in WT thymocytes, while others did not (panel A bottom, track 7 versus 9 and 10). **(B)** Another randomly chosen 3.45 Mb region in X chromosome (panel B top) and its zoom-in view (panel B bottom) shows high incidence of std ChIP-seq peaks in KO thymocytes co-mapping with std ChIP-seq peaks in WT thymocytes (tracks 7 versus 9 and 10).

Figure 5—figure supplement 1

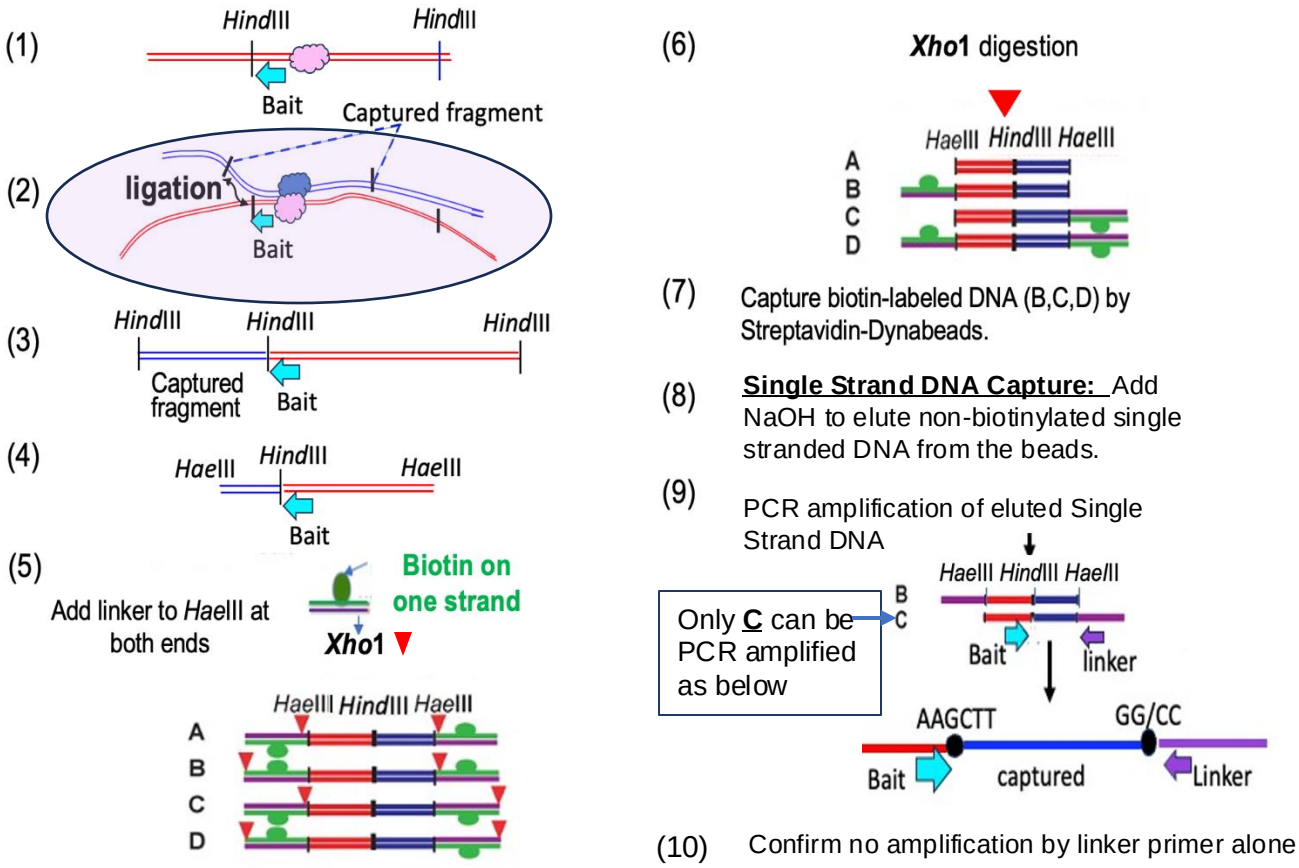

Figure 5—figure supplement 1. **Urea 4C-seq protocol. Starting with urea-ultracentrifugation purified formaldehyde crosslinked chromatin**: **(1)** A bait sequence is designed adjacent to a *Hind*III site of a *Hind*III–*Hind*III fragment containing SATB1 bound site (e.g. BUR-1). **(2)** Ligation is performed to ligate the original SATB1-bound fragment (bait) with other fragments whose close proximity was fixed by formaldehyde at the time of crosslinking and presumably retained after urea purification. The fixed chromatin structure with proximity is illustrated by pink shade. **(3)** Chromatin is decrosslinked and purified. **(4)** Ligated genomic DNA fragments are digested with *Hae*III (secondary restriction enzyme). **(5)** A Linker fragment containing an *Xho*1 site and Biotin labeled on one strand is blunt-end ligated to *Hae*III sites of the ligated genomic DNA fragments shown in step 4 to generate A, B, C, D double stranded fragments. The *Xho* 1 sites are indicated by red arrowhead. **(6)** The ligated products are digested with *Xho*1.
(7) Biotin-labeled double stranded DNA (B, C, and D) are captured by Streptavidin-Dynabeads. **(8)** The beads are treated with NaOH to convert DNA to single strand DNA. This will result in dissociation and elution of non-biotinylated single strand DNA (derived from B and C) from the Dynabeads. **(9)** Using a specific primer including the *Hind*III of the bait sequence at the end and another primer from the Linker, captured DNA fragments are PCR amplified. **(10)** Control experiment is performed to confirm that Linker primer alone does not generate any amplified products. Once this is confirmed, the experiment is expected to contain minimum background signals from non-specific sequences.

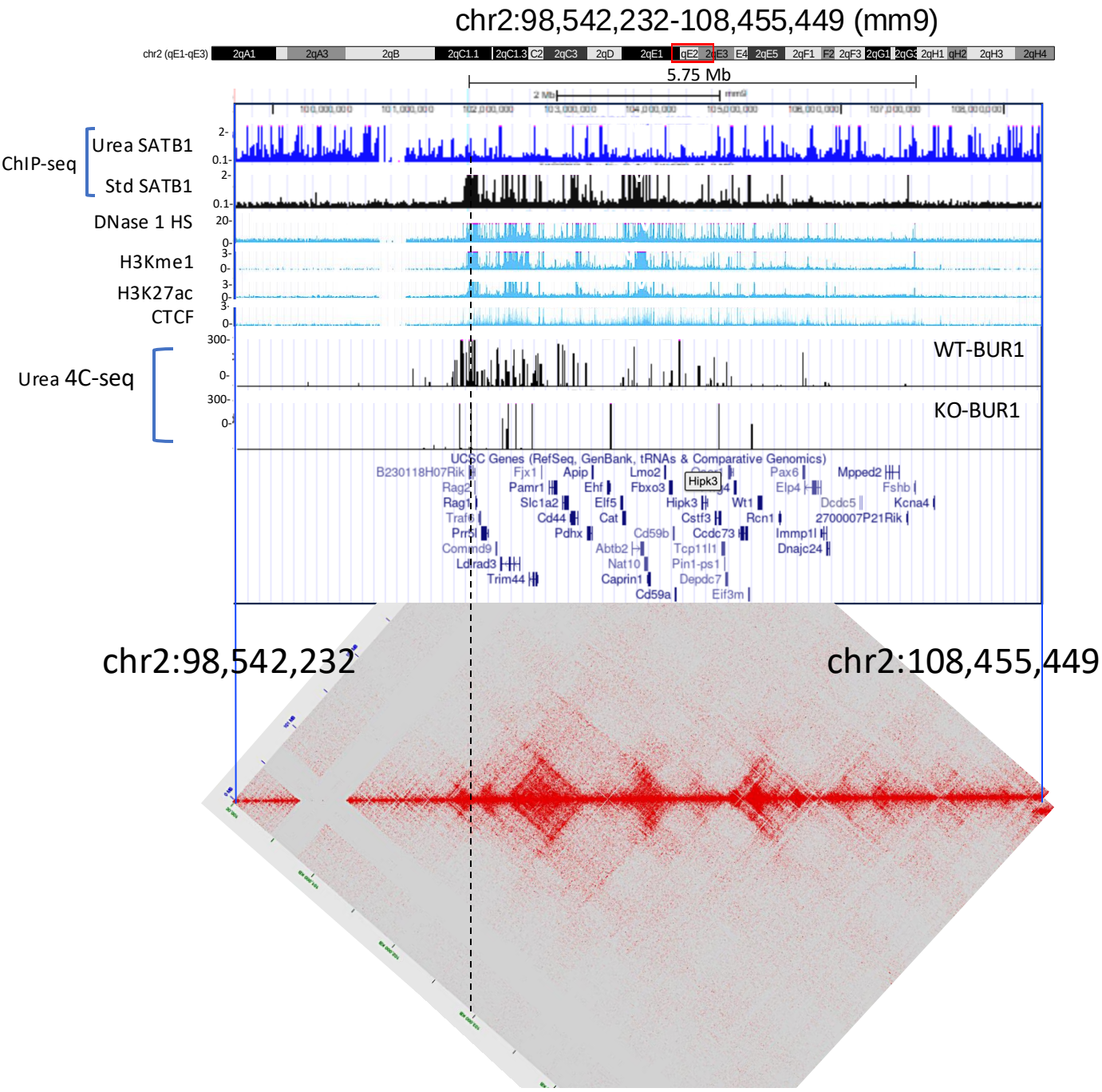

Figure 5—figure supplement 2. **Long-range chromatin interactions from BUR-1 traverse TADs**. BUR-1 interactions determined by urea4C-seq for wild type (WT) and SATB1-KO thymocytes covers the entire 5.75 Mb gene-rich region and these interactions bypass multiple small TADs revealed by the Hi-C heatmap (mm10) generated in the same region. Dotted line indicates the position of BUR-1

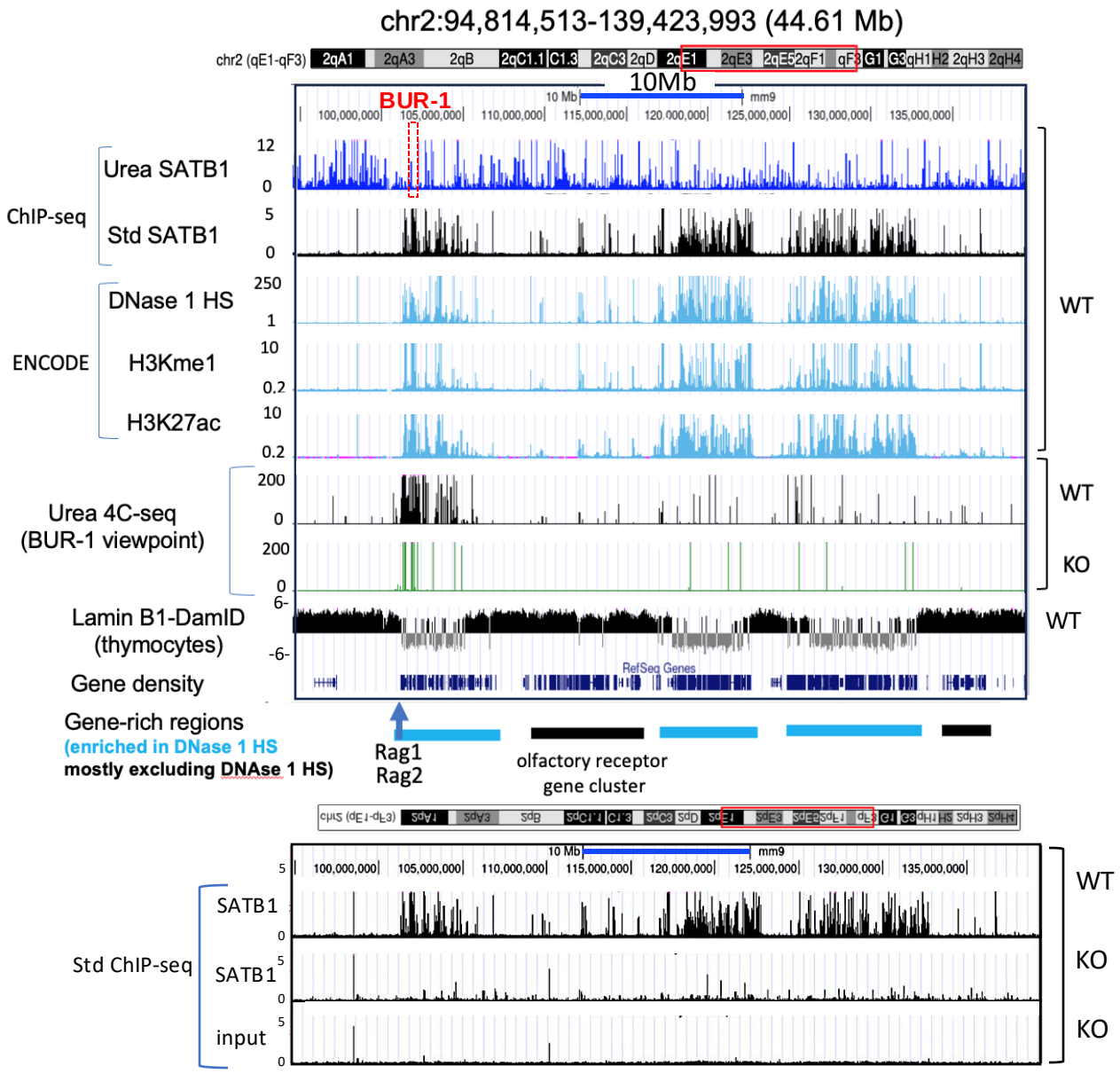

Figure 5—figure supplement 3. **Long-distance interactions covering distal gene-rich regions by BUR-1**. **(A)** A wide view (44.61 Mb) covering distal gene-rich regions shows BUR-1 (red bracket) frequently interacts with distal gene-rich DNase 1 HS regions including clusters of H3Kme1 and H3K27a (indicated by blue horizontal bars). DNase 1 hypersensitive (HS) regions, which indicate highly accessible chromatin (or "**open**" chromatin). These interactions were greatly reduced in SATB1 deficient thymocytes (KO). A gene-rich region (indicated by a black horizontal bar) that does not correspond to DNase 1 HS is enriched in olfactory receptor genes. Lamin B-DamID data shown is from Chen et al., *Cell Rep 2018* (Ref 86). H3Kme1 and H3K27ac data are from ENCODE (LICR) and DNase 1 HS data are from ENCODE (University of Washington). **(B)** SATB1 peaks identified by standard (Std) ChIP-seq in this region are mostly valid and only detected in wildtype (WT) and not in SATB1-null (KO) thymocytes, indicating that SATB1 is binding to these regions, presumably indirectly.

chr2:98,542,232-108,455,449

	Gene Name	log2FoldChange	KO vs WT	p value
SATB1 activated	Rag2	-1.395	0.380	2.29E-14
	Fjx1	-1.138	0.454	0.0074
	Rag1	-0.973	0.509	8.57E-09
	Pamr1	-0.657	0.634	0.0865
	Mpped2	-0.541	0.688	0.1919
	Cd44	-0.521	0.697	0.0299
	Abtb2	-0.502	0.706	0.0055
	Cd59a	-0.369	0.774	0.3787
SATB1 repressed	Rcn1	0.472	1.387	0.0339
	Depdc7	0.518	1.432	0.2204
	Apip	0.543	1.457	0.0224
	Prr5l	0.676	1.598	0.0787
	Prrg4	1.032	2.045	0.0001

Figure 5—figure supplement 4. **Genes within the gene-rich region (chr2:98,542,232-108,455,449) that exhibit SATB1-dependent expression.** Genes showing differential expression for SATB1 with $p<0.05$ are shown in red (SATB1 activated) and in blue (SATB1 repressed). Data are from Zelenka et al., *Nat Commun*.,13, 6954, 2022 (Ref 54).

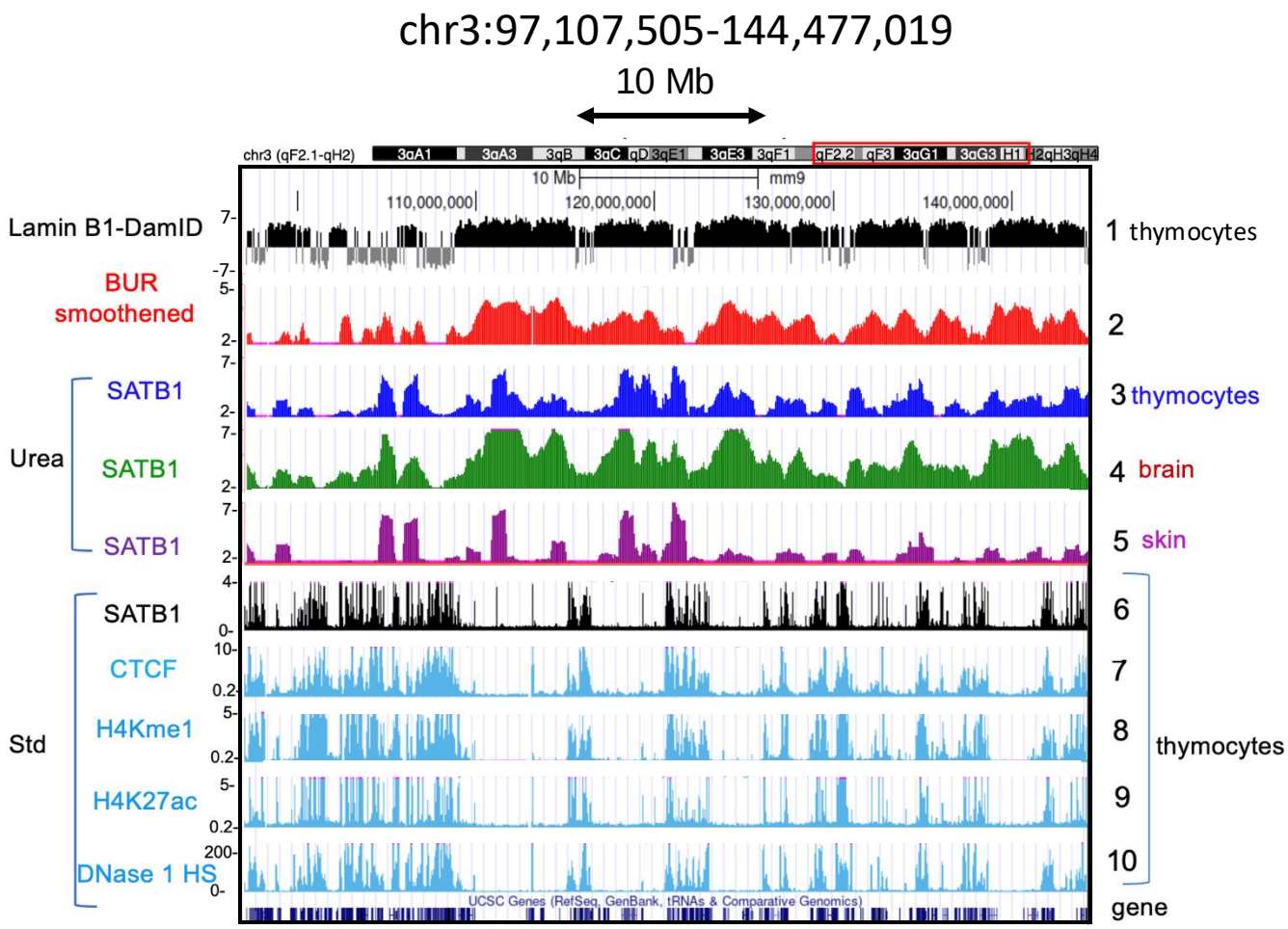

***Figure 7—figure supplement 1*. BURs and BUR-bound SATB1 largely co-map with LaminB1-DamID.** The BUR distribution assessed by the BUR reference map (tracks 2) was compared against Lamin B1-DamID (track 1) over a 47.4Mbp region in chromosome 3. Lamin B1-DamID data are from Chen et al., *Cell Rep 2018* (Ref 86). The BUR distribution shows very similar overall distribution of LADs mapped by Lamin B1-DamID. BUR-binding frequency of SATB1 in thymocytes (track 3) is lower than that in brain (track 4). Distribution of BURs (track 2) and SATB1-binding regions determined by urea ChIP-seq (Urea) (track 3, 4, and 5) largely overlap with LADs (track 1). These regions mostly avoid DNase hypersensitive regions (HS) (track 10), which overlap with SATB1-binding sites determined by standard ChIP-seq (Std) (track 6), CTCF-binding sites (track 7), enhancer marks (H3Kme1 and H3K27ac (tracks 8 and 9, respectively). Data for CTCF, H3Kme1 and H3K27ac are from ENCODE (LICR) and for DNase 1 hypersensitive sites (HS) is from ENCODE (University of Washington).

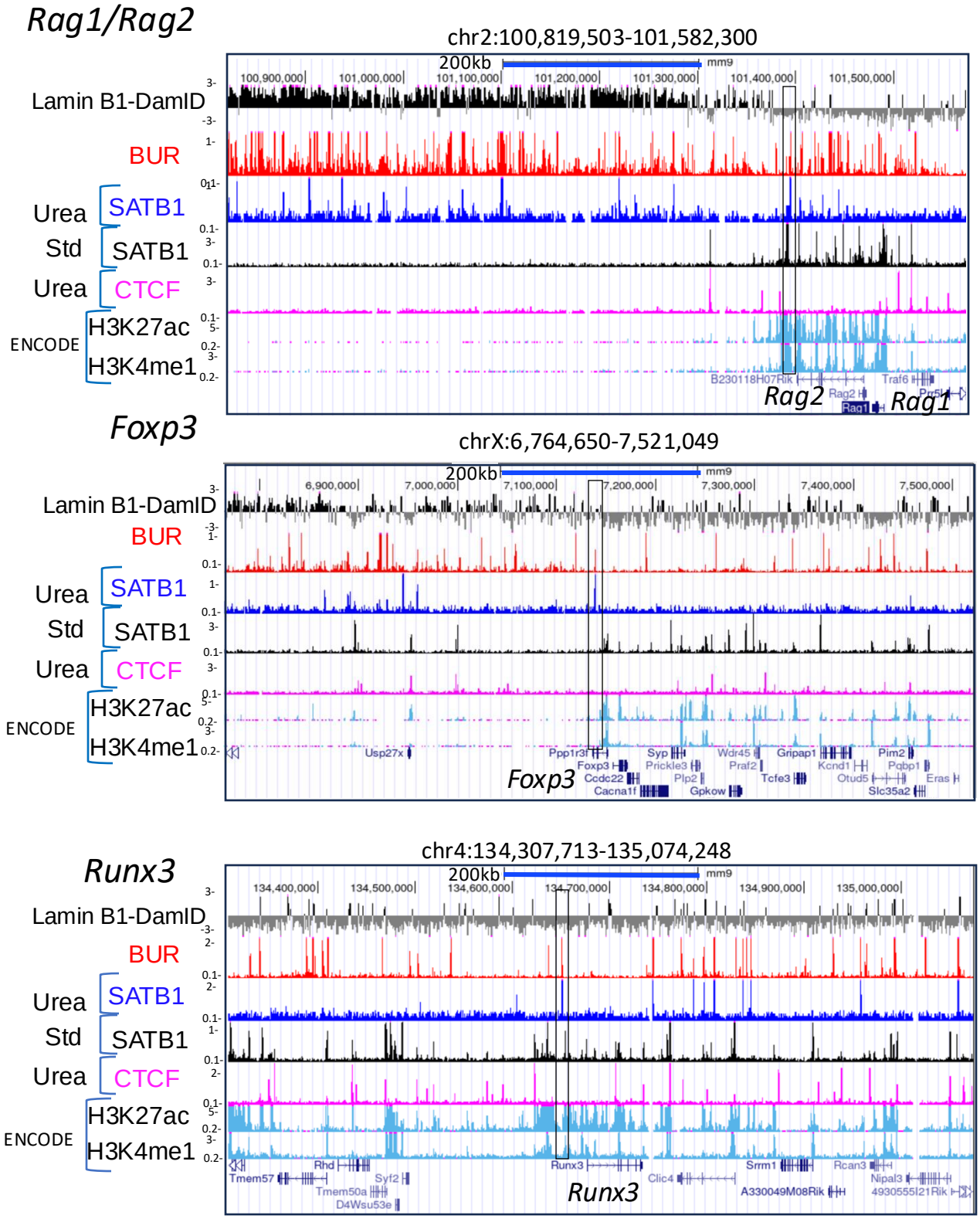

Figure 7—figure supplement 2. **Some SATB1-bound BURs located in SATB1-dependent gene loci are outside of LADs.** SATB1-bound BURs shown in Figure 4 (indicated by black box) in the *Rag1/Rag2, Foxp3, and Runx3* gene loci are found outside LADs mapped by LaminB1-DamID. These are close to H3Kme1 and H3K27ac sites. H3Kme1 and H3K27ac data are from ENCODE (LICR). Lamin B-DamID data shown is from Chen et al., *Cell Rep 2018* (Ref 86).

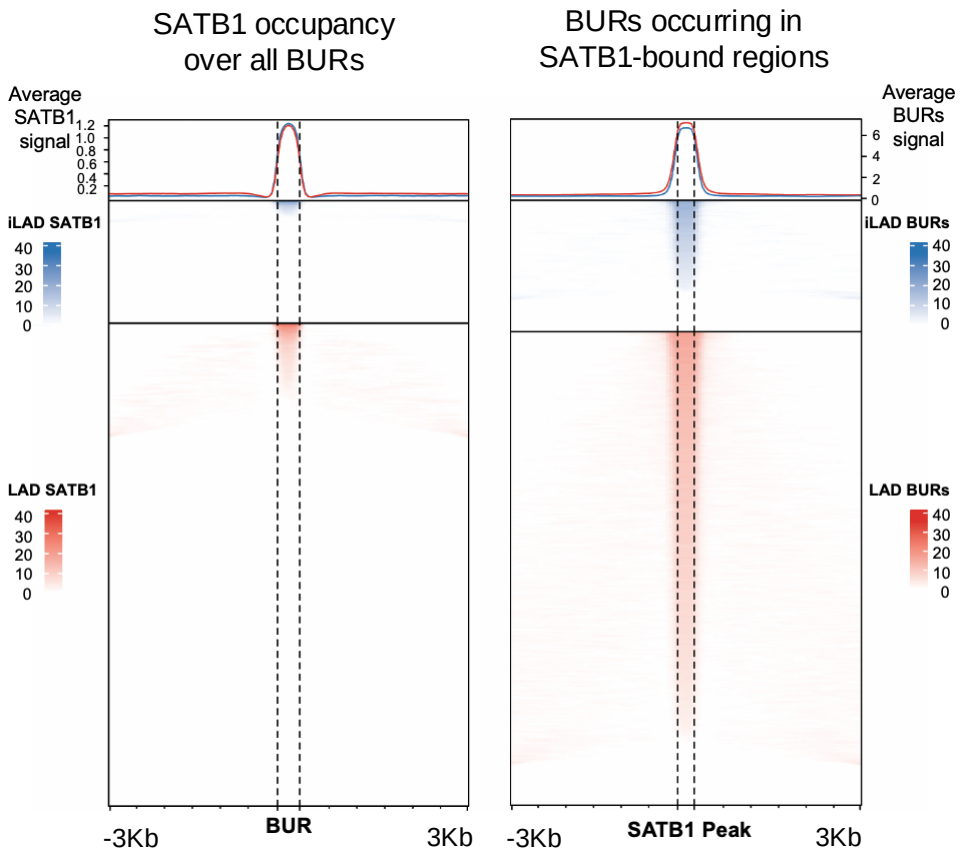

Figure 7—figure supplement 3. **SATB1 occupancy relative to BURs, and BUR signal relative to SATB1-bound loci** *(*Left) Heatmaps showing SATB1 ChIP-seq signal intensity centered on all BUR elements, stratified by lamina association (LAD vs inter-LAD). Signal is plotted within ±3 kb of each BUR center using 50 bp bins using EnrichedHeatmap package (v1.30.0) The line plots above the heatmaps display the average SATB1 signal across all regions. Only a subset of BURs exhibit strong SATB1 binding, consistent with selective occupancy. (Right) Heatmaps showing BUR signal intensity centered on SATB1-bound regions (from ChIP-seq peaks), also separated into LAD and iLAD groups. The vast majority of SATB1 binding events are positioned within BURs, as evidenced by sharp, centered BUR signal at nearly all SATB1 peaks. Line plots reflect the average BUR signal profile across all SATB1 sites in each domain class. BUR intensities are derived from *in vitro* SATB1 BUR-binding assays.

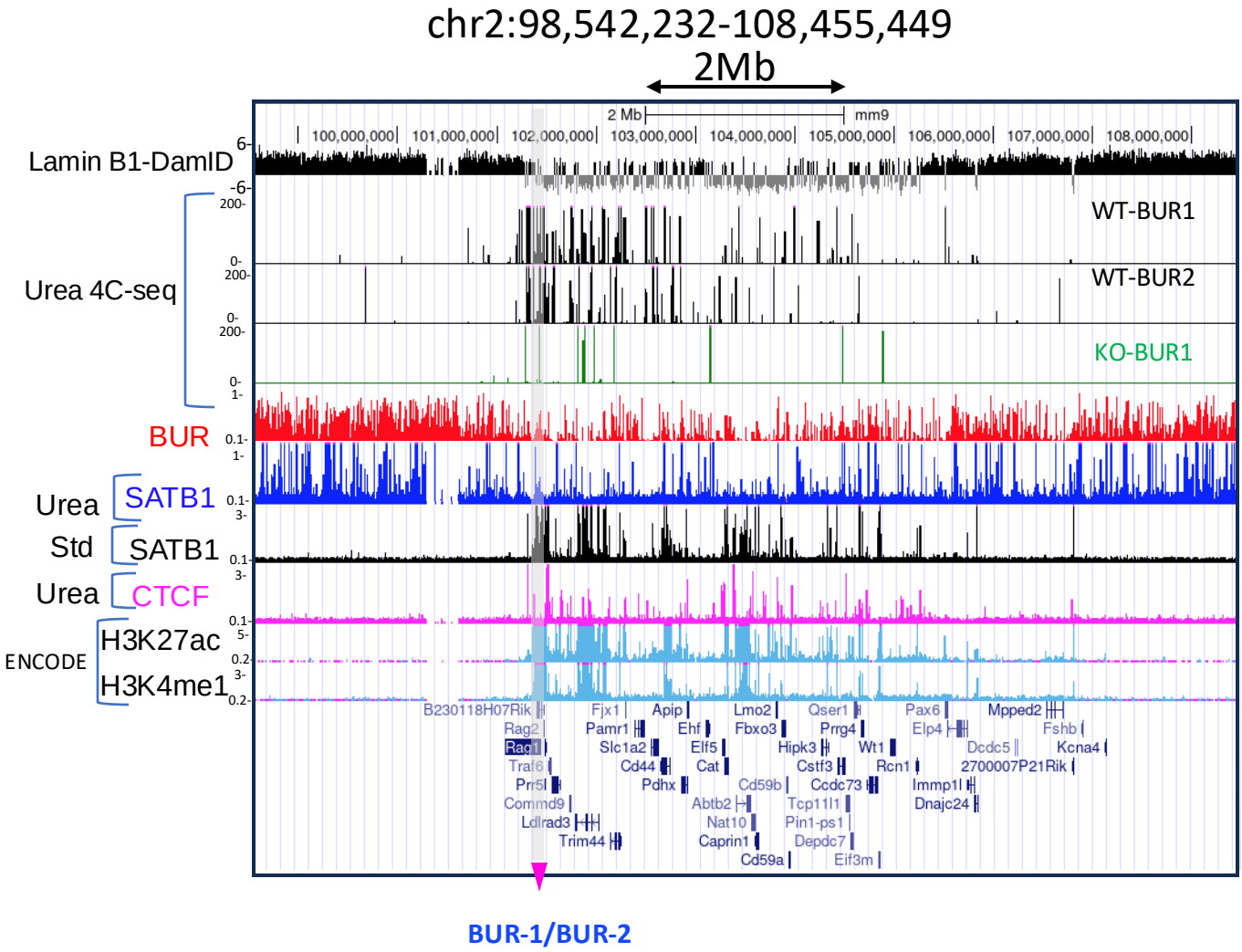

***Figure 7—figure supplement 4*. Interaction sites from BUR-1 or BUR-2 are mostly confined to the inter-LAD region.** The region containing BUR-1 and BUR-2 as baits is light gray shaded with a pink arrowhead. This region is near the border of a LAD and an inter-LAD region, shown by LADs identified by Lamin B-DamID. Interaction profiles from either BUR-1 and BUR-2 obtained in wild-type thymocytes (WT) are found in a region surrounded by LADs. These interactions are greatly reduced in Satb1-KO thymocytes (KO). Many interaction sites are close to H3Kme1 and H3K27ac sites. H3Kme1 and H3K27ac data are from ENCODE (LICR). Lamin B-DamID data shown is from Chen et al., *Cell Rep 2018* (Ref 86).

Supplementary Table 1. Intersection analysis of ChIP-seq samples

	BUR-L	UREA SATB1 thymus	UREA SATB1 thymus	Standard SATB1 thymus	Standard SATB1 thymus	UREA SATB1 brain	UREA SATB1 brain	UREA SATB skin	UREA SATB1 skin	UREA CTCF thymus	UREA CTCF skin	Standard CTCF thymus
%	A	B	C	D	E	F	G	H	I	J	K	L
A-120A		12.68	14.34	0.77	0.60	36.41	33.54	3.69	3.62	0.25	0.58	0.60
B- 355B	77.71		85.02	1.12	0.86	92.07	90.28	24.13	23.56	0.77	1.00	0.86
C-355C	75.87	73.38		0.96	0.75	92.39	91.74	20.82	20.17	0.68	0.93	0.77
D-328B	3.83	0.91	0.90		47.92	1.28	1.11	1.93	1.91	22.35	23.31	36.39
E-408B	5.23	1.23	1.25	85.04		1.72	1.57	3.96	3.59	18.08	21.99	37.71
F-345A	73.58	30.35	35.28	0.52	0.40		78.12	7.80	7.59	0.31	0.58	0.56
G-345B	73.25	32.16	37.86	0.49	0.39	84.42		8.33	8.09	0.30	0.56	0.56
H-404B	78.54	83.69	83.65	8.30	9.59	82.06	81.13		81.06	2.35	12.85	1.78
I-404E	79.49	84.45	83.79	8.47	8.98	82.60	81.45	83.78		2.38	12.17	1.70
J-346D	2.96	1.47	1.52	52.97	24.15	1.78	1.61	1.29	1.27		83.53	60.22
K-403C	4.36	1.23	1.34	35.64	18.94	2.18	1.95	4.57	4.19	53.87		42.86
L-Encode LICR	2.68	0.63	0.65	33.00	19.27	1.24	1.14	0.37	0.35	23.04	25.42	

Supplementary Table 1. Intersection of peaks were determined by deepTools between two samples of choice. Percent of peaks in each sample on the left column intersected with peaks in each of the samples on the top row are indicated.

Supplementary Table 2. ChIP-seq sample identification and peak number

		Sample ID	Total #Peaks
A. BUR-L		A-120A	238380
B. UREA SATB1 thymus	replica 1	B-355B	38882
C. UREA SATB1 thymus	replica 2	C-355C	45049
D. Std SATB1 thymus	replica 1	D-328B	48175
E. Std SATB1 thymus	replica 2	E-408B	27147
F. UREA SATB1 brain	replica 1	F-345A	117963
G. UREA SATB1 brain	replica 2	G-345B	109154
H. UREA SATB1 skin	replica 1	H-404B	11210
I. UREA SATB1 skin	replica 2	I-404E	10846
J. UREA CTCF thymus	replica 1	J-346D	20323
K. UREA CTCF skin	replica 1	K-403C	31509
L. Std CTCF thymus	Encode	L-Encode LICR	53124

Supplementary Table 2. Identification of each sample and their total number of peaks are shown.

Supplementary Table 3. Intersection analysis of WT and KO ChIP-seq samples

	urea ChIP-seq					standard ChIP-seq				
	TKS355B	TKS400B	TKS400D	TKS340A	TKS356A	TKS408B	TKS407D	TKS407B	TKS390A	TKS407C
	SATB1 ChIP	Phantom (KO SATB1 ChIP)	Phantom (KO SATB1 ChIP)	Urea Input	Urea Input	SATB1 ChIP	Phantom (KO SATB1 ChIP)	Phantom (KO SATB1 ChIP)	Standard Input	Standard Input
	UREA	UREA antibody 1	UREA antibody 2	WT	KO	STANDARD	Standard Antibody 1	Standard Antibody 2	WT	KO
TKS355B		0.0	0.0	0.4	0.4	0.8	0.1	0.1	0.5	0.3
TKS400B	1.0		78.5	33.6	6.1	85.7	89.7	93.8	53.0	15.3
TKS400D	0.8	66.1		25.4	4.2	88.9	93.2	93.2	41.5	11.8
TKS340A	10.7	1.4	1.3		51.2	55.6	7.8	10.6	79.2	39.3
TKS356A	17.7	0.4	0.3	90.8		76.1	8.3	12.3	93.4	59.4
TKS408B	1.2	0.3	0.3	4.1	3.1		3.6	4.5	12.7	3.0
TKS407D	2.3	3.1	3.8	6.7	4.3	36.4		90.9	9.6	4.1
TKS407B	1.3	1.3	1.5	3.5	2.3	18.2	37.2		4.9	2.2
TKS390A	3.6	0.7	0.6	25.2	16.9	52.0	3.6	4.6		14.3
TKS407C	16.7	1.2	1.1	75.7	63.9	79.8	8.3	12.0	86.5	

Supplementary Table 3: Intersection of peaks were determined by deepTools between two samples of choice. Percent of peaks in each sample on the left column that intersected with peaks in each sample on the top row are indicated. Important sets of data for comparison are highlighted in blue for urea ChIP-seq and pink for standard ChIP-seq.

Supplementary Table 4. WT and KO ChIP-seq sample identification and total peak number

Sample ID	Description	Total # Peaks
TKS355B	SATB1 ureaChIP-seq	38882
TKS400B	KO SATB1 ureaChIP-seq 1	98
TKS400D	KO SATB1 ureaChIP-seq 2	118
TKS340A	WT Input ureaChIP-seq 1	2381
TKS356A	KO Input ureaChIP-seq 1	1372
TKS408B	SATB1 standard ChIP-seq	27147
TKS407D	KO SATB1 standard ChIP-seq 1	2884
TKS407B	KO SATB1 standard ChIP-seq 2	7003
TKS390A	WT Input Standard ChIP-seq 1	7377
TKS407C	KO Input Standard ChIP-seq 1	1224

Supplementary Table 4: Identification of each sample and their total number of peaks are shown.